
Isolated Neutron Stars

Victoria M. Kaspi and Mallory S. E. Roberts
*Physics Department, McGill University, Rutherford Physics Building,
 3600 University Street, Montreal, QC, Canada, H3A 2T8*

Alice K. Harding
*NASA Goddard Space Flight Center, Laboratory for High Energy Astrophysics,
 Code 661.0, Greenbelt, MD, USA, 20771*

7.1 Introduction

This chapter deals with X-ray emission from isolated neutron stars for which the energy for the observed X-rays is thought to originate from the rotation of the neutron star, or from an internal heat reservoir following formation. Rotation power can manifest itself as pulsed emission, or as nebular radiation produced by a relativistic wind of particles emitted by the neutron star. Residual heat of formation is observed as soft X-ray emission from young neutron stars. Such thermal radiation, however, can also be produced as a result of reheating from internal or external sources. Rotation-powered pulsed and nebular X-ray emission, as well as thermal emission, can often be observed in a single object simultaneously; this is both fascinating and annoying, as one invariably contaminates the study of the other. There are also a handful of neutron stars for which the origin of the observed X-ray emission is unclear but may be related to the above processes; we will discuss those as well.

Rotation-powered neutron stars are generally referred to as “radio pulsars” since it is at radio wavelengths that the vast majority of the catalogued* population (currently numbering ~ 1400) is observed. However, the radio emission is energetically unimportant, and we now know of several rotation-powered neutron stars that are not detected as radio sources in spite of deep searches (e.g. Crawford et al., 1998; McLaughlin et al., 2001). We therefore use the more physically motivated term “rotation-powered.”

The total available spin luminosity in a rotation-powered pulsar is given by the rate of loss of rotational kinetic energy, $\dot{E} \equiv I\omega\dot{\omega} \equiv 4\pi^2 I\dot{P}/P^3$, where I is the stellar moment of inertia and $\omega \equiv 2\pi/P$ is the angular frequency with P the spin period. Thus a simple measurement of P and \dot{P} for an isolated neutron star determines the available rotational power in a model-independent way, assuming a value for I , typically taken to be 10^{45} g cm². Also generally inferred for these sources are their surface di-polar magnetic fields, $B = 3.2 \times 10^{19} (P\dot{P})^{1/2}$ G (for B on the equator), and their characteristic spin-down ages, via $\tau_c = P/2\dot{P}$. Although these latter two inferences are model-dependent (B because it assumes simple magnetic dipole braking in a vacuum – which is almost certainly not the case – and τ_c because it represents the true physical age only for the same assumption and also for a negligible initial

* <http://www.atnf.csiro.au/research/pulsar/psrcat/>

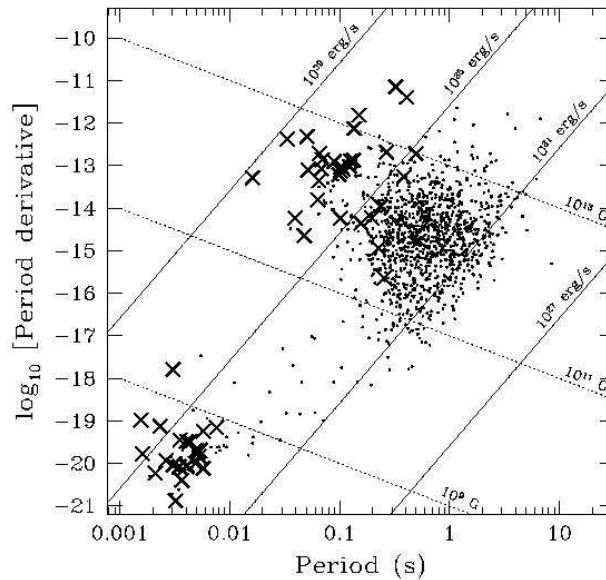


Fig. 7.1. $P-\dot{P}$ diagram for the 1403 currently catalogued rotation-powered pulsars. The 66 X-ray detected sources are indicated with an “X.” Solid lines show constant \dot{E} , and dotted lines show constant inferred surface di-polar magnetic field. “X-ray-detected” means pulsed, unpulsed or nebular emission, be it thermal or non-thermal. X-ray detected sources are generally those with the greatest spin-down luminosity, although the correlation is not perfect because of the wide range of source distances and observational selection effects. The indicated sources are summarized in Tables 7.1, 7.2, and 7.5. Note that the X-ray-detected millisecond pulsars in the globular cluster 47 Tucanae do not have observable intrinsic \dot{P} ’s due to contamination by acceleration in the cluster potential; for those sources (numbering 15), we have used inferred \dot{P} ’s (see Freire et al., 2001; Grindlay et al., 2002).

spin period), the important point is that P and \dot{P} provide, in addition to \dot{E} , at least estimates of other important physical information.

It is for this reason that P - \dot{P} diagrams are so useful. Figure 7.1 shows the P - \dot{P} phase space, with all catalogued rotation-powered neutron stars with measured \dot{P} s indicated as dots. Lines of constant \dot{E} and B are indicated. Note the two different populations of rotation-powered neutron stars: those with periods between ~ 16 ms and ~ 8 s, having $B \gtrsim 10^{11}$ G, and the lower magnetic field ($B \lesssim 10^{10}$ G), very rapidly rotating class ($P \lesssim 100$ ms), the millisecond pulsars. The division is made particularly obvious when binarity is considered, as the latter sources are mostly in binaries, while the former are only rarely in binaries. The millisecond pulsars are often referred to as “recycled” pulsars as they are thought to be formed in a past episode of mass transfer as part of an accreting X-ray binary phase (see chapter 1

by Psaltis). Finally, note the absence of sources having $B \gtrsim 10^{14}$ G. Neutron stars having fields higher than this are thought to be “magnetars,” discussed in chapter 14 by Woods et al.

All sources which have been detected in X-rays are identified with an “X” in Figure 7.1. For the purposes of this Figure, any X-ray detection, be it pulsed, unpulsed or nebular, thermal or non-thermal, is counted. Note the clear correlation with \dot{E} – most X-ray identified rotation-powered neutron stars have large \dot{E} and vice versa. The correlation is not perfect; the main reason for this is that the distances to these sources vary by over two orders of magnitude. Distant high- \dot{E} sources are harder to detect, and nearby low- \dot{E} sources may be detected through their thermal emission. Note also the large number of millisecond pulsar detections is due to many of them being in X-ray studied globular clusters having larger scale heights, hence smaller line-of-sight absorbing column densities.

Tables 7.1, 7.2 and 7.5 provide a summary list of all X-ray-detected rotation-powered neutron stars, along with their most important properties. Note that the number of X-ray detected rotation-powered pulsars has more than doubled in the past 5 years (from 27 in the 1997 review by Becker & Trümper, to 66 today). This is due to improvements in X-ray sensitivity, in particular from the *Rossi X-ray Timing Explorer (RXTE)*, the *Chandra X-ray Observatory* and the *XMM-Newton Telescope*, and also improvements in radio telescope sensitivity, most notably at the Parkes, Arecibo, and Green Bank radio telescopes, which have permitted discoveries of sources that could later be followed up with X-ray observations.

7.2 Magnetospheric Emission

7.2.1 Motivation

After the discovery (Staelin & Reifenstein, 1968; Comella et al., 1969) of the Crab pulsar in 1968 and the realization (Ostriker & Gunn, 1969; Finzi & Wolf, 1969) that the spin-down energy loss of the neutron star, as estimated from its measured P and \dot{P} , could power all the visible radiation of the Crab nebula, it was evident that neutron stars are energetically important sources of particle production and acceleration. It is now believed that the radiating particles in pulsar wind nebulae (see §7.6) are electron-positron pairs produced by electromagnetic cascades within the pulsar magnetosphere. Since the pulsar magnetosphere is also believed to be the origin of the pulsed non-thermal emission, understanding this emission will lead us to an understanding of the energetics of these sources and ultimately how the pulsar converts its spin-down power into both the pulsed and unpulsed observable radiation. However, the pulsed radio emission, which first enabled the discovery of pulsars, makes up a tiny ($\sim 10^{-6}$) portion of the energy budget. Pulsed emission at high energies, although harder to detect, is energetically much more significant (making up $\sim 10^{-3}$ of the spin-down power in the Crab and up to 0.1 in other pulsars) and thus is a more direct probe of the particle acceleration in the magnetosphere.

Aside from the important issue of energetics, we also want to study the non-thermal emission at high energies in order to understand the physical processes in the pair cascades which generate the electron-positron pairs. It is widely believed that generation of a pair plasma is required for the instabilities that produce

4 *Isolated Neutron Stars*

coherent radio emission in pulsars (Melrose, 2000). Why radio pulsars die after they have spun down to periods of several seconds may possibly be understood as their inability to produce pair plasmas when particle acceleration becomes too feeble (Ruderman & Sutherland, 1975; Hibschan & Arons, 2001; Harding et al., 2002a). Studying the radiation and pair cascades at high energy is also a study in the physical processes, such as one-photon pair creation and photon splitting, that occur only in the strong magnetic fields of neutron stars. Finally, the generation of non-thermal emission is intimately linked to the polar-cap heating which contributes to the thermal emission, particularly in older pulsars.

7.2.2 *Summary of Observations*

At X-ray energies, 66 rotation-powered pulsars have been detected, nearly half of which have periods $P < 6$ ms. Many of these detections were first made by *ROSAT* (Becker & Trümper, 1997) and *ASCA* (Saito, 1998), but the number has increased rapidly in recent years with new observations by *RXTE*, *Chandra* and *XMM-Newton* (Becker & Aschenbach, 2002). Table 1.1 lists the pulsars thought to show non-thermal emission components in their X-ray spectra with observed parameters, including detected emission at other wavelengths. The vast majority are also radio pulsars; many of the target sources were chosen from radio pulsar catalogs. However, there have been some detections of X-ray pulsars, such as PSR J0537–6910 (Marshall et al., 1998), PSR J1846–0258 (Gotthelf et al., 2000), PSR J1811–1926 (Torii et al., 1997), and PSR J0205+6449 (Murray et al., 2002), without a radio ephemeris. Radio pulses have since been detected from only one of these (PSR J0205+6449; Camilo et al., 2002c). Clearly, short period pulsars seem to have the highest levels of non-thermal X-ray emission. Most of the field millisecond pulsars have purely non-thermal spectra. On the other hand, the millisecond radio pulsars in the globular cluster 47 Tucanae that have been detected as point sources by *Chandra* (Grindlay et al., 2002) have spectra that are quite soft, and most likely thermal. The longer-period pulsars with detected X-ray emission have spectra that are dominated by thermal emission.

7.2.2.1 *Spectra*

Generally, the X-ray spectra of spin-powered pulsars show a mix of thermal and non-thermal components. Often several thermal components (discussed in §7.3) and sometimes even several non-thermal components can be identified. Cleanly separating the non-thermal, or power-law, components from the thermal components can be difficult, especially in sources where the thermal components dominate (e.g. Geminga, PSRs 0656+14 and B1055–52; Halpern & Wang, 1997; Greiveldinger et al., 1996). Detectors with sensitivity at energies up to at least 10 keV, such as *RXTE*, *Chandra* and *XMM*, have been able to make the best measurements of non-thermal emission components. This non-thermal emission probably originates from the radiation of particles accelerated in the pulsar magnetosphere. Models for this emission will be discussed below.

All of the γ -ray pulsars that have been detected by the *Compton Gamma-Ray Observatory* (*CGRO*) are also X-ray pulsars with measured non-thermal emission components. One interesting question is whether the non-thermal X-ray spectrum

Table 7.1. *Non-Thermal X-ray Detected Rotation-Powered Pulsars*

is part of the same emission as that detected at γ -ray energies. For the youngest of these pulsars (Crab, PSR B1509–58), the total power in pulsed emission peaks in the hard X-ray band (Figure 7.2). There is strong emission through the entire

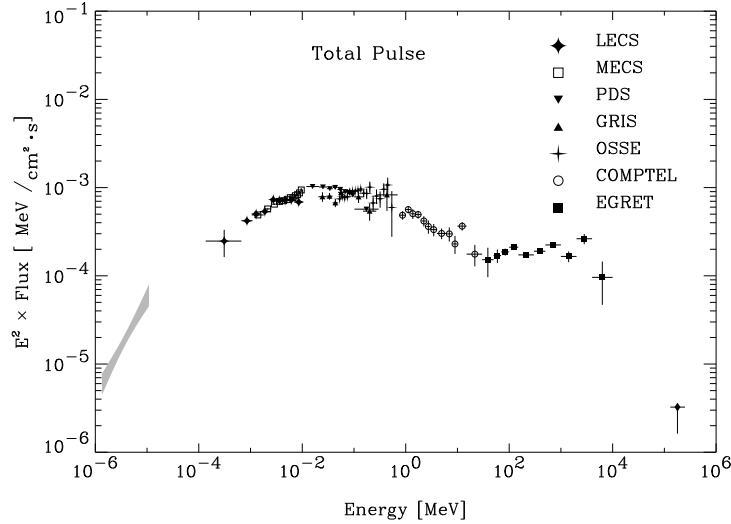


Fig. 7.2. Broadband pulsed spectrum (Kuiper et al., 2001) of the Crab, as an example of emission characteristics of a young pulsar.

X-ray and γ -ray bands and a smooth connection between the two. However, in the case of the Crab the smoothness of the spectrum is misleading as the situation may be more complicated. Kuiper et al. (2001) have argued for several separate emission components in the Crab optical to γ -ray spectrum, evidenced by the strong frequency dependence of the interpeak emission and the peak 2 to peak 1 ratio, both of which have a maximum around 1 MeV. The middle-aged pulsars have comparatively weak non-thermal emission in the X-ray band since their power peaks at GeV energies, and there is a gap in the detected spectrum between the X-ray and γ -ray bands (Figure 7.3). In several cases (Vela, PSR B1055–52) an extrapolation between the two is plausible, but in others (Geminga, PSR B1706–44; Gotthelf et al., 2002) a connection is not clear. In the case of Vela (Figure 7.3), there is strong evidence for two separate non-thermal X-ray components (Harding et al., 2002b), one connecting to the γ -ray (OSSE) spectrum and the other possibly connected with the optical spectrum.

Millisecond pulsars seem to be bright X-ray emitters, as a relatively large number of the known millisecond radio pulsars are X-ray pulsars. Most have hard power-law spectra with photon indices 1.5–2.0 (Becker & Aschenbach, 2002), with the exception of a few (e.g. PSRs J0437–4715, J2124–3358; Zavlin et al., 2002; Sakurai et al., 2001) which also have thermal components. Since they are too old to have detectable cooling emission, the presence of pulsed thermal emission from millisecond pulsars probably requires polar-cap heating.

There are a number of newly discovered X-ray pulsars (PSR J1420–6048; Roberts et al., 2001), (PSR J1930+1852; Camilo et al., 2002a), (PSR J2229+6114; Halpern et al., 2001), (PSR J1105–6107; Kaspi et al., 1997) that lie in or near the error circles of EGRET unidentified γ -ray sources (Hartman et al., 1999). Since these pulsars were

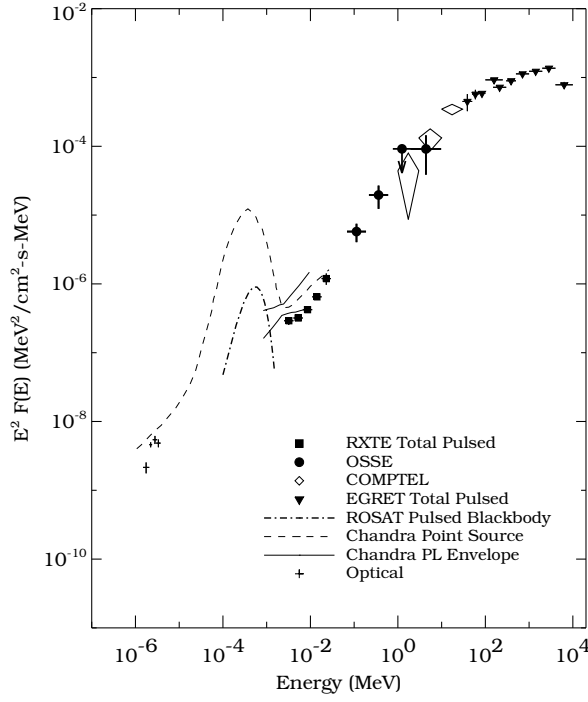


Fig. 7.3. Broadband pulsed spectrum (Harding et al., 2002b) of the Vela pulsar, as an example of emission characteristics of a middle-aged pulsar.

discovered after the end of the *CGRO* mission and EGRET detected too few photons to search for pulsations, it is not known whether they are also γ -ray pulsars. There are also some X-ray pulsars discovered earlier (PSR B1823–13, PSR B1800–21) that are associated with EGRET sources and are candidate γ -ray pulsars (Kanbach, 2002).

7.2.2.2 Pulse Profiles

The pulse profiles of the non-thermal X-ray emission usually show much more modulation and narrower pulses than does the thermal emission. The pulsed fraction for many pulsars with mixed emission rises from around 10% – 20% in the (0.1 - 1 keV) band where the thermal emission dominates, to 80% – 90% where the non-thermal emission dominates (Becker & Aschenbach, 2002). There is often an accompanying phase shift between the thermal and non-thermal pulses of the middle-aged pulsars.

There seems to be no pattern in the relative phases of the non-thermal X-ray, radio and gamma-ray pulses. The non-thermal X-ray and radio pulses of many pulsars that are young or have very short periods, including the Crab (with the exception of the radio pre-cursor), PSRs J1617–5055, J0205+6114, and J1930+1852 and most of the millisecond pulsars, are in phase and/or the profiles look very similar. Somehow for these pulsars, the radio and high-energy emission must originate from

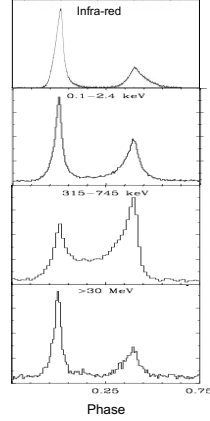


Fig. 7.4. Multiwavelength pulse profiles (Kanbach, 2002) of the Crab, as an example of emission characteristics of a young pulsar.

the same region in the magnetosphere. However, the profiles of these pulsars vary from double-peaked to both broad and narrow single-peaked shapes, and a few young X-ray pulsars (PSRs J1811–1926, J0537–6910 and J1846–0258) have no detected radio counterparts. The non-thermal X-ray pulses of middle-aged pulsars, on the other hand, are not in phase with their radio pulses, indicating a different location in the magnetosphere of the two emission components (e.g. Figure 7.5). The same trend seems to be true for the X-ray and γ -ray pulses of the γ -ray pulsars, with the profiles of the fastest, including millisecond (PSR J0218+4232, Kuiper et al., 2000), pulsars being alike and in phase while the profiles of the slower pulsars are not in phase (Kanbach, 2002). Thus, a fast rotation rate seems to be instrumental in causing alignment of the pulses across the spectrum.

7.2.3 Emission Models

Particle acceleration inside the pulsar magnetosphere gives rise to pulsed non-thermal radiation and possibly also thermal emission from backflowing particles that heat the neutron-star surface. Rotating, magnetized neutron stars are natural unipolar inductors, generating huge vacuum electric fields. However, as was first noted by Goldreich & Julian (1969) in their classic paper, a rotating neutron star will not be surrounded by vacuum, since a large surface charge will build up on the star. This surface charge is unstable, because the induced vacuum electric field has a component parallel to the magnetic field at the stellar surface that exceeds the gravitational force by many orders of magnitude and is capable of pulling charges out of the star. If charges are not trapped in the surface by binding forces (i.e. if the crust is solid) a charge density, known as the Goldreich-Julian or corotation charge density, $\rho_{GJ} \simeq -\omega \cdot \mathbf{B}/(2\pi c)$, builds up in the neutron-star magnetosphere. If the magnetospheric charge reaches the Goldreich-Julian value everywhere, it is able to short out the electric field parallel to the magnetic field (E_{\parallel}), and the dipole magnetic field will corotate with the star. Corotation of the pulsar magnetosphere must break

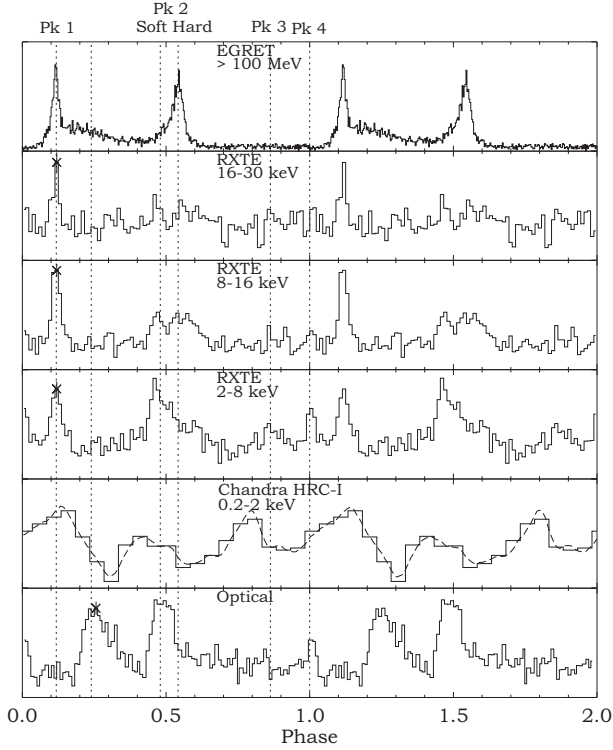


Fig. 7.5. Multiwavelength pulse profiles (Harding et al., 2002b) of the Vela pulsar, as an example of emission characteristics of a middle-aged pulsar.

down at large distances from the neutron star due to particle inertia. Where and how this happens is not yet understood, but it is certain that corotation cannot persist past the speed-of-light cylinder radius, $R_{LC} = c/\omega$, which is the distance at which the corotation velocity reaches c (see Figure 7.6). It is believed that in the outer parts of the magnetosphere there must be a transition to the wind zone, where the energy density of the particles is large enough to distort the poloidal dipole field into a toroidal relativistic wind flow that carries the spin-down energy of the pulsar, in the form of magnetic and particle energy, into a surrounding nebula where (at least in the case of the Crab pulsar) it is dissipated as synchrotron radiation (Rees & Gunn, 1974; Kennel & Coroniti, 1984b). Although the standard picture of a pulsar magnetosphere described above is usually accepted on faith, global magnetospheric simulations (Krause-Polstorff & Michel, 1985; Pétri et al., 2002; Spitkovsky & Arons, 2002) have not yet been able to show whether and how a pulsar magnetosphere reaches the nearly force-free (ideal MHD) state envisioned by Goldreich & Julian. However, if it is assumed that a force-free, corotating magnetosphere has been achieved, then Contopoulos et al. (1999) have found a solution which smoothly connects the corotating magnetosphere to a relativistic wind. Inside the magnetosphere and at the light cylinder, the ratio (known as σ) of the magnetic energy density to the particle energy density is large, primarily because according to the acceleration models to be

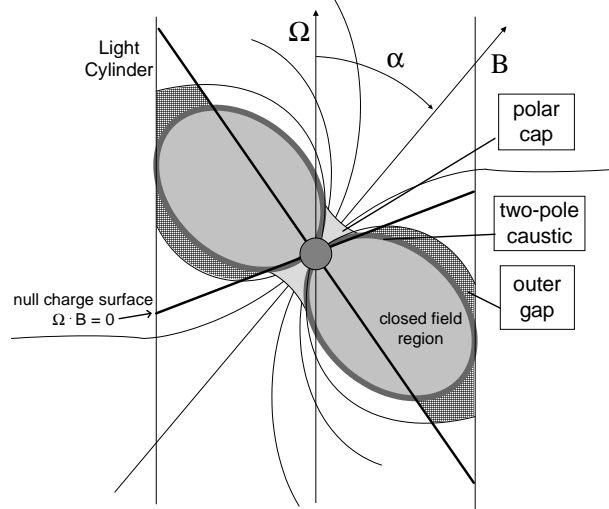


Fig. 7.6. Schematic 2D view of the high-energy emission geometry of several proposed models.

discussed below, the particles receive only a fraction of the full potential drop across the open field lines. Therefore, σ is large at the start of the wind flow, but must drop to 1 or below to accelerate the particles at the wind-termination shock. The pulsed emission is presumed to originate inside the corotating magnetosphere, and strong E_{\parallel} may develop to accelerate particles at two possible sites where $\mathbf{E} \cdot \mathbf{B} \neq 0$. These sites have given rise to two classes of high energy emission models: polar-cap models, where the acceleration and radiation occur near the magnetic poles in the inner magnetosphere, and outer-gap models, where these processes occur in the outer magnetosphere.

7.2.3.1 Polar-Cap Model

Polar-cap models (Daugherty & Harding, 1982; Usov & Melrose, 1995; Daugherty & Harding, 1996) advocate that particle acceleration occurs near the neutron star surface and that high-energy emission results from a curvature radiation or inverse Compton induced pair cascade in a strong magnetic field. There is some variation among polar-cap models, with the primary division being whether or not there is free emission of particles from the neutron-star surface. The subclass of polar-cap models based on free emission of particles of either sign, called space-charge limited flow models, assumes that the surface temperature of the neutron star (many of which have now been measured to be in the range $T \sim 10^5 - 10^6$ K, see §7.3) exceeds the ion and electron thermal emission temperatures. Although $E_{\parallel} = 0$ at the neutron-star surface in these models, the space charge along open field lines above the surface falls short of the corotation charge, due to the curvature of the field (Arons & Scharlemann, 1979) and to general relativistic inertial frame dragging (Muslimov & Tsygan, 1992).

The E_{\parallel} generated by the charge deficit accelerates particles, which radiate inverse Compton (IC) photons (at particle Lorentz factors $\gamma \sim 10^2 - 10^6$) and curvature (CR) photons (at Lorentz factors $\gamma \gtrsim 10^6$). Because lower Lorentz factors are required to produce pairs through IC emission, an IC pair formation front (PFF) will form first, close to the surface. However, it is found (Harding & Muslimov, 2002) that the IC pair formation fronts do not produce sufficient pairs to screen the E_{\parallel} completely, thus allowing acceleration to the Lorentz factors $\sim 10^7$ sufficient to produce a CR PFF, where there are sufficient pairs to completely screen the E_{\parallel} . The CR pair front will therefore limit the particle acceleration voltage and determine the high-energy emission luminosity. The CR photons can produce secondary electrons and positrons through one-photon pair production in the strong magnetic field near the neutron star surface. These pairs are produced in excited Landau states and radiate synchrotron photons which are energetic enough to produce more pairs. The combined curvature and synchrotron radiation from such pair cascades has been shown to produce high-energy phase-resolved spectra similar to observed spectra of X-ray and γ -ray Vela-like pulsars (Daugherty & Harding, 1996). The γ -ray spectra cut off very sharply (as a “super-exponential”) due to one-photon pair production attenuation, at the pair escape energy, i.e. the highest energy at which photons emitted at a given location can escape the magnetosphere without pair producing. A rough estimate of this cutoff energy, assuming emission along the polar-cap outer rim, $\theta_{\text{PC}} \simeq (2\pi r/cP)^{1/2}$, at radius r , is

$$E_c \sim 2 \text{ GeV } P^{1/2} \left(\frac{r}{R} \right)^{1/2} \max \left\{ 0.1, B_{0,12}^{-1} \left(\frac{r}{R} \right)^3 \right\} \quad (7.1)$$

where $B_{0,12}$ is the surface magnetic field in units of 10^{12} G and R is the stellar radius. Although many high-energy photons are attenuated well below 1 GeV near the surface, in polar-cap cascades much of the radiation occurs at least 1-2 stellar radii above the surface, where the photon escape energy for pair production is several GeV (causing a spectral cutoff there). At all but the highest fields there is a prediction that the spectral cutoff energy should be inversely proportional to surface field strength, or $B_0 = 6.4 \times 10^{19} (P\dot{P})^{1/2}$ G for a dipole field at the pole. In fields above $\sim 2 \times 10^{13}$ G, photon splitting, in which a single photon splits into two lower energy photons, becomes the dominant attenuation process and lowers the photon escape energy (Baring & Harding, 2001). The cascade radiation produces a hollow cone of emission around the magnetic pole, with opening angle determined by the polar cap half-angle, θ_{PC} , at the radius of emission r . The polar cap opening angle is very small (a few degrees) unless the emission occurs more than a few stellar radii above the surface. But the pair cascades over most of the polar cap occur within several stellar radii of the stellar surface. Therefore, the wide double-peaked pulses of observed γ -ray pulsars like the Crab, Vela and Geminga, which require beam opening angles of the order of the magnetic inclination angle in this model, cannot be produced unless the pulsar is nearly aligned.

Recently, this seemingly impossible requirement of polar-cap models has been eased somewhat by the realization that emission at the rim of the polar cap will occur at higher altitudes. The height of the CR pair front is within a stellar radius of the neutron-star surface over most of the polar cap. However, near the edge

of the polar cap, at the last open field line which is assumed to be a conducting boundary, the parallel electric field drops to zero. Particles therefore need a longer distance to reach the Lorentz factors necessary to produce pairs, causing the PFF to rise to higher altitude. A slot gap (Arons, 1983) is formed as the PFF turns up to asymptotically approach the last open field line. The pair cascades that form on the edge of the slot gap at altitudes of several stellar radii above the neutron-star surface form a wide hollow cone of high-energy emission (Muslimov & Harding, 2003). Even so, the inclination angles required in this model to reproduce the Crab and Vela profiles are less than $10^\circ - 20^\circ$. This may be at odds with the $\sim 60^\circ$ viewing angle inferred from the *Chandra* image of the Crab nebula (Weisskopf et al., 2000). However, acceleration of primary electrons in the slot gap can continue to high altitudes (Muslimov & Harding, 2004), where the emission may be viewed at larger angles due to the flaring of field lines.

In polar-cap models, surface heating will occur as a result of the screening of the parallel electric field by pairs. Above the pair front, positrons will decelerate and some fraction will turn around and accelerate downward to the neutron-star surface. Because polar-cap heating emission is intimately tied to the pulsar acceleration mechanism, thermal X-ray emission provides very strong constraints on pulsar models. In a space-charge limited flow model, the trapped positrons needed to screen the E_{\parallel} are only a small fraction of the number of primary electrons because this field was created by a small charge imbalance in the first place. The polar-cap heating luminosity is predicted by space-charge limited flow models to be only a few percent of the luminosity of the non-thermal magnetospheric emission, and will fall in the soft X-ray band (Arons, 1981). Recent self-consistent models of polar-cap heating in a space-charge limited flow model (Harding & Muslimov, 2001, 2002) have predicted heating fluxes from positrons trapped at CR and IC pair fronts. The heating from CR pair fronts predicts surface X-ray luminosity

$$L_+^{(CR)} \simeq 10^{31} \text{ erg s}^{-1} \begin{cases} 0.4 P^{-6/7} \tau_6^{-1/7} & \text{if } P \lesssim 0.1 B_{0,12}^{4/9}, \\ 1.0 P^{-1/2} & \text{if } P \gtrsim 0.1 B_{0,12}^{4/9}, \end{cases} \quad (7.2)$$

where τ_6 is the pulsar characteristic age in units of 10^6 yrs. Polar-cap heating may make the dominant contribution to thermal emission from old and middle-aged pulsars. The heating from IC pair fronts, with predicted X-ray luminosity

$$L_+^{(IC)} \simeq 2.5 \times 10^{27} \text{ erg s}^{-1} P^{-3/2} \quad (7.3)$$

can account for thermal emission components detected in the spectrum of some millisecond pulsars.

Polar-cap models predict that emission from the open field line region is visible at all pulse phases. This is because the particles that are accelerated and initiate pair cascades at low altitudes radiate curvature (and possibly inverse Compton) emission at higher altitude on field lines extending to the light cylinder. Such off-pulse emission may have been detected at γ -ray energies by EGRET (Fierro et al., 1998) and at X-ray energies by *Chandra* (Tennant et al., 2001).

7.2.3.2 *Outer-Gap Model*

Outer-gap models (Cheng et al., 1986; Romani, 1996) assume that acceleration occurs in vacuum gaps that develop in the outer magnetosphere, along the last open field line above the null charge surfaces, where the Goldreich-Julian charge density changes sign (see Figure 7.6), and that high-energy emission results from photon-photon pair production-induced cascades. The gaps arise because charges escaping through the light cylinder along open field lines above the null charge surface cannot be replenished from below. Pairs from the polar-cap cascades, which flow out along the open field lines, may pollute the outer gaps to some extent (and vice versa), but this effect has yet to be investigated. The electron-positron pairs needed to provide the current in the outer gaps are produced by photon-photon pair production. In young Crab-like pulsars, the pairs are produced by CR photons from the primary particles interacting with non-thermal synchrotron X-rays from the same pairs. In older Vela-like pulsars, where non-thermal X-ray emission is much lower, the pairs are assumed to come from the interaction of primary particles with thermal X-rays from the neutron-star surface. Some of the accelerated pairs flow downward to heat the surface and maintain the required thermal X-ray emission. The modern outer-gap Vela-type models (Romani, 1996; Zhang & Cheng, 1997) all adopt this picture.

Although there seems to be agreement on the radiation processes involved in the outer gap, the full geometry of the gap is still not solved. Two approaches to such a solution are currently underway, but neither is near to defining the complete three-dimensional gap geometry. One group (Zhang & Cheng, 1997; Cheng et al., 2000) solves the 1D Poisson equation perpendicular to the magnetic field lines, resulting in a gap geometry for young pulsars that is a long, thin sheet bounded below by the last open field line and above by production of pairs. The other group (Hirotani & Shibata, 2001; Hirotani et al., 2003) obtains solutions to the 1D Poisson equation along the magnetic field (assuming a gap width across field lines) and finds that the gap is limited parallel to the field by pair creation. The actual gap geometry is probably somewhere in between. The long narrow outer-gap geometry of Romani & Yadigaroglu (1995) and Cheng et al. (2000), has been successful in reproducing the observed double-peaked pulse profiles for large inclination angles. In these models, the electrons/positrons flowing outward/inward along the last open field line radiate outward/inward from the null surface. The emission forms a wide fan beam which produces in general a wide double-peaked profile, much like the observed Crab profile. The narrow peaks are the result of caustics formed in the observer's frame by the cancelation of the phase shifts from relativistic aberration and light travel time, so that emission from a large range of altitudes is compressed into a narrow phase range. However, due to the fact that no outward emission originates below the null surface, the profile falls off very abruptly at the outer edges (see Figure 7.7) with no leading and trailing or off-pulse emission. The inability to produce trailing and off-pulse emission, as is seen in high-energy pulsar profiles, is thus a serious problem for current outer-gap models. The models of Hirotani & Shibata (2001) and Hirotani et al. (2003) allow external currents to flow through the outer gaps, thus producing a possible extension of the gap below the null surface. In the case of the Crab however, the extent and magnitude of the emission below the null

surface is small and would not produce much off-pulse emission. The formation of the leading peak in double-peaked profiles is also problematic since it requires emission very close to the light cylinder, where the structure of the magnetic field has not been determined.

The spectrum of radiation from the outer gap is a combination of synchro-curvature radiation from pairs inside and outside of the gap and inverse Compton scattering of the synchrotron emission by the pairs. Unlike in polar-cap models, pair production in outer-gap models is essential to the production of the high-energy emission: it allows the current to flow and particle acceleration to take place in the gap. Beyond a death line in period-magnetic field space, and well before the traditional radio-pulsar death line, pairs cannot close the outer gap and the pulsar cannot emit high-energy radiation. This outer-gap death line for high-energy pulsars (Chen & Ruderman, 1993) falls around $P = 0.3$ s for $B \sim 10^{12}$ G. Geminga is very close to the outer-gap death line and recent self-consistent models (Hirotani et al., 2003) have difficulty accounting for GeV γ rays from pulsars of this age. Polar-cap models, on the other hand, predict that all pulsars are capable of high-energy emission at some level, so that detection as a radio-loud high-energy pulsar is thus a matter of sensitivity.

Half of all the particles produced in the outer gaps are accelerated back toward the neutron-star surface and radiate curvature photons that can produce pairs in the strong magnetic field near the surface, initiating pair cascades (Zhang & Cheng, 1997; Wang et al., 1998). But the pairs still have enough residual energy to heat the surface at the footpoints of open field lines that thread the outer gaps. The resulting thermal emission has $T \sim 1$ keV, which is much higher than the thermal emission temperatures observed in pulsars. According to the model, this emission is not observed directly (except right along the poles) but only through the blanket of pairs produced by the downward-going particle cascades. The 1-keV photons are reflected back to the surface by the pair blanket through cyclotron resonance scattering (Halpern & Ruderman, 1993), and are re-radiated from the entire surface at a temperature around 0.1 keV. Thus, these outer-gap models predict three X-ray emission components: hard thermal emission from direct heating of the polar caps (seen only along the poles), soft thermal emission reflected from the pair blanket, and non-thermal emission from the downward pair cascades (Cheng & Zhang, 1999). The components actually observed from a particular pulsar depend on inclination and viewing angle. The predicted X-ray luminosities for pulsars in the *ROSAT* band can account for the observed $L_x = 10^{-3}\dot{E}$ relation.

7.2.4 *It's The Geometry...*

Theoreticians have spent years building pulsar emission models by starting from the fundamental electrodynamics of the particle acceleration and radiation processes, predicting observable pulsar characteristics from the bottom up. This has had some success, but both polar-cap and outer-gap models as currently formulated also have some basic, unresolved problems. Ultimately, it is the emission geometry required by the observations, which tells us the distribution of radiating particles, that will drive us to the correct understanding of pulsar high-energy emission.

Putting together the results of a number of attempts, in different types of models, to reproduce the narrow and often double-peaked pulse profiles of high-energy pul-

sars, one common thread seems to emerge. Nearly all successful geometrical models of pulsar high-energy emission have assumed enhanced particle acceleration and radiation along the last open field lines of a magnetic dipole. In their polar-cap emission model, Daugherty & Harding (1996) were led to assume strongly enhanced particle flow on the rim of the polar cap. Acceleration in the slot gap along the polar-cap rim later provided a physical basis for this idea (Muslimov & Harding, 2003). The outer-gap models of Romani & Yadigaroglu (1995) and Cheng et al. (2000) assumed acceleration and emission essentially only along the last open field line between the null charge surface and the light cylinder in a thin outer gap. But these models cannot produce the non-thermal off-pulse emission seen through the whole pulse phase of the Crab optical and Vela and Geminga γ -ray profiles. Very recently, Dyks & Rudak (2003) have explored a purely geometrical emission model, known as the “two-pole caustic” model in which they assume that particles radiate all along the last open field lines of both poles, from the neutron-star surface to the light cylinder (see Figure 7.6). Taking into account relativistic effects of aberration and light travel time, the phase shifts of photons emitted at different altitudes along the trailing edge of the polar open field line region cancel, so that the emission in the observers frame is compressed into a small range of phase, forming a caustic peak in the profile. The caustic peaks in the two-pole caustic model have the same origin as the caustic peaks that form from outward emission above the null charge surface in the outer-gap models. What makes the two-pole caustic model fundamentally different is the addition of outward emission below the null surface, that allows an observer to view caustic emission from both poles as the neutron star rotates past, in contrast to outer-gap models where an observer can view high-energy emission from only one pole. The resulting profiles for viewing angles crossing caustics from both poles are astonishingly similar to the observed profile of the Crab (see Figure 7.7) and several other high-energy pulsars, and seems to do better than most of the other ‘bottom-up’ models in reproducing the observed geometry. This seems to be telling us that both conventional polar-cap and outer-gap models are missing something critical in their description of the basic electrodynamics. Recently, Muslimov & Harding (2004) have shown that high-altitude radiation from the slot gap could form a physical basis for the two-pole caustic model, producing very similar profiles.

The geometry of emission at different wavelengths is also different in various models. In polar-cap models, the high-energy and radio emission are physically connected, since the electron-positron pairs from the polar-cap cascades are thought to be a necessary ingredient for coherent radio radiation. However, the relative geometry of the two emission regions is not very constrained by observation. Models for radio emission morphology (Rankin, 1993; Lyne & Manchester, 1988) consist of core and conal components, emitted within a distance of about 10-100 stellar radii from the surface. If the polar-cap high-energy emission cone occurs at a lower altitude than the radio emission, as would be expected, then the leading edge of the radio cone would lead the first high-energy peak. The trailing edge of the radio conal emission would then have to be undetected in the *CGRO* pulsars. This type of radio geometry for young pulsars was suggested by Manchester (1996) and a class of pulsars with one-sided radio conal emission was proposed by Lyne & Manchester (1988). This

picture has recently received some observational support by Crawford et al. (2001) and Crawford & Keim (2003).

High-energy emission in the outer gap is generally radiated in a different direction from the radio emission, which allows these models to account for the observed phase offsets of the radio and high-energy pulses. At the same time, there will be fewer radio-high-energy coincidences and thus a larger number of radio-quiet high-energy pulsars. In the Romani & Yadigaroglu (1995) geometrical outer-gap model, the observed radio emission originates from the magnetic pole opposite to the one connected to the visible outer gap. Many observer lines-of-sight miss the radio beam but intersect the outer-gap high-energy beam, having a much larger emission solid angle. When the line-of-sight does intersect both, the radio pulse leads the high-energy pulse, as is observed in most γ -ray and some X-ray pulsars.

In the two-pole caustic model of Dyks & Rudak (2003), trailing-edge radio conal emission would arrive in phase with the high-energy emission due to the fact that emission from a wide range of altitudes is compressed into a narrow phase range to form the caustic. This may be a nice explanation for why the radio and high-energy emission tends to be phase-aligned in some of the fastest rotators, such as the Crab and the millisecond pulsars.

7.2.5 *Polarization Properties*

Phase-resolved polarimetry of rotation-powered pulsars has had enormous diagnostic capability at radio and optical wavelengths and could also be a powerful diagnostic in the X-ray range. Several X-ray polarimeters are planned for the near future (AXP, POGO and MEGA) which could measure X-ray polarization characteristics of the brightest sources, such as the Crab pulsar, Cyg X-1 and Her X-1. The pulsed non-thermal radiation from relativistic particles in the magnetosphere is tightly beamed along the neutron-star magnetic field lines and thus the emitted radiation is believed to be highly polarized either parallel or perpendicular to the field lines. Since the field well inside the speed of light cylinder rotates as a solid body with the star, measurement of the polarization properties as a function of pulse phase can provide a multidimensional mapping of the pulsar emission. The expected signature of emission near the poles of a dipole field, an ‘S’-shaped swing of the polarization position angle through the pulse profile (Radhakrishnan & Cooke, 1969), has been seen from many radio pulsars and has generally been taken as proof that the radio emission originates from the open field lines of a magnetic dipole.

The different high-energy emission models share the common emission mechanisms of curvature, synchrotron and inverse Compton radiation from highly relativistic particles, albeit in very different locations. These mechanisms all intrinsically produce highly polarized radiation (up to 70%, depending on the particle spectrum). Each of the models predicts a distinct variation of position angle and degree of polarization across the pulse profile. Figure 7.7 shows simulations of expected position angle and percent polarization as a function of pulse phase for outer-gap and polar-cap models of the Crab pulsar. Simulations are also shown for the two-pole caustic model (Dyks & Rudak, 2003). The predicted position-angle swing in the polar cap model shows the classic S-shaped pattern of the rotating vector model since the observer is sweeping near the magnetic pole (phase 0). The most rapid change in position angle

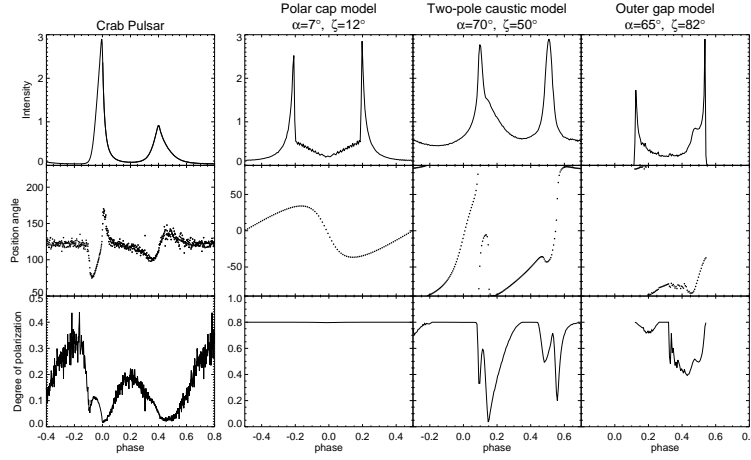


Fig. 7.7. Pulse profiles, polarization position angle and degree of polarization as a function of pulse phase for the Crab pulsar. The left panel the observed optical pulse profile and polarization characteristics as measured by OPTIMA (Kellner, 2002). The right-hand panels are predicted profiles and corresponding polarization characteristics of the polar-cap, two-pole caustic and outer-gap model geometries (Dyks et al., 2004).

occurs near the magnetic axis and there is no predicted decrease in degree of polarization. The two-pole caustic model predicts rapid swings of position angle through the peaks, due to the large change in field orientation, as the viewing angle sweeps past the pole (phase 0) and approaches the trailing edge field line that is the origin of the caustic peaks (Dyks et al., 2004). There is also a predicted decrease in percent polarization on the trailing edges of the peaks, as the observer is viewing emission in the caustics and from rotationally distorted field lines near the light cylinder that fold back and overlap. The outer-gap model (Romani & Yadigaroglu, 1995) predicts position angle swings through the peaks, though they are smaller and occur only for carefully selected combinations of inclination and viewing angle (Dyks et al., 2004). There would also be a predicted dip in degree of polarization, now primarily at the second peak, since the second peak in the outer-gap model originates from the same caustic that is the origin of the dips at both peaks in the two-pole caustic model. The signature of caustic emission is thus a dip in the percent polarization and a rapid swing of the position angle at the pulse peak. A recent measurement by OPTIMA (Kellner, 2002) of optical polarization position angle and degree of polarization as a function of pulse phase for the Crab pulsar exhibits sharp swings in position angle in the peaks and dips in degree in polarization just following each peak. There appears to be a constant, unpulsed background component (at about 120° position angle and 30%) which if subtracted from the data, best matches the predictions of the two-pole caustic model.

7.3 Thermal Emission from Cooling Neutron Stars

7.3.1 Motivation and Background

The existence of magnetospheric emission from neutron stars, as described in §7.2, came as an observational surprise to neutron-star theorists. By contrast, not long after the existence of neutron stars was proposed (Baade & Zwicky, 1934), it was also pointed out that such a star would form hot, with surface temperatures over 10^6 K, and that surface emission might be detectable (Zwicky, 1938). The discovery of cosmic X-ray sources in the 1960's provided hope that neutron stars might one day be observable, and detailed modeling of their potential observational properties began (Morton, 1964; Tsuruta, 1964). Bahcall & Wolf (1965) pointed out that the equation of state of matter at densities comparable to those in atomic nuclei, which cannot be studied in terrestrial laboratories, might be constrained by observations of neutron-star cooling. This is because the magnitude of the stellar neutrino luminosity, which, in the early history of the neutron star, should far exceed that of the photon luminosity, should depend strongly on what species are present in the core, and on how they interact. Prodigious neutrino emission would result in more rapid cooling than photon cooling alone. Studying neutron-star cooling began in quantitative earnest with the computation of the first cooling curves (Tsuruta & Cameron, 1966).

The first actual detections of thermal emission from the surfaces of neutron stars came much later, following the launch of the *Einstein* (Helfand et al., 1980; Harnden et al., 1985; Matsui et al., 1988) and *EXOSAT* (e.g. Brinkmann & Ögelman, 1987) X-ray observatories in the 1980's. The situation pre-1990's was reviewed by Tsuruta (1986). The launch of *ROSAT* in 1990 heralded the next major progress (e.g. Finley et al., 1992; Ögelman et al., 1993; Halpern & Ruderman, 1993), with important contributions made by *ASCA* (e.g. Halpern & Wang, 1997; Zavlin et al., 1998) as well. By 1997, four *bona fide* detections of thermal emission from young or middle-aged pulsars had been reported (from PSRs B0656+14, B0833–45, B1055–52, and the Geminga pulsar) along with interesting upper limits (see Becker & Trümper, 1997, and references therein). The recent launches of the *Chandra* and *XMM-Newton* observatories have already yielded important results (e.g. Pavlov et al., 2001; Marshall & Schulz, 2002; Kargaltsev et al., 2002; Sanwal et al., 2002b; Bignami et al., 2003). Recent reviews of relevant observations include Becker & Pavlov (2002); Pavlov et al. (2002b); Pavlov & Zavlin (2003). Recent reviews of theory include Tsuruta (1998), Page (1998), and Yakovlev et al. (1999).

As discussed in §7.2, thermal emission can also be produced as a byproduct of emission processes in the magnetosphere. Such emission is believed to be unrelated to that originating from initial cooling. Other heating mechanisms are predicted to matter only in the photon-cooling era, i.e. for $t > 10^6$ yr (e.g. Alpar et al., 1984; Umeda et al., 1993; van Riper et al., 1995; Larson & Link, 1999). One notable exception are magnetars, in which the decay of the field is thought to provide a major energy source that dominates over all others (see chapter 14).

7.3.2 Theory of Neutron Star Cooling

Neutron stars are born in the violent collapse of stars having ZAMS mass $\sim 8\text{--}20 M_\odot$, which have core temperatures prior to collapse of $T_c \sim 10^9$ K. Following collapse, it is expected that the neutron star forms with central temperature $T_c \sim 10^{11}$ K, although prodigious neutrino emission results in $T_c \sim 10^9 - 10^{10}$ K within a day or so. Neutrino emission dominates over photon emission until $T_c \sim 10^7 - 10^8$ K (depending on leading neutrino emission process), which is reached at least $\sim 10^3$ yr, and more likely $\sim 10^5 - 10^6$ yr after birth. The thermal behavior before 10^6 yr depends strongly on cooling model. After $t \simeq 10^6$ yr, various internal and external heating mechanisms dominate thermal emission over the initial cooling. Therefore, young, i.e. having age $\lesssim 10^6$ yr, neutron stars for which the surface temperatures T_s are expected to drop either slowly or quickly from $T_s \sim 2 \times 10^6$ to $\sim 2 \times 10^5$ K, with core temperatures dropping from $T_c \sim 10^9$ to $10^7 - 10^8$ K, are interesting targets for studies of neutron-star interior physics. Note that in spite of these apparently high temperatures, from a statistical mechanics point of view, neutron stars can be considered to be at $T = 0$, since for their average densities, the Fermi energy is $\sim 100 - 500$ MeV, while the internal temperature of a one-year old star is certainly below 0.1 MeV. Next we consider in turn the main elements that determine how a neutron star cools.

7.3.2.1 The Stellar Core

During the first $\sim 10^5 - 10^6$ yr, a neutron star cools mainly via neutrino emission from its innermost regions (which have densities $\rho \gtrsim 10^{10} \text{ g cm}^{-3}$). For ages $t \gtrsim 10 - 50$ yrs, the internal layers are isothermal. They have an enormous density gradient which results in different neutrino emissivities at different radii. As a rule, the most efficient neutrino emission is produced in a stellar core, which extends from $\rho \approx \rho_0/2$ to the stellar center $\rho \sim (3 - 15) \rho_0$. Here, $\rho_0 \approx 2.8 \times 10^{14} \text{ g cm}^{-3}$ is the density of nuclear matter in atomic nuclei. The composition and equation of state of supranuclear matter ($\rho \gtrsim 2 \rho_0$) in neutron-star cores are largely unknown but are of considerable interest to basic physics.

The main cooling mechanism in the core is neutrino emission via the “Urca” process*. In its simplest version adopted for neutron-star cores, the Urca process is a sequence of a β -decay and an electron capture, $n \longrightarrow p + e + \bar{\nu}_e$, and $p + e \longrightarrow n + \nu_e$. This is the so-called direct Urca process (Lattimer et al., 1991). However, to proceed at interesting rates in the neutron-star interior for a wide range of expected interior properties, the Urca process requires a spectator reactant to simultaneously conserve energy and momentum. The process with the spectator is called the “modified” Urca process (Chiu & Salpeter, 1964). Neutrons, protons, and other baryon spectators greatly suppress the direct Urca rate (typically, by 5–7 orders of magnitude) because of the lack of phase space due to degeneracy. The most efficient direct Urca cooling, without any spectator, is possible if the proton fraction is sufficiently high. This may happen in the cores of sufficiently massive stars. If hyperons are present in the core, they initiate additional direct Urca processes (Prakash et al., 1992), as

* Urca is the name of a long-since-closed casino in Rio de Janeiro, and was adopted as a name for these reactions by Gamow & Schoenberg (1941) who saw a parallel between how casinos extract money from players and how nature extracts energy in these reactions.

efficient (or nearly as efficient) as the basic direct Urca process with nucleons. If the direct Urca process is forbidden (e.g., if the proton fraction is insufficiently high) but the dense matter contains pion or kaon condensates, weaker processes similar to the direct Urca ones (though stronger than the modified Urca ones) can open (see, e.g. Pethick, 1992, for a review).

7.3.2.2 Equation of State

An equation of state (EOS) is the pressure-density-temperature relationship of matter. In a neutron star, most of the mass is at densities two or three times ρ_0 (the nuclear matter density). At these densities, the EOS is unknown. Nuclear physics can constrain some aspects of the high-density EOS, however certain fundamental parameters, such as the compression modulus, the bulk symmetry energy and the effective nucleon mass remain weakly constrained (Lattimer, 1992; Lattimer & Prakash, 2001). The EOS is crucial to understanding neutron-star structure; it determines, among other things, the mass-to-radius relationship, the stellar binding energy, the stellar moment of inertia and the relative moments of different components, the minimum and maximum masses, and the maximum angular velocity. From a cooling point of view, the most important parameters determined by the EOS are the density, pressure and temperature profiles of the star, as well as its composition. The profiles are important because, for example, the location, amount and type of superfluidities present depend on the density profile, via a critical temperature/density relation (see §7.3.2.3). The composition is important as different species of particles will react differently.

Many EOSs have been proposed, and the range of possible properties of neutron-star matter is large. For example, the range of predicted pressure of matter having density twice ρ_0 is approximately a factor of five, depending on the choice of plausible EOS, where plausible means consistent with available laboratory data on atomic nuclei and nucleon scattering (Lattimer & Prakash, 2001). Phase transitions to kaon, pion or hyperon-rich matter are all possible depending on the core density.

Figure 7.8 (left) shows predicted cooling curves for a commonly (e.g. Yakovlev et al., 2001) assumed core EOS (originally from Prakash et al., 1988) for three different masses. Curves for $M < 1.35 M_\odot$ are very similar to that for $M = 1.35 M_\odot$. Above this mass (to be more exact, above $1.358 M_\odot$), for this EOS, direct Urca cooling sets in; this is clear in the curves. Also shown in the Figure are two schematic curves assuming a pion condensate (but no direct Urca if the pion condensate were absent) in the core at $M > 1.35 M_\odot$. The effect is clearly enhanced cooling, but not as much as for direct Urca.

7.3.2.3 Superfluidity and Superconductivity

Proton and neutron superfluidity in the neutron-star interior can play a very significant role in cooling. (Note that proton superfluidity means superconductivity.) This is because it suppresses traditional neutrino processes involving nucleons. On the other hand, it produces a specific type of neutrino emission (Flowers et al., 1976) associated with Cooper pairing of nucleons. Superfluidity also affects nucleon heat capacity. However, its onset, determined by a critical temperature, is very poorly known at neutron-star densities. Overall, superfluidity in different forms can mimic

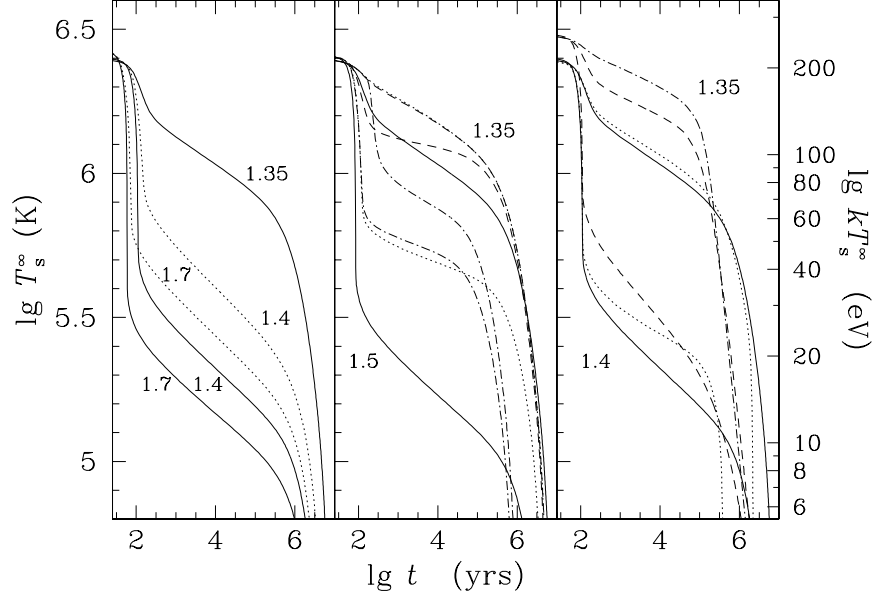


Fig. 7.8. Neutron-star cooling curves for a variety of parameters and models (courtesy D. Yakovlev). All curves are for EOS “A” of Yakovlev et al. (2001), or “model I” of Prakash et al. (1988) with compression modulus of saturated nuclear matter 240 MeV. Left: Curves for non-superfluid stars for three masses (labelled in solar masses) are shown with solid lines. Dotted lines are for pion condensate in the core, for 1.4 and 1.7 M_{\odot} stars (see §7.3.2.2). Middle: Curves for superfluid neutron stars of masses 1.35 and 1.5 M_{\odot} . Four curves are shown for each mass: solid curves are for non-superfluid stars (as in the left plot); dotted curves are for proton superfluidity model “1p” of Kaminker et al. (2002); dashed curves are for proton superfluidity model “2p” of the same reference; dot-dashed curves are for the combination of proton superfluidity model “p1” and neutron superfluidity model “3nt,” also from Kaminker et al. (2002). Note that the 1p and 2p curves for the 1.35 M_{\odot} star coincide as both suppress modified Urca cooling. Also, note that the 2p curve for the 1.5 M_{\odot} star sits among the 1.35 M_{\odot} star curves. Right: Curves for non-superfluid stars for masses 1.35 and 1.4 M_{\odot} for different accreted envelope masses and dipolar magnetic fields: solid curves are for zero accreted mass and zero magnetic field B (as in the left plot); dotted curves are for $B = 10^{14}$ G at the pole; dashed curves are for $B = 0$ and accreted envelope mass $10^{-7} M_{\odot}$. The dot-dashed curve is for a 1.35 M_{\odot} solar mass star having $B = 0$ and accreted envelope mass $10^{-7} M_{\odot}$, but with proton superfluidity included. It is shown to demonstrate the approximate upper bound for temperatures of neutron stars having ages between ~ 1 and ~ 100 kyr.

enhanced cooling, challenging the promise of using cooling to determine the EOS. See Kaminker et al. (2002) and Yakovlev et al. (2002, 2004) for recent reviews of the subject.

The relevance of superfluidity can be summarized as follows. In very low-mass

stars ($M \lesssim 1.35 M_\odot$ for the EOS assumed here), the effect of core singlet-state (1S_0) proton superfluidity is well determined and nearly independent of mass or EOS. These stars cool very slowly as even modified Urca processes are suppressed, so that nucleon-nucleon bremsstrahlung, a slower process, dominates. The hottest young neutron stars are therefore plausibly explained as having the lowest mass. On the other hand, for very high-mass neutron stars ($M \gtrsim 1.5 M_\odot$), proton superfluidity becomes inefficient, and one expects very rapid, model-independent cooling, because direct Urca is too strong to be suppressed. A neutron star that has cooled so rapidly has not yet been observed (see §7.3.4).

For intermediate-mass neutron stars, the situation is highly model dependent, and by assuming an EOS and proton superfluidity model, one can, at least in principle, use observed surface temperatures to determine neutron-star masses (e.g. Yakovlev et al., 2001). In these stars, direct Urca processes would proceed unimpeded were it not for moderate proton superfluidity suppression. Figure 7.8 (middle) shows two different models for proton superfluidity (see Kaminker et al., 2002, and references therein for definitions). Mild 3P_2 pairing of neutrons in the stellar core results in very strongly enhanced cooling of stars with $M \lesssim 1.35 M_\odot$ (Figure 7.8, middle) that is inconsistent with the observations thus far (see §7.3.3).

7.3.2.4 The Stellar Envelope: Composition and Magnetic Field

Interpreting observed thermal emission from neutron stars means mapping the observed surface temperature T_s to that of the stellar core T_c . The temperature gradient from the surface inward is mainly in the stellar envelope, the layer beneath the atmosphere down to the isothermal internal region which effectively acts as a thermal insulator for the bulk of the star. The insulating envelope is commonly defined as the region having density $\rho \lesssim 10^{10} \text{ g cm}^{-3}$. This has thickness only a few tens of metres, much smaller than the stellar radius. The insulating envelope thickness decreases as the star cools.

For envelopes made of iron, for $T_s \simeq 10^6 \text{ K}$, $T_c \simeq 10^8 \text{ K}$ with $T_s \approx T_c^{1/2}$ for a typical surface gravity (Gudmundsson et al., 1983). However, the mapping is highly sensitive to envelope composition. Chabrier et al. (1997) show that even a tiny ($\sim 10^{-13} M_\odot$) amount of accreted light-element matter, such as from fallback after the supernova, from the interstellar medium or from a binary companion, can have a substantial effect on T_s for a given T_c . Specifically, accreted envelopes have lower thermal conductivity. As a consequence, they lead to higher T_s in the neutrino-cooling era but lower T_s in the photon-cooling era. Figure 7.8 (right) shows the effect of an accreted envelope on predicted cooling curves of two different mass neutron stars.

The magnetic field in the envelope can also play a major, though complicated, role (van Riper & Lamb, 1981; Page, 1995; Shibano & Yakovlev, 1996; Heyl & Hernquist, 1997; Potekhin & Yakovlev, 2001; Heyl & Hernquist, 2001). A magnetic field affects all plasma components, especially the electrons. In particular, electron motion perpendicular to the field lines becomes suppressed by classical Larmor rotation. In addition, this motion is quantized in Landau levels. Classical and quantum effects greatly modify the electron thermal and electrical conductivities. Thus the effect of a magnetic field on the thermal structure of the insulating envelope depends strongly

on the field geometry, with radial fields effectively reducing the insulation by the envelope (quantum effect), and fields tangential to the surface increasing it (classical effect). Thus a dipolar field will have a very different effect than an (often assumed) radial field (see Potekhin & Yakovlev, 2001, for a review), with the tangential and radial regions potentially cancelling local deviations when averaging over the surface (Page, 1995; Shibano & Yakovlev, 1996; Potekhin & Yakovlev, 2001; Heyl & Hernquist, 2001; Potekhin et al., 2003). Figure 7.8 (right) shows the effect of a dipolar magnetic field of 10^{14} G (at the pole) on cooling curves for two different masses. Curves for 10^{12} G are close to the zero field case. The net effect is clearly much more subtle than for light elements, mass, or EOS. Note that the above consideration assumes to active magnetic field decay of the type invoked in the “magnetar” model (see Chapter 14).

7.3.2.5 The Stellar Atmosphere

The neutron-star atmosphere, defined as the region having density $\rho \lesssim 10^2 \text{ g cm}^{-3}$, is typically only 0.1–10 cm thick, yet ultimately determines many of the properties of the emerging thermal photon flux. Although in studying thermal radiation the assumption of a blackbody spectrum is often made, every realistic atmosphere model predicts a significant deviation from a Planckian curve. The nature and degree of the deviation, both from the continuum and in the form of lines (see §7.3.3.4) depends strongly on atmospheric composition as well as on magnetic field. A nice review of this subject is given by Zavlin & Pavlov (2002). We summarize the basic issues below.

An unadulterated neutron star might be expected to have an iron atmosphere, in keeping with the pre-collapse composition of the progenitor core. Heavy-element spectra, with even tiny (i.e. $\sim 0.05\%$) metallicities, are expected to contain many spectral features and photoionization edges produced by ions at various stages of ionization (Romani, 1987; Rajagopal & Romani, 1996; Zavlin et al., 1996; Rajagopal et al., 1997). However, blurred to lower resolution, a heavy-element atmosphere resembles a blackbody of comparable effective temperature. Figure 7.9 shows sample atmospheres containing different metal abundances, for comparison with a blackbody spectrum.

On the other hand, a spectrum emerging from a light-element (H or He) atmosphere is predicted to have few absorption lines at X-ray energies (e.g. Ho et al., 2003) – in fact none if the atoms are fully ionized, apart from cyclotron lines. Nevertheless, such an atmosphere has a clear signature: a high-energy tail in the spectrum, resulting in a significant overestimate, by as much as a factor of ~ 3 , of the surface temperature if a blackbody model is fitted instead (see Fig. 7.9; Romani, 1987; Rajagopal & Romani, 1996; Zavlin et al., 1996). For example, fitting a blackbody model to the X-ray spectrum of the Vela pulsar yields $kT_s^\infty = 127 \text{ eV}$, versus $kT_s^\infty = 59 \text{ eV}$ for a hydrogen atmosphere (Pavlov et al., 2001). Also, blackbody fits to hydrogen atmosphere spectra yield emitting radii that are much smaller from those inferred with hydrogen atmosphere models; for example, Marshall & Schulz (2002), as revised by Briskin et al. (2003b), find $R^\infty = 156 \text{ km}$ and 8.5 km for hydrogen and blackbody fits to the X-ray spectrum of PSR B0656+14, respectively. The high-energy tail is produced because light-element opacities decrease rapidly

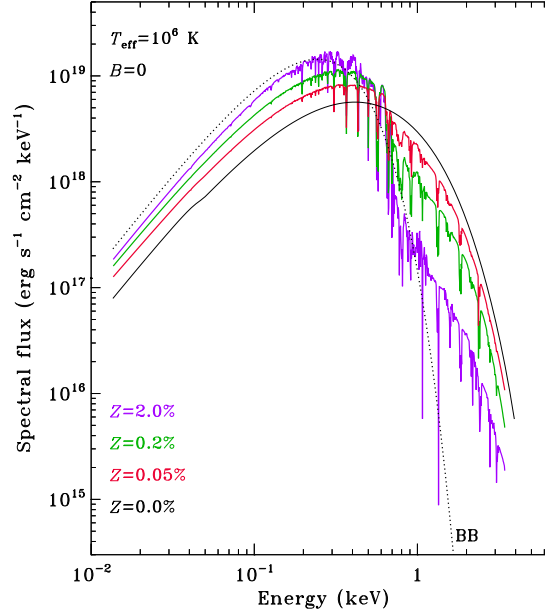


Fig. 7.9. Spectra of emergent radiation in non-magnetic neutron star atmospheres having $T_{\text{eff}} = 10^6$ K for different metallicities Z ($Z = 2.0\%$ corresponds to solar metallicity.) The corresponding blackbody is shown with a dotted line. From Zavlin & Pavlov (2002).

with increasing energy, so that at higher energies one is observing deeper layers of the star which are at higher temperatures. Although an unadulterated neutron star should have an iron atmosphere, even tiny amounts (e.g. $10^{-20} M_{\odot}$) of accreted interstellar material should result in a pure hydrogen atmosphere, because of the short time scale for gravitational settling.

As in the envelope, an appreciable magnetic field can also have a major influence on the atmosphere. The most important issue is the huge difference that exists between the opacities for different polarizations. Specifically, the magnetic atmosphere is much more transparent to photons with electric-field vector perpendicular to the $\mathbf{k} \cdot \mathbf{B}$ plane than is a non-magnetic atmosphere. Thus, the emergent radiation is expected to be highly polarized (see §7.3.3.3). Furthermore, the emergent flux depends on the direction of the magnetic field; hence for non-radial field geometries pulsations are expected even for uniform temperature (which is, in any case, implausible, since variations in surface magnetic field strength result in temperature variations).

For magnetic field strengths greater than a quantum critical field $B_Q \equiv 2\pi m_e^2 c^3 / (eh) = 4.414 \times 10^{13}$ G, so-called “vacuum polarization,” that is the effective dielectric constant of the vacuum, must be accounted for in the radiative transfer equations, given the plasma densities in the envelope. This is interesting physically as, in spite of being predicted by QED theory, this effect has not been confirmed experimentally. The net effect of vacuum polarization is to soften the high-energy tail of the hydrogen spectrum, though the emission is still harder than the blackbody spectrum of the

same effective temperature (Ho & Lai, 2001; Özel, 2001; Zane et al., 2001; Lai & Ho, 2002; Ho & Lai, 2003; Özel, 2003; Lai & Ho, 2003).

7.3.3 Determinations of Neutron-Star Temperatures and Ages

7.3.3.1 Measuring Neutron-Star Temperatures

There are several challenges to measuring neutron-star temperatures. First, the temperature measured by a distant observer T_s^∞ is not that at the neutron star surface T_s . This is due to gravitational redshifting; the two are related via $T_s^\infty = T_s[1 - 2GM/(Rc^2)]^{1/2}$. Here, R is a circumferential neutron-star radius (which determines the proper length $2\pi R$ of the stellar equator). Similarly, the stellar luminosity as measured by a distant observer is given by $L_\gamma^\infty = 4\pi\sigma T_s^4 R^2[1 - 2GM/(Rc^2)]$, where the γ specifies that this is the bolometric photon (as opposed to neutrino) luminosity. The apparent radius which would be measured by a distant observer if the latter could resolve the star is $R^\infty = R/[1 - 2GM/(Rc^2)]^{1/2}$. Thus the determination of T_s from T_s^∞ requires knowledge of M/R , which is unknown, and which depends on the unknown EOS in the stellar core for any M or R that could be determined independently.

Particularly problematic in the pre-*Chandra* era is that young neutron stars that are pulsars with high \dot{E} are ubiquitously associated with pulsar wind nebulae (see §7.6). These extended sources surround the neutron star and contaminate measurements of the thermal emission from the point source. Also, sources with high \dot{E} produce copious non-thermal X-rays from magnetospheric processes (see §7.2). This emission, for example, completely overwhelms any thermal emission from the very young Crab pulsar, hence the availability of only an upper limit on its thermal emission, obtained off-pulse (Table 7.2). Mitigation of both the above problems is best done by avoiding high \dot{E} sources, even though they are often the youngest and hottest (see §7.4).

An additional important difficulty is the degeneracy between the equivalent neutral hydrogen absorption toward the source, N_h , and the measured temperature. For an absorbed blackbody-like spectrum, the low-energy exponential cutoff due to N_h results in higher inferred T_s^∞ for smaller N_h , and vice versa. Generally it is necessary to constrain T_s^∞ via a contour plot in the T_s^∞/N_h plane (e.g. Halpern & Wang, 1997; Zavlin et al., 1999), although frequently authors quote T_s^∞ for only a single assumed N_h (see Table 7.2).

7.3.3.2 Hot Spots and Cyclotron Resonance Scattering

In many instances (see Table 7.2 and §7.5), the effective radius of the star as determined by either a blackbody or an atmosphere spectral fit is much smaller than the expected radius of a neutron star, regardless of assumed EOS. In at least one case, RX J1856.5–3754, this has led to claims that the thermal spectrum therefore implies the target is not a neutron star at all, but a quark star (Drake et al., 2002).

However, localized backheating of a neutron star surface by relativistic electron/positron pairs formed from conversion of γ -rays produced in the magnetosphere in the polar-cap or outer-gap accelerators (see §7.2) can produce “hot spots” which emit thermal radiation. Such hot spots have areas much smaller than the stel-

lar surface and could in principle outshine surrounding thermal emission from initial cooling, thereby dominating the X-ray spectrum. This is the case for the thermal emission detected from millisecond pulsars (e.g. PSRs J0030+0451, J0437–4715, J2124–3358; see e.g. Becker, 2001, for a review), which have ages of $\sim 10^9$ yr hence should have cooled long ago. When hot spots dominate, studying thermal emission is mainly constraining the physics of the magnetosphere, although upper limits on initial cooling emission could still be interesting. For example, the Vela pulsar is a strong γ -ray source, yet a very faint thermal X-ray source (see Tables 7.1 and 7.2); magnetospheric-acceleration-driven hot spots may well dominate the thermal spectrum, but its low effective temperature is still interesting (see Fig. 7.11). Thus, measured temperatures that are associated with small emitting areas are most conservatively taken to be upper limits on cooling temperatures.

Although one might expect stars with hot spots to have higher pulsed fractions than those without, this is not necessarily the case due to strong gravitational light bending expected in neutron stars (see §7.3.3.3). This and a less-than-favourable viewing angle can significantly reduce the pulsed fraction seen from a star with hot spots, as has been argued for RX J1856.5–3754 (e.g. Ransom et al., 2002). The detection of a bow-shock H α nebula around this source supports it being an off-beam rotation-powered pulsar (see 7.5; van Kerkwijk & Kulkarni, 2001). The same is true of other “isolated neutron stars” (see §7.4) as well as of the “central compact objects” (see §7.5).

Ruderman (2003) has argued that cyclotron-resonance scattering of thermal photons by electrons and positrons within a few stellar radii of an energetic rotation-powered pulsar results in a Planck-like X-ray spectrum that is quite changed from the seed thermal spectrum. A pair plasma is thought to surround the star, maintained by conversion of γ -rays from the star’s polar-cap and/or outer-gap accelerators. This is because a thermal X-ray photon’s energy, ~ 1 keV, is less than the cyclotron resonance energy at the stellar surface, $eB\hbar/2\pi mc = 11.6$ keV for $B = 10^{12}$ G. Thus, as the photon passes through the magnetosphere, it goes through a resonance, and the optical depth to cyclotron-resonance scattering becomes large. Ruderman (2003) describes the situation as if the X-rays are reflected back from the surface of a “lightly leaky *Hohlraum* container” and only escape after multiple reabsorptions and re-emissions from the stellar surface. Thus, he argues, measurements of thermal emission from neutron stars teach us only about the stellar magnetosphere, not about initial cooling.

7.3.3.3 Pulsations and Polarization from Thermally Cooling Neutron Stars

The pulsations from the surface of a cooling neutron star have low pulsed fraction and low harmonic content. This is in strong contrast to the high harmonic content and pulsed fractions seen from the magnetospheric component of the emission, which is presumed to be produced well above the stellar surface (see §7.2). Often young neutron stars exhibit emission from both mechanisms, as is clear from the energy dependence of their light curves (e.g. Fig. 7.5).

The low harmonic content results primarily from the presumably low variation of temperature over the neutron-star surface. However, pulsations are further reduced by the strong gravitational bending of light near the surface of the neutron star (e.g.

Page, 1995; Psaltis et al., 2000). This becomes important as the general relativistic compactness parameter $p \equiv Rc^2/2GM \rightarrow 1$ (a Newtonian star is described by $p \rightarrow \infty$). Due to bending, although the observer may be facing one side of the neutron star, she/he may still detect significant emission from the opposite side. Simulations of well defined infinite contrast spots on neutron stars show that the effect is so strong that even for $p = 4$, the maximum pulsed fraction is less than 0.4 for *any* size emitting spot (Psaltis et al., 2000).

Measured temperature is expected to be dependent on pulse phase, as the thermal conductivity of the neutron-star surface depends on the magnetic field strength, which varies over the surface (Page, 1995; Psaltis et al., 2000). However, generally, only phase-averaged temperatures are measured, both because of faint signals, and also because gravitational light bending makes it difficult to do otherwise. Clearly this complicates the interpretation since the averaged value depends on the distribution of temperature over the surface. However, this effect is likely to be small compared to other systematic effects.

X-ray emission from the surface of a cooling neutron star endowed with a magnetic field at the surface of magnitude $\gtrsim 10^{11}$ G is expected to be significantly polarized. This is because atmospheric opacities depend strongly on polarization when the photon energies are much smaller than the electron cyclotron energy. The opacity to light with its electric field vector oriented perpendicular to the magnetic field is smaller by a factor of approximately the squared ratio of the photon energy to the cyclotron energy, if the ratio is small, relative to that for light with electric-field parallel to B (Lodenqual et al., 1974). Thus, radiation with electric-field vector perpendicular to B escapes from greater atmospheric depths where the temperature is higher, hence results in a higher flux. Polarizations from localized regions on the surface should be very high, $\gtrsim 50\%$ (Kanno, 1975; Pavlov & Shibano, 1978). However, an observer sees radiation averaged over a hemisphere, and even beyond due to gravitational light bending, which is strongest for large M/R . This will reduce the observed polarization fraction (e.g. Pavlov & Zavlin, 2000). Similarly, the different magnitudes and directions of the lines of a dipolar B field at the neutron-star surface might be thought to reduce polarization (Pavlov & Zavlin, 2000). However, the QED effect of vacuum polarization, in which the region surrounding the star is effectively birefringent, has recently been shown to counteract the GR and varying B -field effects, because the observed polarization direction of rays from the surface is correlated with the B -field direction far from the surface; a ray bundle that we observe passes through only a small B -field solid angle as it leaves the magnetosphere (Heyl & Shaviv, 2002). This results in very large net polarizations as a function of pulse phase, and even phase-averaged polarization fractions of $\sim 10 - 20\%$ (Heyl et al., 2003; Lai & Ho, 2003). Measurement of polarization light curves should thus allow sensitive constraints on the B field, as well as on M/R and the magnetic geometry of the neutron star. Hence, thermally cooling neutron stars and magnetars (Chapter 14) are expected to be very interesting targets for future X-ray polarimetry experiments.

7.3.3.4 Features in Neutron Star Thermal Spectra

Features in the X-ray spectrum of neutron stars have been an astrophysical “Holy Grail” since their X-ray emission was discovered. This is because the presence

of lines of identifiable origin, with known inertial reference frame energies, would allow the determination of the stellar redshift, z , and hence, at least in principle, the mass-to-radius relationship via $M/R = (c^2/2G)[1 - (1+z)^{-2}]$, which would constrain EOS. (The above is true only under the assumption that General Relativity correctly describes the spacetime around the neutron star; Dedeo & Psaltis, 2003). Atmosphere models with even as little as 0.05% metal abundance predict prolific line production due to the many transitions available for the various atomic ionization stages (Rajagopal et al., 1997). Hydrogen atmosphere models, by contrast, predict few lines. The relevance of spectral features to constraining the neutron-star age is thus that (i) they can help determine the atmosphere composition which can help establish what continuum model to fit; and (ii) they could, in principle, distort the continuum given poor spectral coverage or resolution.

Sanwal et al. (2002b), using *Chandra*’s ACIS CCD detectors, observed two absorption features, at 0.7 and 1.4 keV, in the X-ray spectrum of 1E 1207.4–5209, in the supernova remnant PKS 1209–51/52 (G296.5+10.0). The nature of this object is not understood; see §7.5. Mereghetti et al. (2002a) confirmed the existence of the lines using *XMM-Newton*. A subsequent long *XMM-Newton* exposure revealed an additional absorption feature at 2.1 keV, as well as a possible feature at 2.8 keV (see Fig. 7.10; Bignami et al., 2003; De Luca et al., 2004). These suggest harmonics of a cyclotron line at 0.7 keV. A cyclotron fundamental at this energy implies a magnetic field of 8×10^{10} G for an electron line, or 2×10^{14} G for a proton line. However, Sanwal et al. (2002b) and Hailey & Mori (2002) argue against the cyclotron interpretation, and suggest possible spectral line identification for the most secure 0.7 and 1.4 keV features. In any case, why such lines are not seen, in spite of many comparably sensitive observations of other neutron stars, remains a mystery. This source is discussed further in §7.5.

Very recently, features in spectra of three “isolated neutron stars” have been reported. These are discussed in §7.4.

7.3.3.5 Neutron Star Ages

The standard age estimator for rotation-powered pulsars assumes frequency evolution of the form $\dot{\Omega} = k\Omega^n$, where n is the “braking index,” and k is a constant that depends on the magnetic moment of the neutron star. Assuming k and n to be constant, the braking index can be determined from a measurement of the second time derivative of the frequency, $\ddot{\Omega}$, via $n = \nu\ddot{\Omega}/\dot{\Omega}^2$. The age derived by integrating the above differential equation is:

$$\tau = \frac{P}{(n-1)\dot{P}} \left[1 - \left(\frac{P_0}{P} \right)^{n-1} \right], \quad (7.4)$$

where P_0 is the spin period of the pulsar at the time it became a dipole rotator, generally presumed to coincide with the supernova event. For a simple vacuum dipole spin-down model, $n = 3$. For $P_0 \ll P$ and $n = 3$, Equation 7.4 reduces to $\tau_c = P/2\dot{P}$, the often-used pulsar characteristic age. For the five pulsars for which a constant value of n has been measured (Lyne et al., 1988; Kaspi et al., 1994; Lyne et al., 1996; Deeter et al., 1999; Camilo et al., 2000), the observed values are in

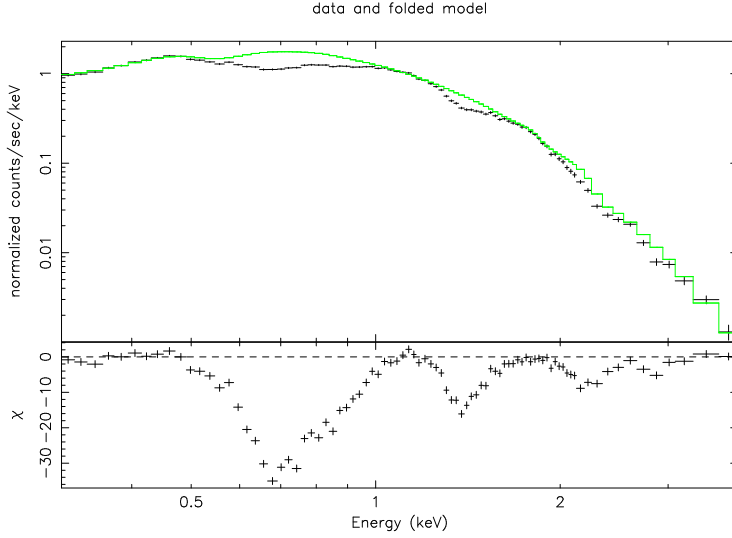


Fig. 7.10. *XMM-Newton* spectrum of 1E 1207.4–5209. The best-fit continuum curve is represented by the sum of two blackbody functions. Four absorption features appear at the harmonically spaced energies of ~ 0.7 keV, ~ 1.4 keV, ~ 2.1 keV and ~ 2.8 keV (De Luca et al., 2004).

the range 1.4–2.91. Though pulsars clearly do not rotate like perfect vacuum dipoles, the range of braking indexes is limited and observationally well constrained.

The situation is less clear for the initial spin period, P_0 . This can be determined from Equation 7.4 if the age is known and n measured. This is only the case for the Crab pulsar, whose estimated $P_0 \sim 19$ ms has led to the generally made assumption that $P_0 \ll P$ for all but the very fastest pulsars. However, the initial spin period distribution of neutron stars is not well predicted by theory, since the rotation rates of the cores of the massive progenitors are largely unknown (Endal & Sofia, 1978). Also, circumstances at core collapse could significantly affect the neutron-star spin independent of the angular momentum properties of the progenitor (e.g. Spruit & Phinney, 1998). As an example, consider PSR J1811–1925 in the supernova remnant G11.2–0.3 (Fig. 7.16; Torii et al., 1999; Kaspi et al., 2001b). The supernova remnant age is well determined to be ~ 2 kyr, while $\tau_c = 24$ kyr, implying $P_0 \simeq P = 65$ ms for reasonable n . In this case, τ_c is certainly over an order of magnitude different from the true age. Similar arguments hold for PSR J0205+6449 in the historic supernova remnant 3C 58 (Murray et al., 2002).

7.3.4 Current Status of Observations Vs Neutron Star Cooling Theory

Chandra and *XMM-Newton* have made by far the best measurements of neutron-star spectra thus far, and so offer the best opportunity for constraining models of neutron-star cooling. The current status of observations of thermally cooling young neutron stars has recently been reviewed by Kaminker et al. (2002), Yakovlev et al. (2002) and Tsuruta et al. (2002), and is summarized in Figure 7.8. There, the data points are actual temperature measurements or upper limits; those

Table 7.2. *Observations of Thermally Cooling Young Rotation-Powered Pulsars*

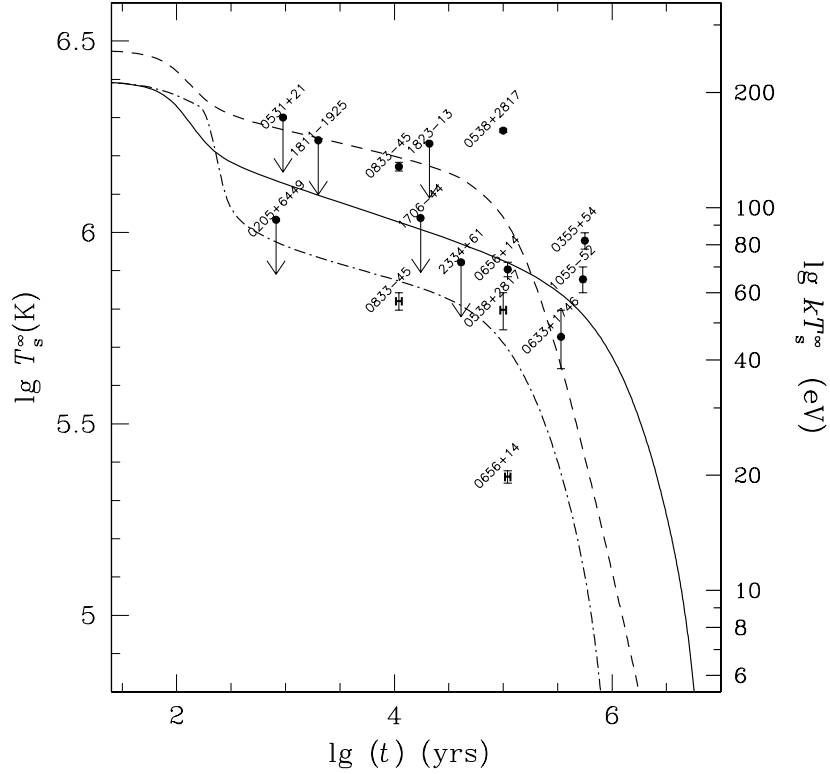


Fig. 7.11. Current best measured rotation-powered pulsar temperature as a function of best age estimate (see Table 7.2). “H” symbols denote that a $B = 0$ hydrogen atmosphere model was used; otherwise, a $B = 0$ blackbody model was assumed. The cooling curves shown are for $1.35 M_{\odot}$ stars, as in Figure 7.8: (solid) non-superfluid star with $B = 0$ and no accreted mass (Fig. 7.8, left); (dot-dash) a combination proton and neutron superfluidity model (Fig. 7.8, middle); (dash) non-superfluid star with $B = 0$ and accreted envelope mass $10^{-7} M_{\odot}$ (Fig. 7.8, right). The curves are illustrative only and do not represent fits to the data.

marked with an “H” are for hydrogen atmosphere models, while the rest are for simple blackbody models. The uncertainty from possible nebular contamination is not indicated; for sources with nebulae, the observations made with *Chandra*, given its superb spatial resolution, are superior to those with other telescopes. Age uncertainties are not indicated, but as discussed in §7.3.3.5, can be an order of magnitude. For PSRs J0538+2817, B0656+14, and B0833–45 (Vela), we show both the blackbody and hydrogen atmosphere temperatures, to illustrate the substantial difference. The plotted data are summarized in Table 7.2.

A striking property of the data is its scatter. Although the above caveats must be applied, the plot remains log-log, and it is hard to explain all the data with iden-

tical neutron stars sharing a common mass and hence EOS and interior structure. Kaminker et al. (2002) argue that on the basis of the data together with models that account for most of the phenomena affecting cooling (they do not consider “exotic” particles, but do consider neutron and proton superfluidity in detail), there are effectively three types of cooling neutron stars (see also Tsuruta et al., 2002): (i) low-mass, slowly cooling stars where there is no direct Urca process occurring; (ii) medium-mass, moderately cooling stars in which some nucleon direct Urca processes occur, but for which proton superfluidity suppresses the bulk of the possible Urca processes; and (iii) high-mass, rapidly cooling stars for which suppression of direct nucleon Urca processes is weak. Of course the mass cuts corresponding to these different categories depend strongly on the EOS and on the possible types of superfluidity. As an example, for the EOS “A” of Yakovlev et al. (2001), for neutron stars having age 4 kyr, for a 2p proton superfluid, the low-mass/medium-mass cut is $1.36 M_{\odot}$, while the medium/high mass cut is $1.64 M_{\odot}$.

What is clear is that we have not yet seen any very rapidly cooling objects. However this may be less of a statement about the interior physics as it is about the mass function of neutron stars, i.e. there may be very few high-mass neutron stars produced for purely astrophysical reasons. According to Kaminker et al. (2002), the Vela pulsar (PSR B0833–45, fit with a hydrogen atmosphere) and Geminga (PSR J0633+1746, fit with a blackbody), as well as presumably PSR J0538+2817 (with a hydrogen atmosphere) the coolest objects, are prime examples of moderately cooling stars for which some direct Urca reactions are occurring, and their masses could be determined assuming some EOS, a model of proton superfluidity (but see Tsuruta et al., 2002) and the dependence of the critical temperature for proton superfluidity on density. Note that the hydrogen-atmosphere model fit to PSR B0656+14 is generally ignored, as it yields a radius much greater than is possible for a neutron star. The apparently higher temperature objects, like PSR B1055–52, must, in this case, be low-mass neutron stars, possibly affected by some internal heating mechanism or by polar-cap heating. The pulsar in 3C 58 recently received fanfare for its relatively low temperature in spite of having likely been born in 1181 AD, hence being very young (Slane et al., 2002). Though the Vela and Geminga pulsars nominally have lower reported temperatures hence might be argued as being closest to rapidly cooling objects (Yakovlev et al., 2002), in fact the 3C 58 upper limit was for a blackbody spectrum. A hydrogen-atmosphere fit to the data (as was done for Vela) could possibly bring the upper limit down to a very constraining level. Indeed, the Vela temperature when fit with a blackbody is well above that of the 3C 58 pulsar.

7.4 “Isolated Neutron Stars”

A relatively recently discovered class of X-ray sources are believed to be thermally cooling neutron stars. Their nature is still not well understood. These are currently being referred to in the literature as “isolated neutron stars” (INSs). This at first glance may seem like a misnomer since this title does not distinguish them from isolated rotation-powered pulsars. Actually, as we describe below, it is possible that at least a subset of the INSs are conventional rotation-powered pulsars. However, the sources known as INSs are currently distinguished as showing no evidence for radio

pulsations, nebulosity, or accretion, and X-ray emission characterized by very soft spectra that are well described by a blackbody, with no apparent magnetospheric contributions. These very properties, as well as their proximity, make them enticing targets, since many of the observational difficulties inherent in using thermal emission to constrain the nuclear EOS that are described above in §7.3 are not present. The name INS therefore does apply to rotation-powered pulsars as well, however the latter are a very special class of the INS population: long after rotation-powered pulsars have spun down past the “death line,” beyond which they no longer produce observable magnetospheric emission (this typically takes ~ 30 Myr), “dead” neutron stars will still populate the Galaxy. INSs, if identified as this “dead” component, may well number as high as 10^9 in the Galaxy, much more than the $\sim 10^5$ active radio pulsars (Lyne et al., 1998).

Prior to the launch of the *ROSAT* satellite, theoretical predictions following an idea first put forth by Ostriker et al. (1970) were that several thousand otherwise dead neutron stars would be detectable in soft X-rays by *ROSAT*, due to their accretion of material from the interstellar medium (Treves & Colpi, 1991; Blaes & Madau, 1993). In fact, well after the rise and fall of *ROSAT*, only 7 objects (Table 7.3; see Treves et al., 2000, for a review) having the predicted properties (such as high X-ray to optical flux ratio) have been found in spite of very careful searches (e.g. Danner, 1998a,b; Rutledge et al., 2003). This is likely due mainly to the much higher than expected average neutron star space velocity (e.g. Lyne & Lorimer, 1994; Hansen & Phinney, 1997; Arzoumanian et al., 2002), which hampers standard Bondi-Hoyle accretion, although other explanations have been suggested (e.g. Perna et al., 2003).

In fact, of the objects in Table 7.3, it now appears likely that *none* is accreting from the ISM; rather, they are visible because of thermal emission from the neutron-star surface. If so, these are unlikely to be extremely old neutron stars as they are too bright; rather they would have to be either off-beam conventional rotation-powered pulsars having ages $\sim 10^6$ yr and magnetic fields $10^{11} - 10^{12}$ G, or even younger quiescent magnetars having magnetic fields 2–3 orders of magnitude higher.

Although 4/7 of the INSs have now been shown to exhibit pulsations, none has had its spin-down rate measured. Their ages are thus not known, which hinders efforts to use them in cooling studies. However, in these sources, one hope is that spectral modeling, coupled with sensitive, high-resolution X-ray observations, could determine their radii. If spectral lines were detectable as well, the stellar masses could in principle be known independently from the lines’ gravitational redshift (§7.3.3.4), thus providing a direct constraint on the neutron-star mass/radius relation and testing EOSs. Spectral modeling in these sources is greatly aided by their low equivalent neutral hydrogen column densities, typically $1 - 2 \times 10^{20} \text{ cm}^{-2}$. Although these ambitious goals have not yet been realized, the recent discoveries of absorption features in the spectra of three INSs is quite encouraging (Haberl et al., 2003, 2004; van Kerkwijk et al., 2004).

The current situation is nicely illustrated by the example of RX J1856.5–3754, which is the best studied of the INSs. This object was discovered in *ROSAT* data (Walter et al., 1996) and optical observations with the *Hubble Space Telescope* revealed a faint blue counterpart (Walter & Matthews, 1997). This suggested emission

Table 7.3. *Reported Isolated Neutron Stars*^a

Name ^b	P (s)	ROSAT PSPC rate (cps)	m_V	$\log f_x/f_{opt}$
RX J0420.0–5022	3.45	0.11	...	> 3.3
RX J0720.4–3125	8.39	1.69	26.8	4.6
RX J0806.4–4132	11.4	0.38	...	> 3.4
RX J1308.6+2127	10.31	0.29	28.7	5.0
RX J1605.3+3249	...	0.88	27.1	4.4
RX J1856.5–3754	...	3.64	25.8	4.4
1RXS J214303.7+065419	...	0.18	...	> 3

^aData from Treves et al. (2000), Kaplan et al. (2003a), and Haberl (2003, 2004); see text for more information.

^bSource names ending with “*” are uncertain members of the class.

that is the Raleigh-Jeans tail of a $kT \simeq 50 - 60$ eV blackbody. The *HST* detection enabled an astrometric study of the source that detected both parallax and proper motion (Walter, 2001). The source is evidently extremely close to the Sun, having parallax 8.5 ± 0.9 mas (Kaplan et al., 2002; Walter & Lattimer, 2002) or distance 117 ± 12 pc. The proper motion of the source, if traced backward, appears to intersect the Upper Sco OB association, if it has a radial velocity of ~ 30 km s⁻¹ (Walter, 2001; Kaplan et al., 2002; Walter & Lattimer, 2002). Assuming the neutron star was born in the association implies an age of 0.4 Myr.

Because of the proximity of the source and the chance for the discovery of spectral features, a 500 ks Director’s Discretionary Time observation with the *Chandra X-ray Observatory* was performed in 2002. The X-ray emission was found to be unpulsed, with stringent upper limits set on the pulsed fraction ($< 1.3\%$ for frequencies less than 50 Hz; Burwitz et al., 2003). The spectral results of the DDT observation were a surprise. Not only were no features detected, but the resulting X-ray spectrum is extremely well modeled by a simple blackbody, with no evidence for the atmospheric distortion so clearly predicted by theory (see §7.3.2.5; Drake et al., 2002; Braje & Romani, 2002; Burwitz et al., 2003). In particular, the emitting radius for a single blackbody fit is $4.3(d/117 \text{ pc})$ km, smaller than expected for any plausible neutron star. This led to speculation that the object is not a neutron star but rather a self-bound quark or strange star (Drake et al., 2002). A very recently revised parallax distance of 175 pc would imply a radius of 7.2 km, more in line with expectations for a neutron star (D. Kaplan, personal comm.). In any case, it is possible that the emitting region is simply a hot spot on a larger stellar surface; this is not completely precluded by the low pulsed fraction upper limits because of the strong effects of gravitational light bending (Burwitz et al., 2003). Interestingly, the optical emission is too bright to be the low-energy extrapolation of the X-ray spectrum. A two-component blackbody model is necessary: the lower temperature, perhaps from the bulk of the surface and accounting for the optical emission, has $kT^\infty < 33$ eV, and the higher temperature, perhaps from a hot spot and accounting

for the X-ray emission, has $kT^\infty \simeq 63.5$ eV. In this case, a strange star is not required (Drake et al., 2002; Braje & Romani, 2002; Burwitz et al., 2003). Of course, the standard caveats regarding the use of blackbody models apply (see §7.3.2.5). van Kerkwijk & Kulkarni (2001) discovered, using H α imaging, a cometary shaped nebula having RX J1856.5–3754 at its apex, similar to those detected around some conventional radio pulsars (see §7.6). This suggests that RX J1856.5–3754 is a conventional neutron star whose emission beam does not intersect our line of sight.

Other sources in Table 7.3 are not yet as well characterized as RX J1856–3754. We discuss each briefly, in order of the degree to which it has been studied.

RX J0720.4–3125 is a 8.39-s soft-X-ray pulsar (Haberl et al., 1997) plausibly identified as an off-beam conventional rotation-powered pulsar and not an accretor (see Kaplan et al., 2003b, and references therein). No spin-down rate has yet been determined, although interesting upper limits on \dot{P} have been established, and imply that $B \lesssim 3.5 \times 10^{13}$ G (Cropper et al., 2004). Its optical through X-ray spectrum is well modelled by two blackbodies (as in RX J1856–3754; Motch et al., 2003) plus a possible power-law component, similar to what is observed in young and middle-aged radio pulsars (e.g. PSR B0656+14). A large inferred velocity seems to preclude it being an accretor (Motch et al., 2003). Intriguingly, Haberl et al. (2004) recently report the discovery of a phase-dependent absorption line in this pulsar’s spectrum. The line has energy ~ 271 eV and an equivalent width that varies from -31 eV to -58 eV depending on pulse phase. The line appears best interpreted as cyclotron resonance of charged particles, presumably either electrons or protons. For the latter, a $\sim 5 \times 10^{13}$ G magnetic field is implied. For electrons, the field must be 2000 times smaller.

RX J1308+2127 (RBS 1223) was identified by Schwöpe et al. (1999) in *ROSAT* data as a relatively bright INS candidate, based on its soft spectrum and the high X-ray to optical flux ratio made possible by the good positional localization. Haberl et al. (2003) showed the source is pulsed with $P = 10.3$ s. Kaplan et al. (2002) reported a possible optical counterpart having flux in excess of the extrapolation of the X-ray blackbody spectrum, as in RX J1856–3754 and RX J0720.4–3125. A broad absorption line feature has been reported in this source (Haberl et al., 2003), and interpreted as a proton cyclotron line in a $> 10^{13}$ G field. Haberl et al. (2003) reported the discovery of a broad absorption feature in this object’s X-ray spectrum. The line energy is at ~ 300 eV and has equivalent width ~ -150 eV. This line is interpreted by the authors as being due to cyclotron resonance absorption, in the $10^{13} - 10^{14}$ G range if protons, and in the $10^{10} - 10^{11}$ G range if electrons.

RX J1605.3+3249 (RBS 1556) was identified by Motch et al. (1999) as being a possible INS, because of the soft source spectrum ($kT \simeq 92$ eV), the lack of X-ray variability, and the absence of any optical counterpart. Kaplan et al. (2003a) reported the detection of a faint, blue optical counterpart, which they argue confirms the INS interpretation. The optical counterpart has flux that is over an order of magnitude above the Rayleigh-Jeans extrapolation of the X-ray blackbody. This is like, though somewhat larger than, the excesses seen in the other sources, and argues either for the X-rays being from a hot polar cap, or, for the optical emission having a non-thermal component. Either is consistent with an off-beam rotation-powered pulsar. Very recently, van Kerkwijk et al. (2004) report the detection of a broad

absorption feature at 450 eV. As for RX J0720.4–3125 and RX J1308+2127, the origin of the line is as yet unclear, although Ho & Lai (2004) show on the basis of approximate calculations that all can be plausibly explained by proton cyclotron absorption.

RX J0806.4–4132 was reported by Haberl et al. (1998) as an interesting INS candidate. It was seen in two *ROSAT* All Sky Survey observations at the same flux, and having a soft spectrum, with $kT \simeq 78$ eV. Haberl et al. (1998) detected no optical counterpart, indicating a high X-ray to optical flux ratio. Haberl & Zavlin (2002) using *XMM-Newton* observations of this source, report a possible 11.4 s periodicity at the 3.5σ level having a small $\sim 6\%$ pulsed fraction, and a blackbody temperature of $kT = 94$ eV. The improved *XMM-Newton* position should allow deeper searches for a possible optical counterpart.

RX J0420.0–5022 is a *ROSAT* soft-spectrum source showing evidence for a 22.7 s periodicity, a high X-ray to optical flux ratio, no apparent variability, and a soft spectrum that is well described by a blackbody of temperature ~ 57 eV (Haberl et al., 1999). All argue for it being an INS, although the period is much longer than has been seen for any rotation-powered pulsar.

7.5 “Central Compact Objects”

There are several putative compact objects that have been studied extensively and which have potential to constrain neutron-star cooling theory (§7.3), yet which are poorly understood. By definition, these sources, known as “Central Compact Objects” (CCOs), are found near the centers of supernova remnants (SNRs), although this could well be a selection effect resulting from SNR X-ray studies. The CCOs share the following distinguishing properties: unusual X-ray spectra that, fit with blackbodies, and, in some cases, hydrogen atmospheres, imply very small radii, and very high effective temperatures (see Table 7.4). The small radii are inconsistent with these objects being neutron stars for any EOS, while the temperatures are inconsistent with any neutron-star cooling models. Other distinguishing characteristics are high X-ray to optical luminosity ratios, no evidence for pulsations (except in one case – see below), no evidence for a wind as seen in conventional young rotation-powered pulsars (§7.6), and no evidence for any companion star that could be powering the X-ray emission via accretion. We discuss the five best studied CCOs briefly below. For a more detailed review, see Pavlov et al. (2002a).

The “first light” of *Chandra* targetted the 300-yr old supernova remnant Cassiopeia A, and revealed, for the first time, the presence of an X-ray point source near the center (Fig. 7.12; Tananbaum, 1999). This object, CXO J232327.9+584843, seems likely to be the long-sought-after compact object formed in this oxygen-rich remnant, clearly a result of the supernova explosion of a massive star. The spectral properties of this source, as well as the absence of any detectable pulsations, make it very different from canonical young neutron stars like the Crab pulsar. Specifically, Pavlov et al. (2000) and Chakrabarty et al. (2001) showed that for either a simple blackbody or hydrogen atmosphere model, the temperature of the emission ($kT = 0.25 - 0.35$ keV) is very high, and the emitting area ($R = 0.2 - 0.5$ km) too small to be consistent with surface thermal emission from initial cooling. A power-law fit yields a photon index ($\Gamma = 2.6 - 4.1$), significantly higher than those seen in

Table 7.4. *Central Compact Objects*^{a,b}

Name	SNR	P	kT_{bb}^∞ (keV)	R_{bb}^∞ (km)	kT^∞ (keV)	R^∞ (km)
CXO J082157.5–430017	Pup A	...	0.4	1.4	0.2	10
CXO J085201.4–461753	G266.1–1.2	...	0.4	0.3	0.3	1.5
RX J121000.8–522625	G296.5+10.0	0.424 s	0.25	1.6	0.1	1
CXO J161736.3–510225	RCW 103	6 hr ?	0.4–0.6	0.2–1.6	0.3	1–8
CXO J232327.9+584843	Cas A	...	0.5	0.5	0.3	1

^aSee Pavlov et al. (2002a), Pavlov et al. (2002b) and references therein.

^bNote: kT_{bb}^∞ and R_{bb}^∞ refer to blackbody models, while kT^∞ and R^∞ refer to magnetic hydrogen atmosphere models.

pulsars. The difference is further evidenced by the absence of any synchrotron nebula around the object (Fig. 7.12), as well as the absence of any radio emission from the source (McLaughlin et al., 2001). The very high X-ray to optical flux ratio, however, does implicate a compact object and render an accreting binary scenario problematic (Kaplan et al., 2001; Ryan et al., 2001). The source spectrum is consistent with it being an “anomalous X-ray pulsar” (see Chapter 14), that is, endowed with an ultrahigh magnetic field ($10^{14} - 10^{15}$ G), or with it being a conventional $B \sim 10^{12}$ -G neutron star having a cooling iron surface and hot hydrogen or helium polar caps (Pavlov et al., 2000; Chakrabarty et al., 2001). More recent *XMM-Newton* observations of the source support these conclusions (Mereghetti et al., 2002b). However, if it is an AXP, why it should be so faint and show no pulsations, and, if it has hot polar caps, why they should be so hot in the absence of any evidence for the pulsar mechanism, is a mystery.

CXO J082157.5–430017 is located in the Puppis A SNR, though significantly off-center (Petre et al., 1982). From *ROSAT* and *ASCA* observations (Petre et al., 1996; Zavlin et al., 1999), the object’s X-ray spectrum is well modeled by a blackbody, however the best-fit radius, 1.4 km, is much smaller than that of neutron star. A magnetized ($B \gtrsim 6 \times 10^{12}$ G) hydrogen atmosphere model yields a more neutron-star-like radius of 10 km, and a temperature more in line with that expected from cooling emission (Zavlin et al., 1999). However, neither pulsations nor evidence for a surrounding nebula has been seen (Gaensler et al., 2000a; Pavlov et al., 2002a), arguing that if this is a rotation-powered pulsar, it must have very low \dot{E} . This argues against the heated-polar-cap interpretation, as in Cas A.

SNR G266.1–1.2, also known affectionately as “Vela Jr,” is in the direction of the southeast corner of the Vela SNR (Aschenbach, 1998). The possible detection of a radioactive ^{44}Ti line suggested an age of ~ 700 yr, and a distance of ~ 200 pc. However, subsequent *ASCA* observations yielded a N_h more consistent with a distance of $\gtrsim 1$ kpc, and an age of several thousand years (Slane et al., 2001). The point source CXO J085201.4–461753 is near the center of the SNR, and has an X-ray to optical flux ratio only consistent with a compact object identification (Pavlov et al.,

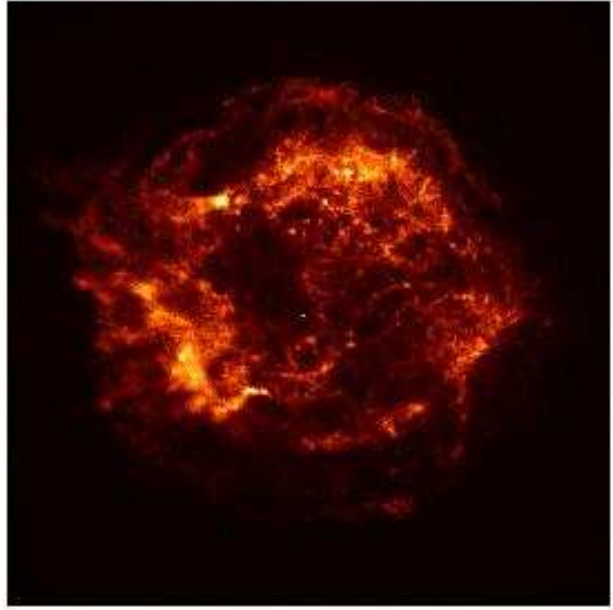


Fig. 7.12. “First light” *Chandra* X-ray image of the supernova remnant Cas A (after Tananbaum, 1999). The image is $6'$ on a side. The previously unknown point source at the center of the remnant is obvious.

2001). This source is not seen to pulsate and shows no evidence of a pulsar wind nebula in *Chandra* data (Kargaltsev et al., 2002). The source spectrum, fit with a blackbody model, yields a radius of only ~ 0.3 km. Atmosphere models do not yield more reasonable radii (Kargaltsev et al., 2002).

RX J121000.8–522625 is a compact source near the center of the large SNR G296.5+10.0 (also known as PKS 1209–51/52). The source was first noticed in *Einstein* IPC observations made by Helfand & Becker (1984). Mereghetti et al. (1996) used *ROSAT* to show that a blackbody model fit the spectral data well. They further demonstrated the absence of any extended emission, and set an optical limit of $V \gtrsim 25$. They did not detect any radio emission from the source at 4.8 GHz, and Kaspi et al. (1996) saw no pulsed radio emission at 436 MHz. Vasisht et al. (1997) and Zavlin et al. (1998) presented *ASCA* observations of the source which again supported the neutron-star interpretation. *Chandra* observations suggested a periodicity in the source, with $P = 424$ ms (Zavlin et al., 2000). Pavlov et al. (2002), using a second *Chandra* observation, reported a spin-down age of 200–900 kyr, much larger than the 3–20 kyr age inferred for the SNR. However, subsequent observations have not found simple spin down as in rotation-powered pulsars, unless the source is an

active glitcher (Zavlin et al., 2004). This is currently not understood. The source spectrum is thermal, and the best-fit continuum blackbody model yields a small 1.6-km emitting radius (Pavlov et al., 2002). This source also shows absorption features in its X-ray spectrum (Fig. 7.10; §7.3.3.4).

1E 161348–5055, the central source in the supernova remnant RCW 103 was the first proposed cooling neutron star (Tuohy & Garmire, 1980). Gotthelf et al. (1999) showed that the source is X-ray variable by as much as an order of magnitude on a time scale of years. A ~ 6 hr periodicity was tentatively reported in data from *Chandra* and *ASCA* observations (Garmire et al., 2000), and a 2002 *Chandra* observation showed a clear 6.4-hr periodicity and apparently phase correlated X-ray flux variations (Sanwal et al., 2002a). This strongly suggests that this object is, in fact, an accreting neutron star having a very low-mass companion.

7.6 Pulsar Wind Nebulae

7.6.1 Physical Overview

Only a small fraction ($\lesssim 10\%$) of the spin-down energy of a young pulsar is converted into observable pulsed emission (§7.2). It is generally accepted that most of the energy leaves the pulsar’s magnetosphere in the form of a magnetized wind (Michel, 1969). In the ideal ($\mathbf{E} \cdot \mathbf{B} = 0$) MHD approximation to the aligned rotating magnetic dipole (Goldreich & Julian, 1969; Contopoulos et al., 1999), it appears that the poloidal field (B_p , the field perpendicular to the toroidal component B_ϕ) goes from a nearly dipolar structure within the light cylinder to a split monopole structure outside the light cylinder (i.e. $B_p = B_r \propto r^{-2}$, a purely radial field whose sign abruptly changes at the equator). The toroidal component B_ϕ , which is small out to the light cylinder grows rapidly outside the light cylinder so that for radii greater than a few times R_{LC} , $B_\phi \gg B_p$. “Cold” (i.e. non-radiating) charged particles flow outward with this magnetic field forming a magnetized wind which is ultimately accelerated to very high energies ($\gamma \gg 1$). This highly relativistic magnetized wind eventually interacts with the surrounding medium, and emits synchrotron radiation from radio to γ -ray wavelengths. This synchrotron emission caused by the pulsar wind is what is generally meant by the term pulsar wind nebula (PWN). However, the winds from rapidly moving pulsars may produce a bow shock in the ISM causing $H\alpha$ emission in what is essentially a thermal process. Optical filaments in the Crab nebula also appear to be thermal emitters (eg. Fesen & Kirshner, 1982), and in principal there could also be thermal X-ray emission at the outer edges of young PWNe, although this is difficult to distinguish from the surrounding supernova remnant (SNR) and has yet to be observed unambiguously.

The details of the structure and luminosity of the PWN should depend on the pulsar’s spin-down energy history and space velocity as well as the density profile of the surrounding medium. It may also depend upon the magnetic inclination angle of the pulsar, although how the wind properties depend on this angle is poorly understood and it is possible that the deviation from the aligned rotator model is negligible in terms of overall growth and energetics of the PWN. What we observe is dependent on the observer’s viewing angle, with Doppler boosting being a non-negligible factor in the surface brightness distribution of the PWN.

Since a pulsar is born in a supernova, the initial environment that the pulsar wind encounters is the (nearly) freely expanding supernova ejecta. The pulsar may be born with a large space velocity and overtake the expanding ejecta shell within a few tens of thousands of years, after which the wind environment is probably the ISM. There appears to be a minimum spin-down energy necessary to create bright PWNe with a significant drop in PWN emission efficiency from pulsars with $\log \dot{E} \lesssim 36$ (Frail & Scharringhausen, 1997; Gaensler et al., 2000b; Gotthelf, 2003), and generally only the youngest isolated pulsars are observed to have PWNe. However, millisecond pulsars can also have a substantial \dot{E} , and both $H\alpha$ (Bell et al., 1995) and X-ray (Stappers et al., 2003) nebulae have been observed around them.

The standard theoretical picture for PWNe from young pulsars (Pacini & Salvati, 1973; Rees & Gunn, 1974; Reynolds & Chevalier, 1984; Kennel & Coroniti, 1984a) is of a synchrotron bubble being blown at the center of an expanding supernova remnant. Initially, the outer edge expands supersonically into the supernova ejecta, so is presumably bounded by a forward shock (R_P of Fig. 7.13). The corresponding reverse shock (R_T) is near the center of the nebula, where the cold relativistic wind from the pulsar is terminated. (Note that the wind is cold only in the sense that $kT \ll (\gamma - 1)mc^2$ and hence in the co-moving frame of the bulk flow the particles have very little time to radiate before encountering the shock.) The bulk flow energy is then converted into random particle motion with a power-law distribution of particle energies. The wind continuously injects high-energy electrons and positrons as well as magnetic field into the bubble. The particles gyrate in the magnetic field, emitting synchrotron radiation from the radio through soft γ -ray regions of the spectrum.

7.6.2 *Observational Properties of PWNe*

Except for a few cases (notably the Crab and Vela nebulae), we have data on PWN emission only at centimeter wavelengths and/or in X-rays below ~ 10 keV. The radio properties of PWNe have been outlined by Weiler & Shaver (1978) among others. A source can be identified as a radio PWN if it has an amorphous (i.e. non-shell) morphology, flat, non-thermal spectrum (energy spectral index $\alpha \simeq 0.0 - 0.3$, where flux $S = \nu^{-\alpha*}$), and high ($\gtrsim 10\%$) fractional linear polarization. The X-ray emission also has a spectrum described by a power law, except the photon index $\Gamma \equiv 1 + \alpha$ is generally between $\sim 1.5 - 2.2$. Hence there is a need for one or more spectral breaks such that the net change in spectral index is $\Delta\alpha = 0.5 - 0.9$. The X-ray nebula tends to be smaller than the radio nebula, and generally has a more defined morphology, sometimes taking the form of a thick torus with perpendicular jets.

The efficiency with which the spin-down energy is converted into synchrotron radiation can be quite high. However, it is often difficult to determine since the observations tend to be restricted to two narrow bands. In general, one can find four observed quantities, with associated errors, quoted in the literature (or minor variants): radio flux density at ~ 1 GHz, $S_{1\text{GHz}}$, radio energy spectral index α_r , 1-10 keV X-ray flux F_x (corrected for interstellar absorption), and X-ray photon spectral

* In radio work, the spectral index is often defined as $S = \nu^\alpha$. However we use the minus sign here to be consistent with the X-ray definition.

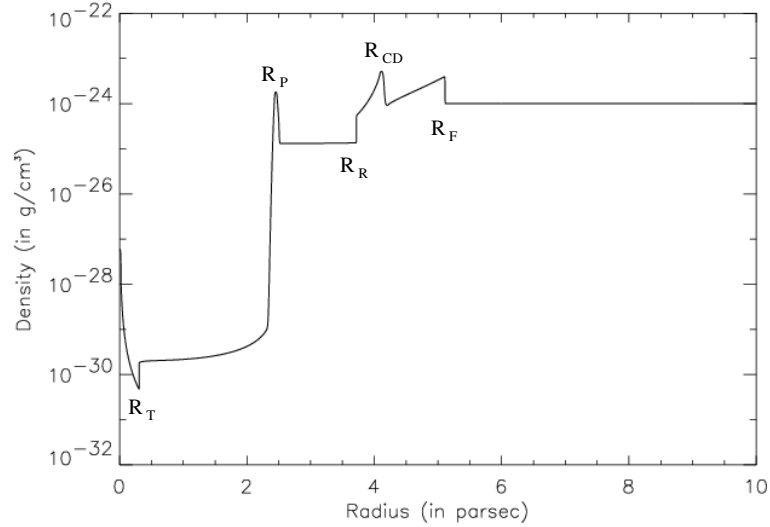


Fig. 7.13. Density profile of a spherically symmetric PWN expanding within a pre-Sedov SNR showing the PWN termination shock R_T , the PWN forward shock R_P , the SNR shell reverse shock R_R , the contact discontinuity between the SNR ejecta and the ISM R_{CD} , and the SNR shell forward shock R_F . Adapted from (van der Swaluw et al., 2001)

index $\Gamma = 1 + \alpha_x$. From these, one can infer a break frequency where the spectral slope changes:

$$\nu_b \equiv \left(\frac{S_x \nu_x^{\alpha_x}}{S_r \nu_r^{\alpha_r}} \right)^{1/(\alpha_x - \alpha_r)}, \quad (7.5)$$

where S_x and S_r are the flux densities at ν_x and ν_r , respectively. Possible physical meanings of this break frequency will be discussed in §7.6.4. At centimeter wavelengths, the spectral index $\alpha_r < 1$, hence the bulk of the energy emitted in this band is at higher frequencies. The radio luminosity L_r therefore depends on what is chosen as the upper frequency limit ν_{ul} of the radio band:

$$L_r = 1.1 \times 10^{30} \frac{S_{1\text{GHz}} d^2 \nu_{ul}^{1-\alpha_r}}{1 - \alpha_r} \text{erg s}^{-1}, \quad (7.6)$$

where d is in kpc, $S_{1\text{GHz}}$ is in Jansky, and ν_{ul} is in GHz. A natural upper limit would be the break frequency, but that is usually not well known due to uncertainties in the radio and X-ray spectral indices and the large extrapolation. Often, an upper limit of 100 GHz is randomly chosen in order to compare different nebulae (Gaensler et al., 2000b).

The X-ray luminosity L_x can be defined as the total power emitted from the break energy up to a high-energy cutoff E_C :

$$L_x = 1.1 \times 10^{32} \frac{F_{x12} d^2 (E_C^{2-\Gamma} - E_B^{2-\Gamma})}{10^{2-\Gamma} - 1} \text{erg s}^{-1}, \quad (7.7)$$

where F_{x12} is the 1–10 keV flux in units of $10^{-12} \text{erg cm}^{-2} \text{s}^{-1}$ and E_C and $E_B = h\nu_b$

are in keV. If the photon index $\Gamma < 2$, the X-ray luminosity depends critically on the high-energy cutoff, which is only known in a very few cases. For the Crab and Vela PWNe, it is in the few to tens of MeV range. If $\Gamma > 2$, then the bulk of the energy is emitted below the X-ray band, peaking near the break frequency. Note that the X-ray luminosity is usually much higher than the radio luminosity. Since the synchrotron lifetime of the X-ray emitting particles is often much shorter than the age of the nebula, the properties of the X-ray emission can be highly dependent on the current spin-down energy of the pulsar. The radio emitting particles generally have synchrotron lifetimes longer than the age of the nebula, and are therefore an indication of the total number of lower-energy relativistic particles injected into the nebula throughout its lifetime.

All known pulsars with detected X-ray or radio PWNe are listed in Table 7.5. Table 7.6 lists other X-ray or radio PWNe from which pulsations have not been detected, while Table 7.7 lists pulsars with $H\alpha$ PWNe. Note that the isolated neutron star RX J1856.5–3754 also has a $H\alpha$ nebula associated with it (see §7.5). A source is considered a PWN if it has one or more of the following observational signatures: a known pulsar embedded in a radio and/or X-ray nebula which appears to be morphologically related to the pulsar; an isolated, filled-center radio nebula with the properties mentioned above; a composite supernova remnant defined as a SNR shell with either a central radio component whose spectrum is flatter than the shell, a compact but extended central X-ray component with a power-law spectrum, or both; an X-ray point source with a very high ratio of X-ray to optical flux and associated extended X-ray emission with a power-law spectrum. The X-ray morphologies are quite varied, but can be loosely placed within the following categories: torus + weak jet (T), jet/trail dominated (J), and mixed or uncertain (M). In the mixed case, sometimes there appears to be a bow-shock or torus as well as a bright trail or jet-like component, but sometimes there is just an indistinct blob. Although a dominant toroid is generally assumed to be the typical structure, only a few of the brightest sources have been clearly determined to have toroidal morphologies. A reference for X-ray morphology is given where available, otherwise for the radio morphology.

There seems to be a change in PWN morphology from toroidal to more of a jet or trail when the pulsar spin-down energy drops below $\log \dot{E} \sim 36.5$ (in erg s^{-1}). This probably simply reflects the on-average greater age of these pulsars so they have moved substantially from their birth sites. The radio and X-ray PWNe largely disappear once the spin-down energy drops below $\log \dot{E} \sim 35.5$. Those few sources listed as being PWNe whose pulsars' spin-down energies are below this tend to have barely detectable X-ray PWN. The fact that they are observable at all, along with the existence of $H\alpha$ nebula seen around pulsars whose $\log \dot{E} < 34.0$ attest to the persistence of the relativistic wind generation mechanism long after the effects on the surrounding medium are readily apparent.

7.6.3 *Evolution of a PWN in a SNR*

The standard evolutionary model of PWNe is a spherical bubble being blown at the center of a spherical SNR shell (Fig. 7.13). Observationally, this picture does not accurately represent the true state of affairs. Many PWNe, including the “canonical” example of the Crab, do not have observable SNR shells, and so there

Table 7.5. *Known Pulsars With Synchrotron Wind Nebulae*

Name	Pulsar	$\log(\dot{E})$ (erg s ⁻¹)	d (kpc)	M ^a	S ^b	γ^c	Reference
N157B	J0537-6910	38.7	50	M	?	Y	Wang et al. 01
Crab	B0531+21	38.7	2.0	T	N	Y	Weisskopf et al. 00
SNR 0540-69.3	B0540-69	38.2	50	T	Y	Y	Gotthelf & Wang 00
3C 58	J0205+6449	37.4	4.5	M	N	N	Murray et al. 02
G106.6+3.1	J2229+6114	37.4	4.0	T	N?	Y	Halpern et al. 01
G320.4-1.2	B1509-58	37.2	5.0	M	Y	Y	Gaensler et al. 02
G292.0+1.8	J1124-5916	37.1	6.5	T	Y	N	Hughes et al. 01
G54.1+0.3	J1930+1852	37.1	9.1	T	N	N	Lu et al. 02
Kookaburra	J1420-6048	37.0	5.6	M	?	Y	Roberts et al. 01
Kes 75	J1846-0258	36.9	21	M	Y	N	Helfand et al. 03
Vela X	B0833-45	36.8	0.29	T	Y	Y	Helfand et al. 01
G11.2-0.3	J1811-1925	36.8	5	M	Y	N	Roberts et al. 03
CTB 80	B1951+32	36.6	3.2	M	Y	Y	Safi-Harb et al. 95
G343.1-2.3	B1706-44	36.5	2.3	M	N	Y	Gotthelf et al. 02
GeV J2020+3658	J2021+3651	36.5	12	T	?	Y	Hessels et al. 03
G18.0-0.7	B1823-13	36.5	3.9	J	N	?	Gaensler et al. 03
Duck	B1757-24	36.4	5.2	J	O	N	Kaspi et al. 01
3EG J1027-5817	J1016-5857	36.4	8.0	M	?	Y	Camilo et al. 01
Mouse	J1747-2958	36.4	5.0	J	N	?	Gaensler et al. 03
G292.2-0.5	J1119-6127	36.4	6	M	Y	N	Gonzalez & Safi-Harb 03
G308.8-0.1	J1341-6220	36.1	11	?	Y	N	Kaspi et al. 92
G270.3-1.0	B0906-49	35.7	2.6	?(J)	N	N	Gaensler et al. 98
W44	B1853+01	35.6	3.1	J	Y	Y	Petre et al. 02
G341.2+0.9	B1643-43	35.6	5.8	?	Y	N	Giacani et al. 01
Black Widow	B1957+20	35.0	2.5	J	N	N	Stappers et al. 03
Geminga	J0633+1746	34.5	0.16	J	N	Y	Caraveo et al. 03

^aX-ray Morphology. T = torus + weak jet, J = jet or trail dominated, M = mixed or uncertain. A ? implies that no X-ray nebula has been clearly detected yet, but if there is a clear radio or H α morphology, that is indicated in parentheses.

^bIndicates if there is an associated SNR shell. O means it is outside the shell, ? means there is a nearby structure that could be interpreted as a related SNR shell.

^cIndicates coincident γ -ray source. ? implies outside nominal γ -ray error box but possibly still related.

is no observational evidence for the expanding blast wave caused by the supernova. However, presumably there is an external blast wave although the surface brightness of the shell might be very low. PWNe appear to be highly aspherical, sometimes with thick torii, sometimes dominated by narrow, jet-like features. How this asphericity may affect the evolution of the PWN is not well understood, although it is plausible that the mere addition of a filling factor to the standard equations could adequately

Table 7.6. *PWNe With No Detected Pulsar*

Nebula	other name	d (kpc)	M	S	γ	Reference
G0.13−0.11		?	M	N	?	Wang et al. 02
G0.9+0.1		8	T	Y	N	Porquet 03
G7.4−2.0	GeV J1809−2327	1.9	J	?	Y	Braje et al. 02
G16.7+0.1		2.2	M	Y	N	Helfand et al. 03
G18.5−0.4	GeV J1825−1310	4.1	J	?	Y	Roberts et al. 01
G20.0−0.2		5.4	?	N	N	Becker & Helfand 85a
G21.5−0.9		5.5	M	N	N	Slane et al. 00
G24.7+0.6			?	N	N	Reich et al. 84
G27.8+0.6			?	N	N	Reich et al. 84
G39.2−0.3	3C 396	7.7	M	Y	Y	Olbert et al. 03
G63.7+1.1		3.8	?	N	N	Wallace et al. 97
G74.9+1.2	CTB 87	12	M	N	Y	Mukherjee et al. 00
G119.5+10.2	CTA 1	2.1	M	Y	Y	Slane et al. 03
G189.1+3.0	IC 443	1.5	J	Y	?	Olbert et al. 01
G279.8−35.8	B0453−685	50	M	Y	N	Gaensler et al. 03
G291.0−0.1	MSH 11−62	?	J	Y	Y	Harrus et al. 03
G293.8+0.6			?	Y	N	Whiteoak & Green 96
G313.3+0.1	Rabbit	?	J	N	Y	Roberts et al. 99
G318.9+0.4			?	Y	N	Whiteoak & Green 96
G322.5−0.1			?	Y	N	Whiteoak & Green 96
G326.3−1.8	MSH 15−56	4.1	?	Y	N	Dickel et al. 00
G327.1−1.1		8.8	M	Y	N	Bocchino & Bandiera 03
G328.4+0.2	MSH 15−57	> 17	M	N	N	Hughes et al. 00
G359.89−0.08		8	J	N	Y	Lu et al. 03

See footnotes to Table 7.5.

account for the morphological variations (Roberts et al., 2003). Pulsars are generally high-velocity objects, so they rapidly leave their birth site, eventually overtaking the supernova blast wave. The interaction of the pulsar wind with the swept-up shell material can reenergize the shell, which seems to be occurring in the case of CTB80 (Shull et al., 1989; van der Swaluw et al., 2003a). To reach the shell usually takes a few tens of thousand years, and so for the first few thousand years assuming the pulsar is near the center of the SNR is reasonable. Well before the pulsar reaches the SNR shell, it will overtake the outer edge of its original bubble, severely distorting the shape, changing from a spherical/toroidal structure to more of a bow-shock. Since the forward shock of the PWN is generally accelerating within the expanding ejecta (Reynolds & Chevalier, 1984), this will usually not happen until after the PWN forward shock encounters the SNR reverse shock. Analytical and numerical models of this transition suggest it occurs at roughly half the pulsar crossing time of the nebula (van der Swaluw et al., 2003b).

Therefore, for the first few thousand years of a pulsar’s life, the assumptions (other

Table 7.7. *Pulsars with H α Bow-Shock Nebulae*

Name	Pulsar	$\log(\dot{E})$ (erg s $^{-1}$)	d (kpc)	v (km s $^{-1}$)	Reference
Black Widow	J0740–28	35.1	1.9	260	Jones et al. 02
	B1957+20	35.0	2.5	220	Stappers et al. 03
	J0437–4715	33.6	0.14	94	Bell et al. 95
	J2124–3358	33.6	0.27	61	Gaensler et al. 02
Guitar	B2224+65	33.1	3.2	1725	Romani et al. 97

than sphericity) of the standard models are probably valid. The evolutionary picture has been described analytically (e.g. Pacini & Salvati, 1973; Reynolds & Chevalier, 1984) and numerically (e.g. van der Swaluw et al., 2001; Blondin et al., 2001). Since the content and structure of the pulsar wind are poorly understood, it is generally assumed that a spherical outflow of energy equal to the spin-down energy of the pulsar (the observed pulsed electromagnetic radiation being a negligibly small fraction of the energy) continuously flows outwards from the pulsar magnetosphere. This energy is split between the kinetic energy of the bulk particle flow and the magnetic-field energy. At some radius which is small compared to the total radius of the nebula, the electron/positron component of the bulk flow is randomized and takes on a power-law distribution of energies. If this transition is caused by a standing shock, then for efficient shock acceleration of the particles to occur, the flow energetics must be dominated by the particle component at the shock. Kennel & Coroniti (1984a), expanding on the work of Rees & Gunn (1974), constructed a steady state MHD model of the Crab nebula, assuming a positronic wind terminated by an MHD shock whose downstream properties are determined by boundary conditions imposed by the size, X-ray luminosity and expansion velocity of the nebula. The upstream flow properties can then be determined from the Rankine-Hugoniot relations. The ratio of magnetic to particle energy flux σ in the unshocked wind of the Crab is inferred to be $\sigma \sim 0.003$ (Kennel & Coroniti, 1984b). This leads to the well-known “sigma problem” of pulsar wind theory, since mechanisms for accelerating the particles within the magnetosphere generally require $\sigma > 1$ (see §7.2). This suggests that the bulk of the acceleration occurs somewhere in the wind zone outside of the pulsar magnetosphere, for which there is no generally accepted model (e.g. Melatos, 1998; Kirk & Skjærraaasen, 2003).

Although shock theory requires the ratio of magnetic to particle energy just downstream of the wind termination shock to be small, it is expected that the magnetic-field will grow rapidly towards equipartition in the downstream flow. This allows the assumption that the magnetic and particle energy densities are roughly equal throughout the bulk of the PWN. For the first few days after the supernova explosion, the magnetic field density rapidly increases within the nebula, but then the

expansion of the nebula causes the magnetic-field strength to decrease with time despite continuous injection of magnetic energy.

The subsequent evolution of the PWNe can then be separated into two eras of the pulsar spin-down \dot{E} and two eras of the SNR expansion (e.g. Reynolds & Chevalier, 1984). For times $t < \tau \equiv P_0/2\dot{P}_0$, the initial spin-down time of the pulsar (note that this is probably the case for systems where the true age $t \ll \tau_c \equiv P/2\dot{P}$, the *observed* characteristic age of the pulsar), energy will be injected at a nearly constant rate ($\dot{E} \simeq \dot{E}_0$), and the radius of the PWN expands as $R \propto t^{6/5}$ while the average magnetic field strength will decrease as $B \propto t^{1/3}$. For large initial spin periods ($P_0 \gtrsim 50$ ms), the time of nearly constant energy input can last for several thousand years. During this time, the outer edge of the PWN bubble is moving supersonically compared to the surrounding medium, and so a forward shock should form, heating the swept-up ejecta which is in a thin shell around the PWN. The total mass of the swept-up material is initially fairly small, and so the thermal luminosity of this material may not be very large. At later times ($t > \tau$ or $t \sim \tau_c$) when $\dot{E} \ll \dot{E}_0$, the expansion slows to $R \propto t$ if the SNR is still in its free expansion phase.

The blast wave of the surrounding SNR shell initially expands almost freely into the ISM (or into a surrounding bubble blown by the wind of the pre-supernova progenitor star Chevalier, 1982), shock heating the swept-up material. As the swept-up mass builds, a reverse shock forms and begins to propagate towards the center of the SNR, heating the ejecta. This reverse shock will reach the center of the SNR when the swept-up ISM mass is much greater than the ejecta mass, marking the beginning of the so-called Sedov-Taylor phase of the SNR (Sedov, 1959). Until this time, there are four shocks in the system: the forward shock of the SNR blast wave propagating into the ISM, the reverse shock of the SNR blast wave propagating back into the freely expanding ejecta interior to the shock, the forward shock of the PWN bubble, and the PWN reverse shock/wind termination shock (Figure 7.13). When the SNR reverse shock encounters the PWN forward shock, numerical simulations show the PWN is initially compressed, and then its radius oscillates a few times over the next several thousand years before settling down into a more compact and probably distorted shape (van der Swaluw et al., 2001). During the compression, the magnetic field is enhanced causing an increase in the synchrotron luminosity and filaments can develop due to Rayleigh-Taylor instabilities (Blondin et al., 2001). If the pulsar wind luminosity is still near its initial luminosity ($\dot{E} \simeq \dot{E}_0$) after this compression, the PWN begins to grow again, but now the expansion is subsonic with $R \propto t^{11/15}$. If, on the other hand, $\dot{E} \ll \dot{E}_0$ then the expansion of the PWN goes as $R \propto t^{1/3}$ (Reynolds & Chevalier, 1984).

7.6.4 Emission Spectra of PWNe

The relativistic particle gas that fills the PWN bubble loses energy through synchrotron radiation and adiabatic expansion. Since the observed radiation spectrum has the form of a broken power law, a power-law electron energy spectrum is suggested, with the particle spectral index s (defined as $N(E) \propto E^{-s}$) related to the radiation spectral index α by $s = 2\alpha + 1$. The simplest model is of a single electron population injected into a uniformly magnetized nebula with a single spectral index S and a high energy cut-off E_{ec} (Chevalier, 2000). Synchrotron radiation is usually

the most important cooling process for the X-ray emitting electrons, with the typical timescale t_c for cooling dependent on the electron energy and the magnetic field. At high energies, $t_c \ll t$, the age of the PWN, and an approximate steady state can be assumed between the injection and cooling of the electrons. In this regime, the average particle spectrum in the nebula is $S + 1$ which corresponds to a steepening of the observed spectrum by $\Delta\alpha = 0.5$. A break in the particle spectrum occurs at an energy where $t_c \sim t$, resulting in a break in the observed photon spectrum at:

$$\nu_b = \frac{1.68}{B^3 t^2} \text{GHz},$$

where B is in Gauss and t is in years. Note that since B decreases with time, this break frequency actually increases as the PWN ages. At low energies ($t_c \gg t$), cooling losses are negligible, and the particle spectral index is simply that of the injection spectrum. At late times when $\dot{E} \ll \dot{E}_0$, the initial cooling of the large number of particles injected at early times can leave an imprint on the particle spectrum in the form of a separate break below ν_b whose frequency decreases with time due to losses from the adiabatic expansion of the nebula. This results in an intermediate particle spectral index $S > s > S + 1$ between the two breaks (Reynolds & Chevalier, 1984). The passage of the reverse shock causes a brightening of the nebula and an enhancement of the magnetic field. The high-energy electrons all rapidly lose their energy, resulting in a spectral cutoff of the electron population. After the reverse shock passes, the low-energy spectrum is dominated by the old electrons with enhanced emission, while the high-energy spectrum is from newly injected particles, with a middle range below the post-reverse-shock cooling break which could have a fairly steep spectrum, i.e. $s_m > S + 1$.

It is tempting to identify the radio emission with the uncooled $s = S$ spectrum and the X-ray emission with the cooled $s = S + 1$ spectrum. However, this predicts $\Delta\alpha = 0.5$ and in many cases it is significantly greater (Woltjer et al., 1997). If the X-ray or radio emitting particles were in the adiabatically cooled regime, $\Delta\alpha < 0.5$. The only time a single injection spectrum would fit this situation is after the reverse shock passage if the cooling break is above the soft X-ray band. In this case, there should be a spectral hardening somewhere in the hard X-ray or soft γ -ray band. Another possibility is that the injection spectrum has changed over time. However, a correlation between PWNe X-ray spectral indices and \dot{E} showing a softening with increasing \dot{E} has been claimed (Gotthelf, 2003), implying the spectral index is decreasing with age. This would again lead to $\Delta\alpha < 0.5$. A third possibility is that more than one electron population is being injected into the nebula, one dominant at low energies and a second at high energies (Bandiera et al., 2002). It is now clear that many, if not most, PWNe consist of both equatorial outflows and polar outflows, the latter in the form of collimated jets. It might be expected that the two flows would inject particles into the PWN with different spectral slopes. Such a situation would often require the polar flows to be relatively underluminous in the X-ray region. A more fundamental problem is the flatness of the PWN spectra in radio. Both theoretical models (Kirk et al., 2000) and observations of other astrophysical shocks which produce radio emitting electrons (eg. SNR shells and AGN jets) tend to produce emission spectral indices of $\alpha \sim 0.6$ and then cool to $\alpha \sim 1.1$. The

only workable mechanism for producing the radio spectra of PWN currently in the literature is one developed for the Crab where a low-energy cut-off which is rapidly cooled during the early spin-down era (Atoyan, 1999). However, this requires some fine tuning of the magnetic field evolution of the PWN as well as a non-standard spin-down history for the pulsar, and it is not clear whether this can be consistently applied to other PWN. Alternative models for the acceleration of the radio emitting particles at sites in the nebula other than the termination shock should be explored.

In the above discussion, it has been implicitly assumed that the electrons have been injected evenly throughout the nebula, the so-called one-zone model (Chevalier, 2000). In a real PWN, the electrons are injected at the termination shock within a few tenths of a parsec from the pulsar and then propagate outwards, initially at the typical post-shock velocity $v \simeq c/3$ but then with the bulk velocity typically decreasing as $1/r^2$ (this is true whatever the emission geometry, since the nebula will have an r^2 expansion as long as the external confinement is spherically symmetric; this is probably not the case for some rPWN – see §7.6.7). If the PWN bubble is large enough, the X-ray emitting particles will have a chance to cool significantly before reaching the outer edge, and it is expected that the X-ray spectral index will increase as a function of distance from the pulsar. For all energies where the travel time to the outer edge of the PWN is more than the synchrotron cooling time, then the PWN should decrease in size with increasing energy. Therefore, we should expect the radio PWN to be larger than the X-ray PWN. Kennel & Coroniti (1984b) modelled this in detail, and found the integrated X-ray spectral index should be $\Delta\alpha = (4+\alpha/9)$ larger than that of the uncooled particles emitting just downstream of the termination shock. For reasonable values of $\alpha = 0.0 - 1.0$, $\Delta\alpha = 0.44 - 0.56$, very close to the simple, one-zone model estimate of $\Delta\alpha = 0.5$. The spatial resolution of *Chandra* and *XMM-Newton* has allowed this increase in spectral index with radius to be observed in several PWNe (e.g. Weisskopf et al., 2000; Slane et al., 2000; Porquet et al., 2003).

7.6.5 *The Crab and Other Classic “Plerions”*

Until recently, observational and theoretical studies of PWNe have been dominated by the Crab nebula. It contains the most energetic pulsar known in the Galaxy, it is bright at all wavelengths, has a precisely known age due to historical records of the associated supernova, and has been intensely studied for over 100 years. It had been the defining member of the class of “supernova remnants” with no observable shells, sometimes called *plerions* meaning filled center (Weiler, 1978), and provided the conclusive proof that neutron stars are born in Type II supernovae. Ironically, although it has been known as the remnant of SN 1054 A.D. for many years, it is something of a misnomer to call it a SNR since the nebula is a result of the pulsar wind and not the blast wave of the supernova itself. Why there is no observable radio shell is still uncertain, with explanations including that it is in a low density region of the ISM and that SN 1054 was an anomalously low-energy event (Frail et al., 1995). There are several other PWNe in the Galaxy with no observable shell, typified by 3C 58 (Reynolds & Aller, 1985). They tend to have much lower X-ray luminosities and harder spectra than the Crab. The inferred break energies between the radio and X-ray spectra of these other PWNe also tend to be much lower than that of the Crab’s breaks (Woltjer et al., 1997). Whether these differences can

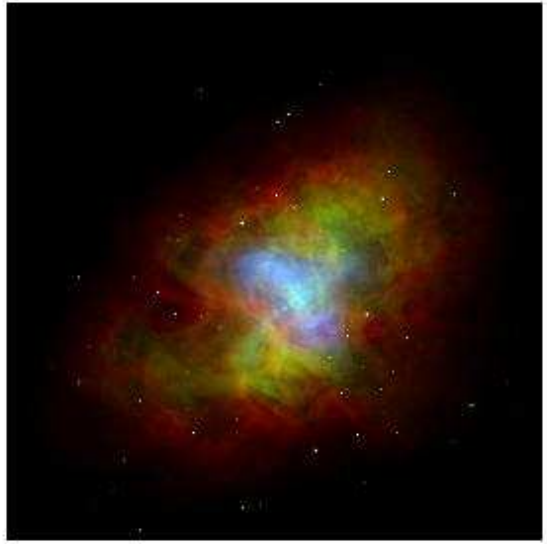


Fig. 7.14. A composite image of the Crab Nebula showing X-ray in blue, optical in green, and radio in red. (Credits: X-ray: NASA/CXC/ASU/J. Hester et al.; Optical: NASA/HST/ASU/J. Hester et al.; Radio: VLA/NRAO) (from Chandra website <http://chandra.harvard.edu>)

be ascribed completely to the difference in spin-down energies is debatable, but since observations of the Crab tend to be of much higher quality than of all other PWNe, attempting to interpret what is viewed by scaling from the Crab is somewhat inevitable. The PWN whose properties are most similar to the Crab's is that around PSR B0540–69, often referred to as the Crab's twin, in the Large Magellenic Cloud (Chanan et al., 1984; Manchester et al., 1993; Gotthelf & Wang, 2000).

At radio energies, the Crab appears as an ovoid blob with a superimposed filamentary structure. The radio spectral index is remarkably spatially uniform (Bietenholz et al., 1997), and the emission is mostly constant except for a slow expansion (Velusamy et al., 1992) and a long term overall decline in its flux (Aller & Reynolds, 1985b). Recently, variations in the form of small ripples in the nebula have been detected whose general morphology correspond to the regions of activity seen in the optical and X-ray nebulae (Bietenholz et al., 2001). The radio emission is highly linearly polarized and well organized, showing that the emission mechanism is almost certainly synchrotron (Bietenholz & Kronberg, 1990).

At optical energies the Crab is somewhat smaller than in the radio, and consists of thermal filaments superimposed on a polarized non-thermal continuum. Near the pulsar, there is an underluminous region probably associated with the unshocked wind. Outside of this zone, there is a series of bright, non-thermal enhancements, re-

ferred to as wisps, that have been known for a long time to be variable on timescales of months (Lampland, 1921; Oort & Walraven, 1956; Scargle, 1969). Monitoring observations with the Hubble Space Telescope have shown the enhancements, the innermost one starting at the edge of the underluminous zone which is presumably at the wind termination shock, move outwards over several weeks to months (Hester et al., 1996). One model of the radial placement of the wisps posits that if the wind contains a significant fraction of ions, the post-shock ions would cause enhancements in the magnetic field at multiples of their cyclotron radius, and hence be sites of enhanced synchrotron emission (Gallant & Arons, 1994).

In X-rays, the Crab has a very definite toroidal morphology with polar jets. Again, surrounding the pulsar is an underluminous zone ending in a bright ring with knotty enhancements which have been observed with *Chandra* to form and move outwards at $v \sim 0.5c$ and then diffuse, similar to the optical wisps (Hester et al., 2002). Outside of this region is a thick torus, which ends rather abruptly well within the boundaries of the optical and radio nebula (Fig. 7.14). There is clear evidence of spectral steepening with increasing radius in the torus. The jets emit a much smaller fraction of the X-ray luminosity than does the torus, and overall have a harder spectrum. Outward motion of features within the jets has also been observed. The proper motion of the pulsar is along the line of the jets, suggesting the natal kick was along the spin axis of the pulsar (Caraveo & Mignani, 1999; Weisskopf et al., 2000).

The unpulsed, and hence presumably nebular, emission spectrum is seen to extend smoothly from the X-rays all the way to ~ 25 MeV. Above this is a sharp, possibly variable cut-off (de Jager et al., 1996a) indicating some limiting factor in the particle acceleration mechanism. Above ~ 100 MeV, a rising unpulsed component is seen which can be observed all the way into the TeV energy range (Weekes, 1991). This is most likely due to inverse Compton scattering off the synchrotron emitting electrons in the nebula.

Since the Crab is energetically unique among Galactic pulsars, it is valid to wonder if its properties can be legitimately scaled down over two orders of magnitude to other pulsars with more typical spin-down energies. 3C 58 was the second plerion to be identified and is thought to be a result of SN 1181. Its pulsar, which was only recently discovered through X-ray and very deep radio observations (Murray et al., 2002; Camilo et al., 2002c), has a spin-down energy of $2.7 \times 10^{37} \text{ erg s}^{-1}$, second only to the Crab among Galactic PWNe. Although its spin-down energy is only a factor of ~ 15 less than the Crab's and the nebular radio luminosity is a factor of ~ 10 less than the Crab nebula, the nebular X-ray luminosity is a factor of ~ 1000 less (Becker et al., 1982; Murray et al., 2002). There appears to be an unusually sharp spectral break (Green & Scheuer, 1992) at ~ 50 GHz. The radio luminosity appears to be increasing, suggesting the unseen SNR reverse shock may already be affecting the PWN (Aller & Reynolds, 1985a).

The Vela pulsar is generally considered to be the prototype of pulsars with $\tau_c \sim 10,000$ yr and spin-down energies in the $10^{36} - 10^{37} \text{ erg s}^{-1}$ range. Its PWN appears very bright and can be well-resolved at X-ray energies because of its proximity to Earth, being only ~ 290 pc away (Dodson et al., 2003a). There is an associated radio SNR shell, but it is patchy, uneven, and diffuse, as is typical of older remnants (Clark & Caswell, 1976), having three sections called Vela X, Y, and Z.

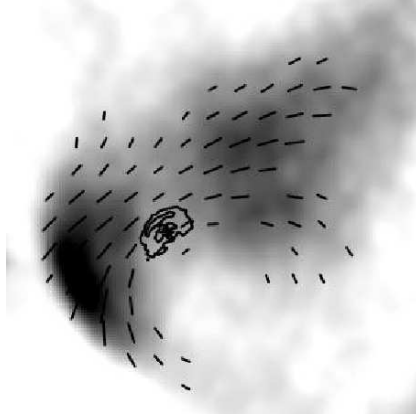


Fig. 7.15. 5 GHz *ATCA* image of the Vela radio lobes near the pulsar with polarization vectors showing how highly structured the magnetic field is. The contours near the center are of the X-ray nebula as seen with *Chandra*. Note this is only a small part of the Vela X radio region. Adapted from Fig. 10 of Dodson et al. (2003b)

Weiler & Panagia (1980) noted that the Vela X region had radio properties more similar to the Crab and other plerions than to ordinary SNR shells. Due to the age of the Vela SNR, it is likely that the reverse shock encountered the PWN long ago, although there may still be some transient effects. The morphology of the Vela PWN in X-rays is a double arc with narrow, jet-like enhancements, again near the line of proper motion. While this has sometimes been interpreted as a bow-shock morphology, it is now usually interpreted as a double torus (Helfand et al., 2001). An apparently variable, extended jet feature is sometimes prominent (Pavlov et al., 2003) outside of the arcs. There is no clear indication of an underluminous region near the pulsar, although that may be due to an unfortunate viewing angle, and the observed double-arc system may be the location of the termination shock.

The physical size of the bright part of the Vela X-ray PWN is about an order of magnitude smaller than the Crab, and its X-ray efficiency in the 1–10 keV band is more than two orders of magnitude less. The X-ray spectrum is flatter and the high-energy cut-off is probably less than 10 MeV (de Jager et al., 1996b). Whether these are indicative of a general trend of lower efficiency, spectral hardening, and lower maximum particle energies with lower \dot{E} is difficult to say, although there is some evidence for a dependency of spectral index on \dot{E} (Gotthelf, 2003) and the maximum potential drop across the open field lines $E_{max} \propto \dot{E}^{1/2}$ so there is a theoretical expectation for a lower high-energy cutoff (de Jager et al., 1996a). The X-ray PWN is centered between two radio lobes which are much larger than the X-ray PWN (Fig. 7.15 Dodson et al., 2003b), and are themselves just a small part near the edge of the filamentary, flat spectrum Vela X radio complex. It is likely the reverse shock has displaced the larger radio nebula which is why the proper motion vector of the pulsar is not directed away from the center of Vela X (Blondin et al., 2001).

7.6.6 Young Composite SNR

The standard theoretical picture of a PWN growing within the expanding shell of the supernova blast wave has been around since the early eighties. Although quite a few young composite SNR were known at that time (Helfand & Becker, 1987), in embarrassingly few cases had the exciting pulsar been observed. While the unknown radio beaming could be invoked to account for the lack of observable radio pulsations, this situation made it difficult to confront theoretical expectations with observational realities. Since the mid-nineties, several pulsars have been discovered within young composites by deep radio searches (Camilo et al., 2000, 2002b) or with sensitive X-ray searches (Torii et al., 1997; Gotthelf et al., 2000), representing different stages and scenarios in the early evolution of PWN systems.

Perhaps the system whose observational properties best match the assumptions made in the models is G11.2–0.3. This bright, remarkably circular remnant is often associated with a “Guest Star” observed by the Chinese in 386 A.D. (Clark & Stephenson, 1977) and the age inferred from expansion measurements of shell support this association (Tam & Roberts, 2003). HI absorption measurements place the remnant at a distance of ~ 5 kpc (Green et al., 1988). A 65-ms X-ray pulsar is within a few arcseconds of the geometrical center of the shell (Kaspi et al., 2001b) which has a characteristic age of 24,000 yr; over ten times that of the SNR (Torii et al., 1997) strongly implying $P_0 \simeq P$ and $\dot{E} \simeq \dot{E}_0$. High-resolution radio and X-ray observations have separated the PWN from the shell and measured its spectrum (Tam et al., 2002; Roberts et al., 2003).

We therefore have in G11.2–0.3 an example of a composite remnant where the assumptions of near spherical symmetry of the shell and negligible displacement of the pulsar from its birthsite are demonstrably true, the energy output history is well constrained to be nearly constant, the age is known, and the distance is fairly well determined. Given its age and estimates of the swept-up mass, it should be nearing the Sedov phase, so the reverse shock should be nearing the PWN. However, the radio PWN is one of the largest relative to the shell and there is marginal evidence it is expanding (Tam & Roberts, 2003), suggesting the reverse shock has not yet begun to crush the PWN bubble. It therefore should still be expanding supersonically, and may be shock-heating the surrounding ejecta. There is thermal X-ray emission which seems to be morphologically related to the radio PWN, but may also be a region of enhanced shell emission seen in projection (Fig. 7.16). The velocity of the shell inferred from the thermal emission is consistent with that inferred from the expansion rate and HI distance estimates (Tam & Roberts, 2003).

Current estimates of the X-ray and radio spectral indices are consistent with a single cooling break in between. However, given the age of the nebula, the implied magnetic field is unusually high. If it uniformly fills a region of the apparent bubble size, then the required magnetic energy is much larger than could have been supplied by the pulsar. This may indicate that the pulsar wind is highly non-spherical, predominantly coming from within $\sim 10^\circ$ of either the poles or the equator. The narrowness of the X-ray emission may support this interpretation (Roberts et al., 2003). Varying X-ray spots are seen in this nebula as well, with apparent motions of $\sim c$, much faster than the expected $c/3$ of a standard post-shock flow. So even with

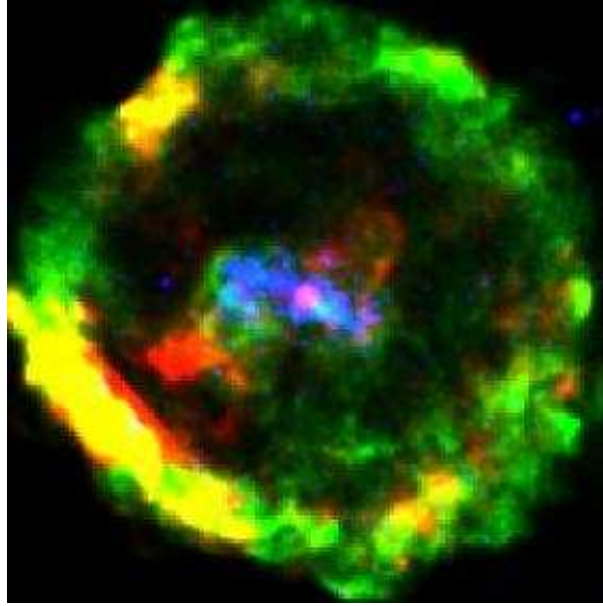


Fig. 7.16. *Chandra* and VLA image of G11.2–0.3 and its central PWN showing the relationship between the soft thermal X-ray emission (red), the radio synchrotron emission (green) and the hard, non-thermal X-ray emission (blue). The point source at the center is the pulsar, only seen in X-rays. Adapted from Fig. 1 of Roberts et al. (2003).

this most “simple” of PWN/SNR systems where our knowledge is most complete, there are anomalies which are not well understood.

Kes 75 is a young ($\tau \lesssim 2000$ yr) distant ($d \sim 19$ kpc Becker & Helfand, 1984) composite SNR in many ways similar to G11.2–0.3. It contains a 324 ms X-ray pulsar with the youngest known characteristic age, ~ 700 yr (Gotthelf et al., 2000). The *Chandra* image of Kes 75 (Helfand et al., 2003b) of both the shell and PWN in both X-rays and radio of Kes 75 look very similar to G11.2–0.3, and the pulsars powering both PWN are very X-ray efficient and have unusually broad profiles. However, on closer examination, there are remarkable differences. The X-ray efficiency in the 0.5–10 keV band of the PWN in Kes 75 is $\sim 6.5\%$, which is the highest known, while that of G11.2–0.3 is only $\sim 0.2\%$, a much more typical value. The pulsar’s spin parameters imply both an unusually large magnetic field ($B \sim 5 \times 10^{13}$ G) and that $P_0 \ll P$, so that the energy input into the PWN has changed dramatically over its short history. The implied size of the shell of Kes 75 requires an enormous expansion velocity ($v \sim 13,000 \text{ km s}^{-1}$) and therefore implies a remarkably energetic explosion or else the neutron star was born spinning very rapidly and a significant fraction of its rotational kinetic energy was somehow transferred to the expanding ejecta (Helfand et al., 2003b).

SNR G292.0+1.8 is an example of a slightly older ($\tau \sim 3000$ yr) composite system. *Chandra* imaging shows a remnant filled with ejecta material, but there is also a clear X-ray PWN slightly offset from the geometrical center (Hughes et al., 2001). In this

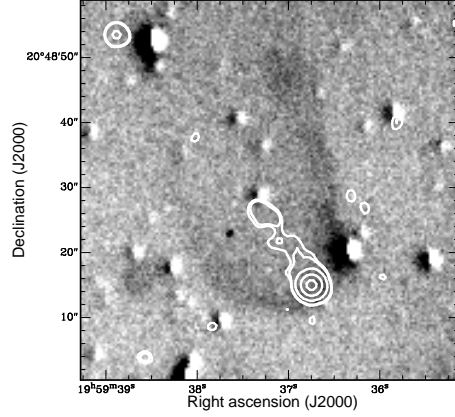


Fig. 7.17. $H\alpha$ image of Black Widow pulsar PSR B1957+20 with *Chandra* X-ray contours. Adapted from Fig. 2 of Stappers et al. (2003).

case there is no clear morphological separation between the radio PWN and shell and it seems likely that the SNR reverse shock has recently begun to interact with the PWN (Gaensler & Wallace, 2003).

7.6.7 The Duck and Other PWNe with Trail Morphologies

Several PWNe show a predominantly trail morphology at X-ray, and sometimes radio, wavelengths extending from an X-ray point source, presumably the pulsar, back towards the apparent birth-site. This has been observed in pulsars both within the SNR shell, such as PSR B1853+01 in W44 (Petre et al., 2002), and outside such as coming from PSR B1757–24, the head of the Duck system (Kaspi et al., 2001a). X-ray trails have also been seen from sources with $H\alpha$ bow-shock nebulae, such as the Black Widow binary millisecond pulsar system PSR B1957+20 (Stappers et al., 2003, see Fig. 7.17). The apparent radio bow-shock PWNe source associated with the possibly variable γ -ray source GeV J1809–2328 also shows a clear point source and trail morphology in X-rays (Braje et al., 2002). These type of PWNe are the most common around pulsars with spin-down energies $\log \dot{E} \lesssim 36.5$ (in erg s^{-1}). These nebulae are sometimes referred to as bow-shock nebulae or ram-pressure confined nebulae, however it is not clear if either of these terms accurately reflect the physical situation in respect to the X-ray and radio nebulae. Therefore, we will simply refer to these nebulae as rapidly-moving PWNe (rPWN), where the pulsar’s motion is rapid relative to the radial expansion of the nebula and probably relative to the local sound speed.

The Duck is an illustrative case. Upper limits on the proper motion of the pulsar (Gaensler & Frail, 2000; Thorsett et al., 2002) rule out the X-ray emission being an actual trail, since the synchrotron lifetime of the X-ray emitting particles is too short for the pulsar to have moved the length of the X-ray emitting region in the required time (Kaspi et al., 2001a). The X-ray emission is therefore due to a collimated out-flow, somehow constrained to move within a cavity created by the pulsar’s passage.

A spectacular *Chandra* X-ray image of the Mouse shows the structure of the X-ray nebula to consist of a narrow tail region in a broader, fainter, bow-shaped nebula which may be too faint to see clearly in the Duck (Gaensler et al., 2003c). The extremely long radio tail of the Mouse (Predehl & Kulkarni, 1995) is another example where it seems something must continue to confine the flow well beyond where ram-pressure from the pulsar’s passage should no longer be relevant. The extraordinary jet/trail coming from PSR B1509–58 (Gaensler et al., 2002) also demonstrates that in many cases pulsar outflows can be narrowly confined over large distances even while still within the parent SNR.

The Black Widow pulsar PSR 1557+20 (Fruchter et al., 1988), so called because its wind is believed to be destroying its white dwarf companion, is interesting for several reasons. Unlike the other sources with X-ray trails, it is a millisecond pulsar, demonstrating that old, recycled pulsars also have relativistic winds. It also has an $H\alpha$ nebula (Kulkarni & Hester, 1988) which clearly delineates the forward bow-shock as well as a narrow trail of non-thermal X-ray emission (Stappers et al., 2003) which can serve as a test bed for simulations of rPWNe (Bucciantini, 2002).

7.6.8 The γ -Ray Connection

The magnetosphere of a young pulsar is one of the few places in the universe where particles can be accelerated such that they will emit high-energy γ -ray emission through either the synchrotron process, curvature radiation, or inverse Compton scattering. Approximately 1/3 of the known PWNe are coincident with sources of emission at $E > 100$ MeV observed by the EGRET instrument on the *Compton Gamma Ray Observatory* (Hartman et al., 1999). Some of these are the known γ -ray pulsars (Thompson et al., 1999), and this may be an indication that the potential needed to produce pulsed γ -ray emission observable at typical Galactic distances is similar to that needed to produce observable PWNe. However, several of the PWNe are associated with unidentified EGRET sources which appear to be variable (Roberts et al., 2001; Nolan et al., 2003) on timescales of a few months, similar to the synchrotron cooling timescale at these energies, indicating that the PWN may be the source of emission. Practically speaking, γ -ray sources can serve as tracers of PWNe. Six of the PWNe listed in Tables 7.5 and 7.6 were initially discovered through X-ray imaging of a γ -ray error box. In addition, the shape of PWNe can be used to infer the viewing angle, and possibly the magnetic inclination angle, of the pulsar (e.g. Ng & Romani, 2004) which is critical information for testing models of pulsed γ -ray emission (§7.2). Observations from the upcoming GeV energy telescopes *AGILE* and *GLAST* will be able to distinguish between pulsed and unpulsed emission from many of these sources, verify any variability, and locate more PWNe buried deep in the Galactic plane.

Steady, unpulsed emission up to several TeV has been observed towards three pulsars (Crab, Vela, and PSR B1706–44 Weekes, 1991; Yoshikoshi et al., 1997; Kifune et al., 1993) with PWNe, presumably caused by inverse Compton scattering by electrons in the inner nebula. This is direct evidence of very high energy acceleration and puts constraints on the magnetic field in the inner nebula. As the new generation of ground based Cerenkov air shower telescopes comes on line, many more PWNe will undoubtedly be observed at energies of ~ 100 GeV to a few TeV.

7.6.9 *Current Trends and Future Directions*

The high-resolution X-ray imaging capabilities of the *Chandra* and *XMM-Newton* telescopes are allowing detailed study of the structure of many PWNe. The presence of collimated jet-like outflows as a common feature of PWNe is a surprise which most models of PWNe, dominated by a toroidal equatorial flow, did not allow for. New analytical and numerical models are now being developed with varying amount of power being lost through polar outflows (Khangoulia & Bogovalov, 2003; Komissarov & Lyubarsky, 2003; Shibata et al., 2003). PWNe have also been shown to be dynamical X-ray systems with observable variations on timescales as short as a few weeks (Hester et al., 2002). As quantitative measurements of these variations are made in more PWNe the need for the further development of models of acceleration in the inner nebula becomes more acute.

The remarkable diversity of PWNe has also been a surprising result of the new X-ray images. Many of the observations currently archived are too short to distinguish different spectral characteristics of the various features within PWNe. There is a suggestive correlation between the X-ray spectral index of PWNe and the magnetospheric potential (Gotthelf, 2003), but whether this will be born out by further observations and whether there is a different correlation for jet-like and toroidal structures will require deep observations of many more PWNe. The structure of the PWNe also seems to depend on the magnitude and direction of the pulsar's velocity, but so far only a few young pulsars have had their proper motions measured. Radio interferometry campaigns now underway (e.g. Briskin et al., 2003a) promise to greatly increase the number of measured pulsar transverse velocities, allowing the determination of how well jets are aligned with velocity vectors (e.g. Dodson et al., 2003a), if at all. New 2-D and 3-D numerical simulations of PWN evolution are beginning to yield intriguing results. For example: relaxing the spherical symmetry outflow constraint but keeping axial symmetry leads to a multiplicity of shock regions that can mimic the Crab morphology (Komissarov & Lyubarsky, 2003). Toroidal magnetic outflows can cause an elongation of PWNe with spherical particle outflows, reminiscent of the shape of 3C58 (van der Swaluw, 2003), and interactions with the reverse shock can lead to complicated, asymmetric morphologies (Blondin et al., 2001; Bucciantini et al., 2003).

7.7 **X-rays from Rotation-Powered Pulsars in Binary Systems**

For completeness, we mention briefly another related source of X-rays from rotation-powered pulsars – shock emission in binary systems. Although these systems do not obviously satisfy the mandate of this chapter on “isolated neutron stars,” the nature of their X-ray emission is very similar to that in a PWN. For high- \dot{E} pulsars in binary systems, the confining medium can be the wind of the companion star. In this case, the confinement, particularly for eccentric binaries, is strongly orbital-phase dependent, leading to a PWN of luminosity (and, presumably, size) that varies systematically with orbital phase. Even circular orbits are of interest since the orientation of the PWN, which, in this case, is not expected to be isotropic, changes with orbital phase. In principle, such systems are an excellent diagnostic of shock acceleration and the pulsar wind as they have regular, repeating and predictable dynamical properties. They also represent a new form of “X-ray binary,” one not

7.7 X-rays from Rotation-Powered Pulsars in Binary Systems 57

powered by accretion. However, only two such systems have been detected in X-rays: PSRs 1259–63 and B1957+20. Their rarity is because of the need to have a high \dot{E} pulsar in a binary system in which the two components come sufficiently close to each other for the shock to be strong, but not too close so that accretion occurs.

The 48-ms radio pulsar PSR B1259–63 is in a 3.4 yr binary orbit having eccentricity 0.87 (Johnston et al., 1992). From radio timing, the pulsar is known to have $B = 3 \times 10^{11}$ G and $\tau_c = 3 \times 10^5$ yr. The pulsar’s companion, identified by its location within the $< 1''$ pulsar timing error box, is the 10th mag B2Ve star SS 2883. It has mass $\sim 10 M_\odot$ and radius $\sim 6 R_\odot$, deduced from its spectral type. The system provides an evolutionary link between the rotation-powered pulsars and the high-mass X-ray binaries. For PSR B1259–63, near periastron, the pulsar approaches its companion to within ~ 25 Be star radii. Cominsky et al. (1994) detected variable X-rays from the system near apastron. This ruled out standard wind accretion scenarios, magnetospheric emission, and emission from the companion. Cominsky et al. (1994) suggested either some form of non-standard accretion or the pulsar wind shocked by the companion wind as possible mechanisms for the X-ray emission. Tavani et al. (1994) considered pulsar/Be star wind interactions in detail, in particular, shock emission at the location of pressure balance between the pulsar and Be star winds. They suggested this mechanism produced the apastron X-rays, and predicted PSR 1259–63 would be a moderately strong, unpulsed X-ray source near periastron, unable to accrete due to the shock distance from the pulsar being much larger than the accretion radius. Kaspi et al. (1995) and Hirayama et al. (1996) reported on *ASCA* observations around the periastron of 1994; Hirayama et al. (1999) summarize all the X-ray observations including two more made at the subsequent apastron. The source was clearly seen to increase in intensity by a factor of > 10 near periastron relative to apastron, with the peak luminosity $\sim 10^{34}$ erg s $^{-1}$. The emission was well described at each epoch by a power law, however the photon index clearly varied from 1.6 to 2.0, with the emission softest at periastron. Tavani & Arons (1997) considered the X-ray radiation mechanisms and interaction geometry in detail, showing that a synchrotron/inverse-Compton scattering model of emission of electron/positron pairs accelerated at the inner shock front of the pulsar cavity and adiabatically expanding in the MHD flow explains well the observed time-variable X-ray flux and spectrum. They conclude that most likely the Be-star spin axis is misaligned with the orbital angular momentum, and its mass outflow rate was constant over the ~ 2 -yr period in question. Campana et al. (1995) argue that an unusual Galactic X-ray source, LSI+61°303, is a similar system to PSR B1259–63, but with the radio pulsations permanently eclipsed.

PSR B1957+20 is a 1.6-ms recycled radio pulsar in a 9-hr binary system with a low-mass companion (Fruchter et al., 1988). The pulsar has $\dot{E} = 10^{35}$ erg s $^{-1}$. For $\sim 10\%$ of every orbit, the radio pulsations are eclipsed by the wind from the companion, which is being ablated and, eventually, evaporated, by the pulsar wind. For this reason, the pulsar is sometimes known as the “Black Widow,” as it seems to be destroying the star that gave it new life as a recycled pulsar. The system is surrounded by an H α bow shock nebula, oriented with apex in the direction of the pulsar’s known proper motion, a result of the interaction of the pulsar wind with the ambient interstellar medium (Kulkarni & Hester, 1988). Arons & Tavani

(1994) argued that intra-binary shock emission ought to be observable, because of the interaction of the pulsar wind with material being ablated off the companion. They also argued that X-rays might originate from the bow shock. Of course, magnetospheric X-rays might be detectable from this pulsar as well. The first X-ray detection of PSR B1957+20 came from *ROSAT*, although only handful of photons were detected (Fruchter et al., 1992; Kulkarni et al., 1992), and the conclusions that could be drawn were limited. More recently, *Chandra* observed the PSR B1957+20 system (see Fig. 7.17), and detected both a point source as well as an extended X-ray tail (Stappers et al., 2003). The tail emission is likely related to the bow shock nebula, and represents the first proof that millisecond pulsars have relativistic winds like their much younger counterparts. The origin of the point-source emission is less clear as the observation's time resolution was insufficient to detect pulsations. Planned *XMM-Newton* observations should be able to decide with certainty whether the point source is due to magnetospheric emission, or if it is from the intra-binary shock, as in PSR B1259–63.

The authors thank B. Gaensler and D. Yakovlev for discussions, for careful reading of the manuscript and for many helpful comments. We also thank P. Jaikumar, D. Lai, M. Lyutikov, G. Pavlov, S. Ransom, R. Turolla, M. van Kerkwijk, and S. Zane for helpful conversations, and M. Strickman and J. Dyks for help with figures.

Bibliography

- Aller, H. D. & Reynolds, S. P. 1985a, in *The Crab Nebula and Related Supernova Remnants* (Cambridge University Press), 75–78
- Aller, H. D. & Reynolds, S. P. 1985b, *ApJ*, 293, L73
- Alpar, M. A., Anderson, P. W., Pines, D., & Shaham, J. 1984, *ApJ*, 276, 325
- Arons, J. 1981, *ApJ*, 248, 1099
- . 1983, *ApJ*, 266, 215
- Arons, J. & Scharlemann, E. T. 1979, *ApJ*, 231, 854
- Arons, J. & Tavani, M. 1994, *ApJS*, 90, 797
- Arzoumanian, Z., Chernoff, D. F., & Cordes, J. M. 2002, *ApJ*, 568, 289
- Aschenbach, B. 1998, *Nature*, 141
- Atoyan, A. M. 1999, *A&A*, 346, L49
- Baade, W. & Zwicky, F. 1934, *Proc. Nat. Acad. Sci.*, 20, 254
- Bahcall, J. N. & Wolf, R. A. 1965, *ApJ*, 142, 1254
- Bandiera, R., Neri, R., & Cesaroni, R. 2002, *A&A*, 386, 1044
- Baring, M. G. & Harding, A. K. 2001, *ApJ*, 547, 929
- Becker, R. H. & Helfand, D. J. 1984, *ApJ*, 283, 154
- Becker, R. H. & Helfand, D. J. 1985, *ApJ*, 297, L25
- Becker, R. H., Helfand, D. J., & Szymkowiak, A. E. 1982, *ApJ*, 255, 557
- Becker, W. 2001, in *AIP Conf. Proc. 599: X-ray Astronomy: Stellar Endpoints, AGN, and the Diffuse X-ray Background*, ed. N. White, G. Malaguti, & G. G. Palumbo, 13–24
- Becker, W. & Aschenbach, B. 2002, in *Neutron Stars, Pulsars, and Supernova Remnants*, ed. W. Becker, H. Lesch, & J. Trümper (Garching bei München: Max-Planck-Institut für extraterrestrische Physik), 64
- Becker, W., Brazier, K. T. S., & Trümper, J. 1996, *A&A*, 306, 464
- Becker, W. & Pavlov, G. G. 2002, in *The Century of Space Science*, ed. J. Bleeker, J. Geiss, & M. Huber (Dordrecht: Kluwer)
- Becker, W. & Trümper, J. 1997, *A&A*, 326, 682
- Becker, W. & Trümper, J. 1999, *A&A*, 341, 803
- Becker, W., Weisskopf, M. C., Tennant, A. F., Jessner, A., Dyks, J., Harding, A. K., & Zhang, S. N. 2004, *ApJ*, submitted
- Bell, J. F., Bailes, M., Manchester, R. N., Weisberg, J. M., & Lyne, A. G. 1995, *ApJ*, 440, L81
- Bietenholz, M. F., Frail, D. A., & Hester, J. J. 2001, *ApJ*, 560, 254
- Bietenholz, M. F., Kassim, N., Frail, D. A., Perley, R. A., Erickson, W. C., & Hajian, A. R. 1997, *ApJ*, 490, 291
- Bietenholz, M. F. & Kronberg, P. P. 1990, *ApJ*, 357, L13
- Bignami, G. F., Caraveo, P. A., De Luca, A., & Mereghetti, S. 2003, *Nature*, 423, 725
- Blaes, O. & Madau, P. 1993, *ApJ*, 403, 690
- Blondin, J. M., Chevalier, R. A., & Frierson, D. M. 2001, *ApJ*, 563, 806
- Bocchino, F. & Bandiera, R. 2003, *A&A*, 398, 195
- Braje, T. M. & Romani, R. W. 2002, *ApJ*, 580, 1043
- Braje, T. M., Romani, R. W., Roberts, M. S. E., & Kawai, N. 2002, *ApJ*, 565, L91
- Brinkmann, W. & Ögelman, H. 1987, *A&A*, 182, 71

60 *Bibliography*

- Briskin, W. F., Fruchter, A., Goss, W., Herrnstein, R., & Thorsett, S. 2003a, *AJ*, 126, 3090
- Briskin, W. F., Thorsett, S. E., Golden, A., & Goss, W. M. 2003b, *ApJ*, 593, L89
- Bucciantini, N. 2002, *A&A*, 387, 1066
- Bucciantini, N., Blondin, J. M., Del Zanna, L., & Amato, E. 2003, *A&A*, 405, 617
- Burwitz, V., Haberl, F., Neuhäuser, R., Predehl, P., Trümper, J., & Zavlin, V. 2003, *A&A*, 399, 1109
- Camilo, F. et al. 2001, *ApJ*, 557, L51
- Camilo, F., Kaspi, V. M., Lyne, A. G., Manchester, R. N., Bell, J. F., D'Amico, N., McKay, N. P. F., & Crawford, F. 2000, *ApJ*, 541, 367
- Camilo, F., Lorimer, D. R., Bhat, N. D. R., Gotthelf, E. V., Halpern, J. P., Wang, Q. D., Lu, F. J., & Mirabal, N. 2002a, *ApJ*, 574, L71
- Camilo, F., Manchester, R., Gaensler, B., Lorimer, D., & Sarkissian, J. 2002b, *ApJ*, 567, L71
- Camilo, F. et al. 2002c, *ApJ*, 571, L41
- Campana, S., Stella, L., Mereghetti, S., & Colpi, M. 1995, *A&A*, 297, 385
- Caraveo, P. A., Bignami, G. F., DeLuca, A., Mereghetti, S., Pellizzoni, A., Mignani, R., Tur, A., & Becker, W. 2003, *Science*, 301, 1345
- Caraveo, P. A. & Mignani, R. P. 1999, *A&A*, 344, 366
- Chabrier, G., Potekhin, A. Y., & Yakovlev, D. G. 1997, *ApJ*, 477, L99
- Chakrabarty, D., Pivovarov, M., Hernquist, L., Heyl, J., & Narayan, R. 2001, *ApJ*, 548, 800
- Chanan, G. A., Helfand, D. J., & Reynolds, S. P. 1984, *ApJ*, 287, L23
- Chen, K. & Ruderman, M. 1993, *ApJ*, 408, 179
- Cheng, K. S., Ho, C., & Ruderman, M. 1986, *ApJ*, 300, 500
- Cheng, K. S., Ruderman, M. A., & Zhang, L. 2000, *ApJ*, 537, 964
- Cheng, K. S. & Zhang, L. 1999, *ApJ*, 515, 337
- Chevalier, R. A. 1982, *ApJ*, 259, 302
- Chevalier, R. A. 2000, *ApJ*, 539, L45
- Chiu, H. Y. & Salpeter, E. E. 1964, *Phys. Rev. Lett.*, 12, 413
- Clark, D. & Stephenson, F. 1977, *MNRAS*, 179, 87P
- Clark, D. H. & Caswell, J. L. 1976, *MNRAS*, 174, 267
- Comella, J. M., Craft, H., Lovelace, R., Sutton, J., & Tyler, G. 1969, *Nature*, 221, 453
- Cominsky, L., Roberts, M., & Johnston, S. 1994, *ApJ*, 427, 978
- Contopoulos, J., Kazanas, D., & Fendt, C. 1999, *ApJ*, 511, 351
- Crawford, F., Kaspi, V. M., Manchester, R. N., Lyne, A. G., Camilo, F., & D'Amico, N. 1998, in *Proc. of the Elba Workshop: Neutron Stars and Supernova Remnants*, Vol. 69 (*Memorie della Societa' Astronomica Italiana*), 951–954
- Crawford, F. & Keim, N. C. 2003, *ApJ*, 590, 1020
- Crawford, F., Manchester, R. N., & Kaspi, V. M. 2001, *AJ*, 122, 2001
- Cropper, M., Haberl, F., Zane, S., & Zavlin, V. 2004, *MNRAS*, 351, 1099
- Danner, R. 1998a, *A&AS*, 128, 331
- . 1998b, *A&AS*, 128, 349
- Daugherty, J. K. & Harding, A. K. 1982, *ApJ*, 252, 337
- . 1996, *ApJ*, 458, 278
- de Jager, O. C., Harding, A. K., Michelson, P. F., Nel, H. I., Nolan, P. L., Sreekumar, P., & Thompson, D. J. 1996a, *ApJ*, 457, 253
- de Jager, O. C., Harding, A. K., Sreekumar, P., & Strickman, M. 1996b, *Astronomy & Astrophysics Supplements*, 120, C441+
- De Luca, A., Mereghetti, S., Caraveo, P. A., Moroni, M., Mignani, R. P., & Bignami, G. F. 2004, *A&A*, 418, 625
- Dedeo, S. & Psaltis, D. 2003, *Phys. Rev. Lett.*, 90, 141101
- Deeter, J. E., Nagase, F., & Boynton, P. E. 1999, *ApJ*, 512, 300
- Dickel, J. R., Milne, D. K., & Strom, R. G. 2000, *ApJ*, 543, 840
- Dodson, R., Legge, D., Reynolds, J. E., & McCulloch, P. M. 2003a, *ApJ*, 596, 1137
- Dodson, R., Lewis, D., McConnell, D., & Deshpande, A. A. 2003b, *MNRAS*, 343, 116
- Drake, J. J. et al. 2002, *ApJ*, 572, 996
- Dyks, J., Harding, A. K., & Rudak, B. 2004, *ApJ*, 606, 1125
- Dyks, J. & Rudak, B. 2003, *ApJ*, 598, 1201
- Endal, A. S. & Sofia, S. 1978, *ApJ*, 220, 279
- Fesen, R. A. & Kirshner, R. P. 1982, *ApJ*, 258, 1

- Fierro, J. M., Michelson, P. F., Nolan, P. L., & Thompson, D. J. 1998, *ApJ*, 494, 734
- Finley, J. P., Ogelman, H., & Kiziloglu, U. 1992, *ApJ*, 394, L21
- Finzi, A. & Wolf, R. A. 1969, *ApJ*, 155, 107
- Flowers, E. G., Ruderman, M., & Sutherland, P. G. 1976, *ApJ*, 205, 241
- Frail, D. A., Kassim, N. E., Cornwell, T. J., & Goss, W. M. 1995, *ApJ*, 454, L129
- Frail, D. A. & Scharringhausen, B. R. 1997, *ApJ*, 480, 364
- Freire, P. C., Kramer, M., Lyne, A., Camilo, F., Manchester, R., & D'Amico, N. 2001, *ApJ*, 557, L105
- Fruchter, A. S., Bookbinder, J., Garcia, M. R., & Bailyn, C. D. 1992, *Nature*, 359, 303
- Fruchter, A. S., Stinebring, D. R., & Taylor, J. H. 1988, *Nature*, 333, 237
- Gamow, G. & Schoenberg, S. 1941, *Phys. Rev.*, 59, 539
- Gaensler, B. M., Arons, J., Kaspi, V., Pivovarov, M., Kawai, N., & Tamura, K. 2002, *ApJ*, 569, 878
- Gaensler, B. M., Bock, D. C.-J., & Stappers, B. W. 2000a, *ApJ*, 537, L35
- Gaensler, B. M. & Frail, D. A. 2000, *Nature*, 406, 158
- Gaensler, B. M., Hendrick, S. P., Reynolds, S. P., & Borkowski, K. J. 2003a, *ApJ*, 594, L111
- Gaensler, B. M., Jones, D. H., & Stappers, B. W. 2002, *ApJ*, 580, L137
- Gaensler, B. M., Schulz, N., Kaspi, V., Pivovarov, M., & Becker, W. 2003b, *ApJ*, 588, 441
- Gaensler, B. M., Stappers, B. W., Frail, D. A., & Johnston, S. 1998, *ApJ*, 499, L69
- Gaensler, B. M., Stappers, B. W., Frail, D. A., Moffett, D. A., Johnston, S., & Chatterjee, S. 2000b, *MNRAS*, 318, 58
- Gaensler, B. M., van der Swaluw, E., Camilo, F., Kaspi, V. M., Baganoff, F. K., Yusef-Zadeh, F., & Manchester, R. N. 2003c, *ApJ*, in press (astro-ph/0312362)
- Gaensler, B. M. & Wallace, B. J. 2003, *ApJ*, 594, 326
- Gallant, Y. A. & Arons, J. 1994, *ApJ*, 435, 230
- Garmire, G. P., Pavlov, G. G., Garmire, A. B., & Zavlin, V. E. IAU circular 7350
- Giacani, E. B., Frail, D. A., Goss, W. M., & Vieytes, M. 2001, *AJ*, 121, 3133
- Goldreich, P. & Julian, W. H. 1969, *ApJ*, 157, 869
- Gonzalez, M. & Safi-Harb, S. 2003, *ApJ*, 591, L143
- Gotthelf, E. V. 2003, *ApJ*, 591, 361
- Gotthelf, E. V., Halpern, J. P., & Dodson, R. 2002, *ApJ*, 567, L125
- Gotthelf, E. V., Petre, R., & Vasisht, G. 1999, *ApJ*, 514, L107
- Gotthelf, E. V., Vasisht, G., Boylan-Kolchin, M., & Torii, K. 2000, *ApJ*, 542, L37
- Gotthelf, E. V. & Wang, Q. D. 2000, *ApJ*, 532, L117
- Green, D. A., Gull, S. F., Tan, S. M., & Simon, A. J. B. 1988, *MNRAS*, 231, 735
- Green, D. A. & Scheuer, P. A. G. 1992, *MNRAS*, 258, 833
- Greiveldinger, C. et al. 1996, *ApJ*, 465, L35
- Grindlay, J. E., Camilo, F., Heinke, C., Edmonds, P., Cohn, H., & Lugger, P. 2002, *ApJ*, 581, 470
- Gudmundsson, E. H., Pethick, C. J., & Epstein, R. I. 1983, *ApJ*, 272, 286
- Haberl, F. 2003, in *High Energy Studies of Supernova Remnants and Neutron Stars*, ed. W. Becker & W. Hermsen, in press (astro-ph/0302540)
- Haberl, F. 2004, in *Memorie della Societa Astronomica Italiana*
- Haberl, F., Motch, C., Buckley, D. A. H., Zickgraf, F.-J., & Pietsch, W. 1997, *A&A*, 326, 662
- Haberl, F., Motch, C., & Pietsch, W. 1998, *Astronomische Nachrichten*, 319, 97
- Haberl, F., Pietsch, W., & Motch, C. 1999, *A&A*, 351, L53
- Haberl, F., Schwobe, A. D., Hambaryan, V., Hasinger, G., & Motch, C. 2003, *A&A*, 403, L19
- Haberl, F. & Zavlin, V. E. 2002, *A&A*, 391, 571
- Haberl, F., Zavlin, V. E., Trüper, J., & Burwitz, V. 2004, *A&A*, 419, 1077
- Hailey, C. J. & Mori, K. 2002, *ApJ*, 578, L133
- Halpern, J. P., Camilo, F., Gotthelf, E. V., Helfand, D. J., Kramer, M., Lyne, A. G., Leighly, K. M., & Eracleous, M. 2001, *ApJ*, 552, L125
- Halpern, J. P. & Ruderman, M. 1993, *ApJ*, 415, 286
- Halpern, J. P. & Wang, F. Y.-H. 1997, *ApJ*, 477, 905
- Hansen, B. & Phinney, E. S. 1997, *MNRAS*, 291, 569
- Harding, A. K. & Muslimov, A. G. 2001, *ApJ*, 556, 987
- . 2002, *ApJ*, 568, 862
- Harding, A. K., Muslimov, A. G., & Zhang, B. 2002a, *ApJ*, 576, 366
- Harding, A. K., Strickman, M. S., Gwinn, C., Dodson, R., Moffet, D., & McCulloch, P. 2002b, *ApJ*, 576, 376

62 *Bibliography*

- Harnden, F. R., Grant, P. D., Seward, F. D., & Kahn, S. M. 1985, *ApJ*, 299, 828
- Harrus, I., Slane, P., Gaensler, B., Hughes, J., Moffett, D., & Dodson, R. 2003, in *IAU Symposium* 218, *Young Neutron Stars and their Environment*, ed. F. Camilo & B. Gaensler (ASP)
- Hartman, R. C. et al. 1999, *ApJS*, 123, 79
- Helfand, D. J., Agüeros, M. A., & Gotthelf, E. V. 2003a, *ApJ*, 592, 941
- Helfand, D. J. & Becker, R. H. 1984, *Nature*, 307, 215
- . 1987, *ApJ*, 314, 203
- Helfand, D. J., Chanan, G. A., & Novick, R. 1980, *Nature*, 283, 337
- Helfand, D. J., Collins, B. F., & Gotthelf, E. V. 2003b, *ApJ*, 582, 783
- Helfand, D. J., Gotthelf, E. V., & Halpern, J. P. 2001, *ApJ*, 556, 380
- Hessels, J. W., Roberts, M. S., Ransom, S. M., Kaspi, V. M., Tam, C., & Freire, P. C. 2003, in *IAU Symposium* 218, *Young Neutron Stars and their Environment*, ed. F. Camilo & B. Gaensler (ASP)
- Hester, J. J., Mori, K., Burrows, D., Gallagher, J. S., Graham, J. R., Halverson, M., Kader, A., Michel, F. C., & Scowen, P. 2002, *ApJ*, 577, L49
- Hester, J. J. et al. 1996, *ApJ*, 456, 225
- Heyl, J. S. & Hernquist, L. 1997, *ApJ*, 491, L95
- . 2001, *MNRAS*, 324, 292
- Heyl, J. S. & Shaviv, N. J. 2002, *Phys. Rev. D*, 66, 23002
- Heyl, J. S., Shaviv, N. J., & Lloyd, D. 2003, *MNRAS*, 342, 134
- Hibschman, J. A. & Arons, J. 2001, *ApJ*, 546, 382
- Hirayama, M., Cominsky, L. R., Kaspi, V. M., Nagase, F., Tavani, M., Kawai, N., & Grove, J. E. 1999, *ApJ*, 521, 718
- Hirayama, M., Nagase, F., Tavani, M., Kaspi, V. M., Kawia, N., & Arons, J. 1996, *PASJ*, 48, 833
- Hirotsu, K., Harding, A. K., & Shibata, S. 2003, *ApJ*, 591, 334
- Hirotsu, K. & Shibata, S. 2001, *MNRAS*, 325, 1228
- Ho, W. C. G. & Lai, D. 2001, *MNRAS*, 327, 1081
- Ho, W. C. G. & Lai, D. 2003, *MNRAS*, 338, 233
- Ho, W. C. G. & Lai, D. 2004, *ApJ*, 607, 420
- Ho, W. C. G., Lai, D., Potekhin, A. Y., & Chabrier, G. 2003, *ApJ*, 599, 1293
- Hughes, J. P., Slane, P. O., Burrows, D. N., Garmire, G., Nousek, J. A., Olbert, C. M., & Keohane, J. W. 2001, *ApJ*, 559, L153
- Hughes, J. P., Slane, P. O., & Plucinsky, P. 2000, *ApJ*, 542, 386
- Johnston, S., Manchester, R. N., Lyne, A. G., Bailes, M., Kaspi, V. M., Qiao, G., & D’Amico, N. 1992, *ApJ*, 387, L37
- Jones, D. H., Stappers, B. W., & Gaensler, B. M. 2002, *A&A*, 389, L1
- Kaminker, A. D., Yakovlev, D. G., & Gnedin, O. Y. 2002, *A&A*, 383, 1076
- Kanbach, G. 2002, in *Neutron Stars, Pulsars, and Supernova Remnants*, ed. W. Becker, H. Lesch, & J. Trümper (Garching bei München: Max-Planck-Institut für extraterrestrische Physik), 91
- Kanno, S. 1975, *PASJ*, 27, 287
- Kaplan, D. L., Kulkarni, S. R., & Murray, S. S. 2001, *ApJ*, 558, 270
- Kaplan, D. L., Kulkarni, S. R., & van Kerkwijk, M. H. 2002, *ApJ*, 579, L29
- . 2003a, *ApJ*, 588, L33
- Kaplan, D. L., van Kerkwijk, M. H., & Anderson, J. 2002, *ApJ*, 571, 447
- Kaplan, D. L., van Kerkwijk, M. H., Marshall, H. L., Jacoby, B. A., Kulkarni, S. R., & Frail, D. A. 2003b, *ApJ*, 590, 1008
- Kargaltsev, O., Pavlov, G. G., Sanwal, D., & Garmire, G. P. 2002, *ApJ*, 580, 1060
- Kaspi, V. M., Bailes, M., Manchester, R. N., Stappers, B. W., Sandhu, J. S., Navarro, J., & D’Amico, N. 1997, *ApJ*, 485, 820
- Kaspi, V. M., Gotthelf, E. V., Gaensler, B. M., & Lyutikov, M. 2001a, *ApJ*, 562, L163
- Kaspi, V. M., Manchester, R. N., Johnston, S., Lyne, A. G., & D’Amico, N. 1992, *ApJ*, 399, L155
- . 1996, *AJ*, 111, 2028
- Kaspi, V. M., Manchester, R. N., Siegelman, B., Johnston, S., & Lyne, A. G. 1994, *ApJ*, 422, L83
- Kaspi, V. M., Roberts, M. S. E., Vasisht, G., Gotthelf, E. V., Pivovarov, M., & Kawai, N. 2001b, *ApJ*, 560, 371
- Kaspi, V. M., Tavani, M., Nagase, F., Hirayama, M., Hoshino, M., Aoki, T., Kawai, N., & Arons, J. 1995, *ApJ*, 453, 424

- Kellner, S. 2002, PhD thesis, Technische Universitt Mnchen
- Kennel, C. F. & Coroniti, F. V. 1984a, *ApJ*, 283, 694
- . 1984b, *ApJ*, 283, 710
- Khangouliau, D. V. & Bogovalov, S. V. 2003, *Astronomy Letters*, 29, 495
- Kifune, T. et al. IAU circular 5905
- Kirk, J. G., Guthmann, A. W., Gallant, Y. A., & Achterberg, A. 2000, *ApJ*, 542, 235
- Kirk, J. G. & Skjæraasen, O. 2003, *ApJ*, 591, 366
- Komissarov, S. S. & Lyubarsky, Y. E. 2003, *MNRAS*, 344, L93
- Krause-Polstorff, J. & Michel, F. C. 1985, *MNRAS*, 213, 43P
- Kuiper, L., Hermsen, W., Cusumano, G., Diehl, R., Schnfelder, V., Strong, A., Bennett, K., & McConnell, M. L. 2001, *A&A*, 378, 918
- Kuiper, L., Hermsen, W., Verbunt, F., & Belloni, T. 1998, *A&A*, 336, 545
- Kuiper, L., Hermsen, W., Verbunt, F., Thompson, D. J., Stairs, I. H.; Lyne, A. G., Strickman, M. S., & Cusumano, G. 2000, *A&A*, 359, 615
- Kulkarni, S. R. & Hester, J. J. 1988, *Nature*, 335, 801
- Kulkarni, S. R., Phinney, E. S., Evans, C. R., & Hasinger, G. 1992, *Nature*, 359, 300
- Lai, D. & Ho, W. 2003, *Phys. Rev. Lett.*, 91, 071101
- Lai, D. & Ho, W. C. G. 2002, *ApJ*, 566, 373
- . 2003, *ApJ*, 588, 962
- Lampland, C. O. 1921, *PASP*, 33, 79
- Larson, M. B. & Link, B. 1999, *ApJ*, 521, 271
- Lattimer, J. M. 1992, in *The Structure and Evolution of Neutron Stars*, ed. D. Pines, R. Tmagaki, & S. Tsuruta (USA: Addison-Wesley)
- Lattimer, J. M. & Prakash, M. 2001, *ApJ*, 550, 426
- Lattimer, J. M., Prakash, M., Pethick, C. J., & Haensel, P. 1991, *Phys. Rev. Lett.*, 66, 2701
- Lodenqual, J., Canuto, V., Ruderman, M., & Tsuruta, S. 1974, *ApJ*, 190, 141
- Lu, F. J., Wang, Q. D., Aschenbach, B., Durouchoux, P., & Song, L. M. 2002, *ApJ*, 568, L49
- Lu, F. J., Wang, Q. D., & Lang, C. C. 2003, *AJ*, 126, 319
- Lyne, A. G. & Lorimer, D. R. 1994, *Nature*, 369, 127
- Lyne, A. G. & Manchester, R. N. 1988, *MNRAS*, 234, 477
- Lyne, A. G., Manchester, R. N., Lorimer, D. R., Bailes, M., D'Amico, N., Tauris, T. M., Johnston, S., Bell, J. F., & Nicastro, L. 1998, *MNRAS*, 295, 743
- Lyne, A. G., Pritchard, R. S., Graham-Smith, F., & Camilo, F. 1996, *Nature*, 381, 497
- Lyne, A. G., Pritchard, R. S., & Smith, F. G. 1988, *MNRAS*, 233, 667
- Manchester, R. N. 1996, in *Pulsars: Problems and Progress*, IAU Colloquium 160, ed. S. Johnston, M. A. Walker, & M. Bailes (San Francisco: ASP), 193–196
- Manchester, R. N., Staveley-Smith, L., & Kesteven, M. J. 1993, *ApJ*, 411, 756
- Marshall, F. E., Gotthelf, E. V., Zhang, W., Middleditch, J., & Wang, Q. D. 1998, *ApJ*, 499, L179
- Marshall, H. L. & Schulz, N. S. 2002, *ApJ*, 574, 377
- Matsui, Y., Long, K. S., & Tuohy, I. R. 1988, *ApJ*, 329, 838
- McGowan, K. E., Kennea, J. A., Zane, S., Córdova, F. A., Cropper, M., Ho, C., Sasseeen, T., & Vestrand. 2003, *ApJ*, 591, 380
- McLaughlin, M. A., Cordes, J. M., Deshpande, A. A., Gaensler, B. M., Hankins, T. H., Kaspi, V. M., & Kern, J. S. 2001, *ApJ*, 547, L41
- Melatos, A. 1998, *Mem. della Soc. Ast. It.*, 69, 1009
- Melrose, D. B. 2000, in *Pulsar Astronomy - 2000 and Beyond*, IAU Colloquium 177, ed. M. Kramer, N. Wex, & R. Wielebinski (San Francisco: ASP), 721
- Mereghetti, S., Bignami, G. F., & Caraveo, P. A. 1996, *ApJ*, 464, 842
- Mereghetti, S., De Luca, A., Caraveo, P. A., Becker, W., Mignani, R., & Bignami, G. F. 2002a, *ApJ*, 581, 1280
- Mereghetti, S., Tiengo, A., & Israel, G. L. 2002b, *ApJ*, 569, 275
- Michel, F. C. 1969, *ApJ*, 158, 727
- Morton, D. C. 1964, *ApJ*, 140, 460
- Motch, C., Haberl, F., Zickgraf, F.-J., Hasinger, G., & Schwöpe, A. D. 1999, *A&A*, 351, 177
- Motch, C., Zavlin, V. E., & Haberl, F. 2003, *A&A*, 408, 323
- Mukherjee, R., Gotthelf, E. V., Halpern, J., & Tavani, M. 2000, *ApJ*, 542, 740
- Murray, S. S., Slane, P. O., Seward, F. D., Ransom, S. M., & Gaensler, B. M. 2002, *ApJ*, 568, 226

64 *Bibliography*

- Muslimov, A. G. & Harding, A. K. 2003, *ApJ*, 588, 430
—, 2004, *ApJ*
Muslimov, A. G. & Tsygan, A. I. 1992, *MNRAS*, 255, 61
Ng, C. . & Romani, R. W. 2004, *ApJ*, 601, 479
Nicastro, L., Cusumano, G., Löhmer, O., Kramer, M., Kuiper, L., Hermsen, W., Mineo, T., & Becker, W. 2004, *A&A*, 413, 1065
Nolan, P. L., Tompkins, W. F., Grenier, I. A., & Michelson, P. F. 2003, *ApJ*, 597, 615
Ögelman, H., Finley, J. P., & Zimmermann, H. U. 1993, *Nature*, 361, 136
Olbert, C. M., Clearfield, C., Williams, N., Keohane, J., & Frail, D. 2001, *ApJ*, 554, L205
Olbert, C. M., Keohane, J. W., Arnaud, K. A., Dyer, K. K., Reynolds, S. P., & Safi-Harb, S. 2003, *ApJ*, 592, L45
Oort, J. & Walraven, T. 1956, *Bull. Astr. Inst. Netherlands*, 12, 285
Ostriker, J. P. & Gunn, J. E. 1969, *ApJ*, 157, 1395
Ostriker, J. P., Rees, M. J., & Silk, J. 1970, *Astrophys. Lett.*, 6, 179
Özel, F. 2001, *ApJ*, 563, 276
—, 2003, *ApJ*, 583, 402
Pacini, F. & Salvati, M. 1973, *ApJ*, 186, 249
Page, D. 1995, *ApJ*, 442, 273
Page, D. 1998, in *The Many Faces of Neutron Stars*. Edited by R. Buccheri, J. van Paradijs, and M. A. Alpar. Dordrecht ; Boston : Kluwer Academic Publishers, 1998., p.539, 539+
Pavlov, G. G., Sanwal, D., Garmire, G., & Zavlin, V. 2002a, in *Neutron Stars in Supernova Remnants*, ed. P. Slane & B. Gaensler (San Francisco: ASP), 247
Pavlov, G. G., Sanwal, D., Kızıltan, B., & Garmire, G. P. 2001, *ApJ*, 559, L131
Pavlov, G. G. & Shibano, I. A. 1978, *Astronomicheskii Zhurnal*, 55, 373
Pavlov, G. G., Teter, M. A., Kargaltsev, O., & Sanwal, D. 2003, *ApJ*, 591, 1157
Pavlov, G. G. & Zavlin, V. E. 2000, in *Pulsar Astronomy - 2000 and Beyond*, IAU Colloquium 177, ed. M. Kramer, N. Wex, & R. Wielebinski (San Francisco: ASP), 613–618
Pavlov, G. G. & Zavlin, V. E. 2003, in *Proc. of the XXI Texas Symposium on Relativistic Astrophysics*, ed. R. Bandiera, R. Maiolino, & F. Mannucci (World Sci. Publishing Co.), 319
Pavlov, G. G., Zavlin, V. E., Aschenbach, B., Trümper, J., & Sanwal, D. 2000, *ApJ*, 531, L53
Pavlov, G. G., Zavlin, V. E., & Sanwal, D. 2002b, in *Heraeus Seminar on Neutron Stars, Pulsars, and Supernova Remnants*, MPE Report 278., ed. W. Becker, H. Lesch, & J. Trümper, 273
Pavlov, G. G., Zavlin, V. E., Sanwal, D., Burwitz, V., & Garmire, G. P. 2001, *ApJ*, 552, L129
Pavlov, G. G., Zavlin, V. E., Sanwal, D., & Trümper, J. 2002, *ApJ*, 569, L95
Perna, R., Narayan, R., Rybicki, G., Stella, L., & Treves, A. 2003, *ApJ*, 594, 936
Pethick, C. J. 1992, *Reviews of Modern Physics*, 64, 1133
Petre, R., Becker, C. M., & Winkler, P. F. 1996, *ApJ*, 465, L43
Petre, R., Kriss, G. A., Winkler, P. F., & Canizares, C. R. 1982, *ApJ*, 258, 22
Petre, R., Kuntz, K. D., & Shelton, R. L. 2002, *ApJ*, 579, 404
Pétri, J., Heyvaerts, J., & Bonazzola, S. 2002, *A&A*, 384, 414
Porquet, D., Decourchelle, A., & Warwick, R. S. 2003, *A&A*, 401, 197
Potekhin, A., Yakovlev, D., Chabrier, G., & Gnedin, O. 2003, *ApJ*, 594, 404
Potekhin, A. Y. & Yakovlev, D. G. 2001, *A&A*, 374, 213
Prakash, A. Y., Ainsworth, T. L., & Lattimer, J. M. 1988, *Phys. Rev. Lett.*, 61, 2518
Prakash, M., Prakash, M., Lattimer, J. M., & Pethick, C. J. 1992, *ApJ*, 390, L77
Predehl, P. & Kulkarni, S. R. 1995, *A&A*, 294, L29
Psaltis, D., Özel, F., & DeDeo, S. 2000, *ApJ*, 544, 390
Radhakrishnan, V. & Cooke, D. J. 1969, *Astrophys. Lett.*, 3, 225
Rajagopal, M. & Romani, R. W. 1996, *ApJ*, 461, 327
Rajagopal, M., Romani, R. W., & Miller, M. C. 1997, *ApJ*, 479, 347
Rankin, J. M. 1993, *ApJ*, 405, 285
Ransom, S. M., Gaensler, B. M., & Slane, P. O. 2002, *ApJ*, 570, L75
Rees, M. J. & Gunn, J. E. 1974, *MNRAS*, 167, 1
Reich, W., Fürst, E., & Sofue, Y. 1984, *A&A*, 133, 4
Reynolds, S. P. & Aller, H. D. 1985, *AJ*, 90, 2312
Reynolds, S. P. & Chevalier, R. A. 1984, *ApJ*, 278, 630
Roberts, M. S. E., Romani, R. W., & Johnston, S. 2001, *ApJ*, 561, L187

- Roberts, M. S. E., Romani, R. W., Johnston, S., & Green, A. J. 1999, *ApJ*, 515, 712
- Roberts, M. S. E., Romani, R. W., & Kawai, N. 2001, *ApJS*, 133, 451
- Roberts, M. S. E., Tam, C. R., Kaspi, V. M., Lyutikov, M., Vasisht, G., Pivovarov, M., Gotthelf, E. V., & Kawai, N. 2003, *ApJ*, 588, 992
- Romani, R. W. 1987, *ApJ*, 313, 718
- . 1996, *ApJ*, 470, 469
- Romani, R. W., Cordes, J. M., & Yadigaroglu, I.-A. 1997, *ApJ*, 484, L137
- Romani, R. W. & Yadigaroglu, I.-A. 1995, *ApJ*, 438, 314
- Ruderman, M. 2003, in *X-ray and Gamma-ray Astrophysics of Galactic Sources*, in press (astro-ph/0310777)
- Ruderman, M. A. & Sutherland, P. G. 1975, *ApJ*, 196, 51
- Rutledge, R. E., Fox, D. W., Bogosavljevic, M., & Mahabal, A. 2003, *ApJ*, submitted (astro-ph/0302107)
- Ryan, E., Wagner, R. M., & Starrfield, S. G. 2001, *ApJ*, 548, 811
- Safi-Harb, S., Ogelman, H., & Finley, J. P. 1995, *ApJ*, 439, 722
- Saito, Y. 1998, PhD thesis, University of Tokyo
- Sakurai, I., Kawai, N., Torii, K., Negoro, H., Nagase, F., Shibata, S., & Becker, W. 2001, *PASJ*, 53, 535
- Sanwal, D., Garmire, G. P., Garmire, A., Pavlov, G. G., & Mignani, R. 2002a, *BAAS*, 200, 7201
- Sanwal, D., Pavlov, G. G., Zavlin, V. E., & Teter, M. A. 2002b, *ApJ*, 574, L61
- Scargle, J. D. 1969, *ApJ*, 156, 401
- Schwope, A. D., Hasinger, G., Schwarz, R., Haberl, F., & Schmidt, M. 1999, *A&A*, 341, L51
- Sedov, L. I. 1959, *Similarity and Dimensional Methods in Mechanics* (New York: Academic Press)
- Shibanov, Y. A. & Yakovlev, D. G. 1996, *A&A*, 309, 171
- Shibata, S., Tomatsuri, H., Shimanuki, M., Saito, K., & Mori, K. 2003, *MNRAS*, 346, 841
- Shull, J. M., Fesen, R. A., & Saken, J. M. 1989, *ApJ*, 346, 860
- Slane, P. O. 1994, *ApJ*, 437, 458
- Slane, P. O., Chen, Y., Schulz, N., Seward, F., Hughes, J., & Gaensler, B. 2000, *ApJ*, 533, L29
- Slane, P., Hughes, J. P., Edgar, R. J., Plucinsky, P. P., Miyata, E., Tsunemi, H., & Aschenbach, B. 2001, *ApJ*, 548, 814
- Slane, P., Zimmerman, E. R., Hughes, J. P., Seward, F. D., Gaensler, B. M., & Clarke, M. J. 2003, *ApJ*, 601, 1045
- Slane, P. O., Helfand, D. J., & Murray, S. S. 2002, *ApJ*, 571, L45
- Spitkovsky, A. & Arons, J. 2002, in *Neutron Stars in Supernova Remnants*, ed. P. O. Slane & B. M. Gaensler (San Francisco: ASP), 81
- Spruit, H. & Phinney, E. S. 1998, *Nature*, 393, 139
- Stappers, B. W., Gaensler, B. M., Kaspi, V. M., van der Klis, M., & Lewin, W. H. G. 2003, *Science*, 299, 1372
- Staelin, D. H. & Reifstein, E. C. III, 1968, *Science*, 162, 1481
- Tam, C. & Roberts, M. S. E. 2003, *ApJ*, 598, L27
- Tam, C., Roberts, M. S. E., & Kaspi, V. M. 2002, *ApJ*, 572, 202
- Tananbaum, H. IAU circular 7246
- Tavani, M. & Arons, J. 1997, *ApJ*, 477, 439
- Tavani, M., Arons, J., & Kaspi, V. M. 1994, *ApJ*, 433, L37
- Tennant, A. F. et al. 2001, *ApJ*, 554, L173
- Thompson, D. J. et al. 1999, *ApJ*, 516, 297
- Thorsett, S. E., Briskin, W. F., & Goss, W. M. 2002, *ApJ*, 573, L111
- Torii, K., Kinugasa, K., Toneri, T., Asanuma, T., Tsunemi, H., Donati, T., Mitsuda, K., Gotthelf, E. V., & Petre, R. 1998, *ApJ*, 494, L207
- Torii, K., Tsunemi, H., Dotani, T., & Mitsuda, K. 1997, *ApJ*, 489, 145
- Torii, K., Tsunemi, H., Dotani, T., Mitsuda, K., Kawai, N., Kinugasa, K., Saito, Y., & Shibata, S. 1999, *ApJ*, 523, L69
- Treves, A. & Colpi, M. 1991, *A&A*, 241, 107
- Treves, A., Turolla, R., Zane, S., & Colpi, M. 2000, *PASP*, 112, 297
- Tsuruta, S. 1964, PhD thesis, Columbia University
- Tsuruta, S. 1986, *Comments on Astrophysics*, 11, 151
- Tsuruta, S. 1998, *Phys. Rep.*, 292, 1
- Tsuruta, S. & Cameron, A. G. W. 1966, *Can. J. Phys.*, 44, 1863

- Tsuruta, S., Teter, M. A., Takatsuka, T., Tatsumi, T., & Tamagaki, R. 2002, *ApJ*, 571, L143
- Tuohy, I. & Garmire, G. 1980, *ApJ*, 239, 107
- Umeda, H., Shibazaki, N., Nomoto, K., & Tsuruta, S. 1993, *ApJ*, 408, 186
- Usov, V. V. & Melrose, D. B. 1995, *Aust. J. Phys.*, 48, 571
- van der Swaluw, E. 2003, *A&A*, 404, 939
- van der Swaluw, E., Achterberg, A., Gallant, Y., Downes, T., & Keppens, R. 2003a, *A&A*, 397, 913
- van der Swaluw, E., Achterberg, A., Gallant, Y. A., & Tóth, G. 2001, *A&A*, 380, 309
- van der Swaluw, E., Downes, T. P., & Keegan, R. 2003b, *A&A*
- van Kerkwijk, M. H., Kaplan, D. L., Durant, M., Kulkarni, S. R., & Paerels, F. 2004, *ApJ*, 608, 432
- van Kerkwijk, M. H. & Kulkarni, S. R. 2001, *A&A*, 380, 221
- van Riper, K. A. & Lamb, D. Q. 1981, *ApJ*, 244, L13
- van Riper, K. A., Link, B., & Epstein, R. I. 1995, *ApJ*, 448, 294
- Vasisht, G., Kulkarni, S. R., Anderson, S. B., Hamilton, T. T., & Kawai, N. 1997, *ApJ*, 476, L43
- Velusamy, T., Roshni, D., & Venugopal, V. R. 1992, *MNRAS*, 255, 210
- Wallace, B. J., Landecker, T. L., & Taylor, A. R. 1997, *AJ*, 114, 2068
- Walter, F. M. 2001, *ApJ*, 549, 433
- Walter, F. M. & Lattimer, J. M. 2002, *ApJ*, 576, L145
- Walter, F. M. & Matthews, L. D. 1997, *Nature*, 389, 358
- Walter, F. M., Wolk, S. J., & Neuhauser, R. 1996, *Nature*, 379, 233
- Wang, F. Y.-H., Ruderman, M., Halpern, J. P., & Zhu, T. 1998, *ApJ*, 498, 373
- Wang, Q. D., Gotthelf, E. V., Chu, Y.-H., & Dickel, J. R. 2001, *ApJ*, 559, 275
- Wang, Q. D., Lu, F., & Lang, C. C. 2002, *ApJ*, 581, 1148
- Webb, N. A., Olive, J. F., Barret, D., Kramer, M., Cognard, I., & Lohmer, O. 2004, *A&A*, 419, 269
- Weekes, T. C. 1991, *Space Sci. Rev.*, 59, 315
- Weiler, K. W. 1978, in *Proc. from the Workshop on Supernovae and Supernova Remnants*, Vol. 49, 545–552
- Weiler, K. W. & Panagia, N. 1980, *A&A*, 90, 269
- Weiler, K. W. & Shaver, P. A. 1978, *A&A*, 70, 389
- Weisskopf, M. C. et al. 2000, *ApJ*, 536, L81
- Weisskopf, M. C., O'Dell, S. L., Paerels, F., Elsner, R. F., Becker, W., Tennant, A. F., & Schwarz, D. A. 2004, *ApJ*, 601, 1050
- Whiteoak, J. B. Z. & Green, A. J. 1996, *A&AS*, 118, 329,
- Woltjer, L., Salvati, M., Pacini, F., & Bandiera, R. 1997, *A&A*, 325, 295
- Yakovlev, D. G., Gnedin, O. Y., Kaminker, A. D., Levenfish, K. P., & Potekhin, A. Y. 2004, *Adv. Space Res.*, 33, 523
- Yakovlev, D. G., Gnedin, O. Y., Kaminker, A. D., & Potekhin, A. Y. 2002, in *Proc. of the 270. Heraeus Seminar on Neutron Stars, Pulsars and Supernova Remnants*, MPE Report 278., ed. W. Becker, H. Lesch, & J. Trümper, Bad Honnef., in press (astro-ph/0111429)
- Yakovlev, D. G., Kaminker, A. D., & Gnedin, O. Y. 2001, *A&A*, 379, L5
- Yakovlev, D. G., Kaminker, A. D., Haensel, P., & Gnedin, O. Y. 2002, *A&A*, 389, L24
- Yakovlev, D. G., Levenfish, K. P., & Shibano, Y. A. 1999, *Phys. Usp.*, 42, 737
- Yoshikoshi, T. et al. 1997, *ApJ*, 487, L65
- Zane, S., Turolla, R., Stella, L., & Treves, A. 2001, *ApJ*, 560, 384
- Zavlin, V. E. & Pavlov, G. G. 2002, in *Proc. of the 270. Heraeus Seminar on Neutron Stars, Pulsars and Supernova Remnants*, ed. W. Becker, H. Lesch, & J. Trümper (Bad Honnef.), 273
- Zavlin, V. E., Pavlov, G. G., & Sanwal, D. 2004, *ApJ*, 606, 444
- Zavlin, V. E., Pavlov, G. G., Sanwal, D., Manchester, R. N., Trümper, J., Halpern, J. P., & Becker, W. 2002, *ApJ*, 569, 894
- Zavlin, V. E., Pavlov, G. G., Sanwal, D., & Trümper, J. 2000, *ApJ*, 540, L25
- Zavlin, V. E., Pavlov, G. G., & Shibano, Y. A. 1996, *A&A*, 315, 141
- Zavlin, V. E., Pavlov, G. G., & Trümper, J. 1998, *A&A*, 331, 821
- Zavlin, V. E., Trümper, J., & Pavlov, G. G. 1999, *ApJ*, 525, 959
- Zavlin, V. E., Trümper, J., & Pavlov, G. G. 1999, *ApJ*, 525, 959
- Zhang, L. & Cheng, K. S. 1997, *ApJ*, 487, 370
- Zwicky, F. 1938, *ApJ*, 88, 522